MAGNETIC ANISOTROPY IN thin SINGLE CRYSTAL NICKEL FILMS.

by

EPHRAIM SECEMSKI, B. Sc., A.R.C.S.

A Thesis presented for the Degree
of Doctor of Philosophy in the
University of London.

December 1968. Materials Section,
Dept. of Electrical Engineering,
Imperial College of Science & Technology,
London S.W.7.

ABSTRACT.

A review of past work on the origins of the uniaxial anisotropy in thin ferromagnetic films revealed that progress in this direction could possibly be achieved by performing epitaxial depositions under rigorously controlled conditions.

Accordingly, an ultra high vacuum system has been designed and built, in which it was possible to maintain c. 5×10^{-9} torr. at best, whilst depositing nickel at 5 Å/sec. 20 cm. from the electron bombardment source. An important feature was the accurate knowledge and control of substrate temperature.

An investigation of anisotropy measurement techniques indicated torque magnetometry as being the most suitable. A manual torque magnetometer of high sensitivity and accuracy was therefore constructed. Calculations on the effect of the deviation of $\underline{M}_S$ from $\underline{H}$ when plotting torque curves in non-infinite fields have been performed, and successfully accounted for the torque-reversal phenomenon.

Torque magnetometry combined with electron microscopic analysis on films deposited under widely varying conditions have produced the following results:

1) K_1 for monocrystalline Ni films has the same value as

for bulk Ni. Their magnetostrictive behaviour is predictable from bulk magnetostriction properties. An estimate of the sign of K_3 is also obtained.

2) The uniaxial anisotropy can be reduced to extremely low levels (500 erg./cc.) by taking steps to exclude all known mechanisms.

3) The effects of stress mechanisms on K_1 and K_u have been investigated, and the two results correlated. In particular, a constraint temperature well below the substrate temperature has been established.

4) There seems to be no contribution to K_u from mechanisms specifically involving oxygen impurities, at least for films grown at up to 2×10^{-5} torr O_2.

5) The effects of lattice imperfections and impurities seem quite important in the as- grown films, and can be the predominant K_u source. Imperfections arising from the growth process itself seem more important than imperfections arising from included gas atoms.

ACKNOWLEDGEMENTS.

To Professor J.C. Anderson, D. Sc., for suggesting the project and for taking a constant interest in it, together with Dr. K.D. Leaver, throughout its progress.

To Mr. E.C. Hall, Materials Section technician, for his assistance on technical problems.

To the various central services of Imperial College, including the Departmental Workshop for the fabrication of some of the larger parts of the vacuum system, to the Centre for Computing and Automation for the use of the I.B.M. 7094 computer, to the Analytical Services Laboratory for the X- ray fluorescence measurements on the films.

To the Science Research Council for financial assistance during the major part of the project.

To Mrs. S. Hibbs, for her patient typing of the thesis.

CONTENTS.

APPENDICES.

CHAPTER 1.

Introduction to Magnetic Anisotropy and its Measurement.

1.1. The Meaning of Magnetic Anisotropy.

A sample of magnetic material is said to be magnetically anisotropic if its internal energy is a function of the orientation of its spontaneous magnetisation $\underline{M}_s$. An energy term of this kind is called a magnetic anisotropy energy. It implies that it is energetically more favourable for $\underline{M}_s$ to lie in certain preferred, or "easy" directions, rather than in higher energy "hard" directions. Thus, if the magnetisation is rotated out of a preferred direction by the application of an external field, there must be an increase in the anisotropy energy. This anisotropy energy term, where present, must be added to the magnetostatic energy term and the usual thermodynamic ones of enthalpy and entropy to give the total free energy of a magnetically anisotropic material. Since the anisotropy energy varies with α_i, the direction cosines of $\underline{M}_s$ relative to a fixed reference direction in the sample, it can be written as $E_k(\alpha_i)$.

There are several forms of anisotropy commonly encountered, of which, following Kittel and Galt[K5], four are here mentioned in an introductory manner.

1.1.1. The Induced Uniaxial Anisotropy, taking the form:

$$E_{K_u} = K_u \sin^2 \theta$$

where G is the angle between M_s and the easy axis, and K_u is known as the anisotropy constant. This form of anisotropy can be induced into some bulk ferromagnets by heat treating or cold rolling in a magnetic field. Uniaxial anisotropy can also be induced in magnetic thin films by depositing them in a magnetic field.

Induced uniaxial anisotropy has a very complicated origin which is undoubtedly an involved mixture of the three, physically more basic, anisotropies now to be listed.

1.1.2. The Magnetocrystalline Anisotropy.

Single crystals of most magnetic materials exhibit an intrinsic anisotropy associated with the crystal lattice, i.e., in the absence of external fields, M_s takes up one of several specific directions relative to the crystal axes. This magneto-crystalline anisotropy, as it is known, generally reflects the spatial symmetry of the crystal structure with which it is associated.

The way in which this comes about is not straightforward. The electron orbital motion, which determines the lattice structure is generally immobilised in the lattice and virtually unaffected by externally applied fields. In the pair model of crystal anisotropy, first developed by Van Vleck(V2) in 1937, spin-orbit coupling is invoked to explain how the spin - which is directly affected by external magnetic fields - interacts

with the crystal lattice to give rise to crystalline anisotropy. This formulation is described in greater detail in the magnetics text books (A1), (B1), (C9) and so need not be elaborated here.

The simplest form of magnetocrystalline anisotropy is, in fact, a uniaxial anisotropy. If, for example, the slight anisotropy in the basal plane is neglected for the moment, hexagonal cobalt exhibits a uniaxial anisotropy which makes the easy direction of $\underline{M}_s$ parallel to the C-axis at room temperature. As $\underline{M}_s$ rotates away from the C-axis, the anisotropy energy increases with angle of rotation, θ, reaching a maximum value at $\theta = 90^\circ$, and thence decreasing to its original value as $\underline{M}_s$ again reaches the C-axis in the opposite direction. The energy can be expressed by a power series in sin θ, including only even terms, i.e., $E_k = K_{u1} \sin^2 \theta + K_{u2} \sin^4 \theta + \ldots$ where K_{u1}, K_{u2} ... are the magnetocrystalline anisotropy constants. Usually, the first term is sufficient to express the actual anisotropy energy. The anisotropy must, of course, also be dependent on the azimuthal angle about the C-axis, but this term is even smaller than the second term above. In the more general case, the magnetocrystalline anisotropy is defined by referring $\underline{M}_s$ to three axes, not necessarily orthogonal, by the direction cosines α_1, α_2 and α_3. As an example iron, which is a cubic crystal, has the easy axis of magnetisation

along the cube edges [100], and the hard direction the cube diagonals [111], with the [110] directions intermediate. The case for cubic crystals will be discussed in more detail later.

1.1.3. Magnetoelastic Anisotropy.

A magnetoelastic, or magnetostrictive anisotropy can arise from the interaction between the magnetisation and the mechanical strain of the lattice. In its simplest form, where a uniform tensile stress, T, is applied to the specimen, the anisotropy energy is given by $E_{\lambda} = \frac{3}{2} \lambda T \sin^2 \theta$ where λ is the magnetostriction constant and θ the angle between $\underline{M}_s$ and the direction in which the tension acts.

1.1.4. Shape Anisotropy.

That part of the magnetostatic energy due to the self-energy of a magnetised material in its own field also gives rise to an anisotropy, known as shape anisotropy. This is dependent on the demagnetising factor of the sample, N, which in turn depends on its shape. The expression for the self-energy of a ferromagnet is $-\frac{1}{2}\underline{M}.\underline{H}_d$ per unit volume, where $\underline{H}_d$ is the demagnetising field. For regularly shaped specimens, $\underline{H}_d = -N\,\underline{M}$, so that the magnetostatic self-energy becomes $E_d = \frac{1}{2} N M^2$. N can be calculated for simple regular shapes, all of them being special cases of the general ellipsoid. This is the only

general shape for which the demagnetising field is uniform throughout the volume for uniform magnetisation distribution (01). Now, for a non-spherical shaped sample, since N is a function of the dimensions of the sample, the magnetostatic self-energy will vary with orientation of $\underline{M}_s$. Taking the ellipsoid as an example:

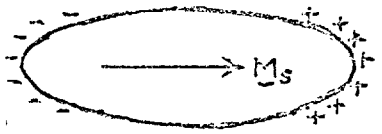

E_d is small when $\underline{M}_s$ lies along the long axis, and is large if $\underline{M}_s$ is swung perpendicular to the long axis. This anisotropy is thus yet another form of a uniaxial anisotropy, expressed for the ellipsoid by: $E_d = \frac{1}{2}(N_\perp - N_{||}) M_s^2 \sin^2\theta$ where $N_\perp$ and $N_{||}$ are the demagnetising factors along the minor and major axes of the ellipsoid in the plane considered.

1.2. The Mathematical Formalism of Cubic Magnetocrystalline Anisotropy.

It is now proposed to investigate the mathematical form of the magnetocrystalline anisotropy for cubic crystals, e.g., nickel or iron. Because of the orthogonality of the cube edges, it is most convenient to express the anisotropy energy in terms of the direction cosines $(\alpha_1, \alpha_2, \alpha_3)$ of M_s with respect to

these cube edges. Cartesian trigonometric relationships can then simply be used to manipulate the algebraic expressions involved. Because of the very high symmetry of the cubic system, there are many equivalent directions in the cubic lattice in which the anisotropy energy is the same. This symmetry implies that if we expand E_k as a polynomial series in the direction cosines α_i, $i = 1, 2, 3$, two simplifying factors can be taken into account:

(i) Terms including odd powers of α_i must vanish, since a change in sign of any of the α_i must bring the M-vector to an energetically equivalent direction.

(ii) The expression must be invariant to interchange of any two α_i's, since all the cube directions must be magnetically indistinguishable.

The use of various algebraic simplifying expressions and the fulfilment of the two above conditions leads to a form for the anisotropy energy up to 6th order in α of:

$$E_k = K_1(\alpha_1^2\alpha_2^2 + \alpha_2^2\alpha_3^2 + \alpha_3^2\alpha_1^2) + K_2\alpha_1^2\alpha_2^2\alpha_3^2 + \ldots$$

(See, for instance, Anderson[A1], p. 115-116). K_1 and K_2 are known as the first and second anisotropy constants respectively.

The magnitude of the constants decrease very rapidly as higher order terms are taken, and normally, only the first two terms noted above are sufficient. By similar algebraic

manipulation to that in the work quoted, it is possible to reduce even the higher order terms to simpler symmetrical expressions. The eighth and tenth order terms then become:

$$K_3(\alpha_1^4\alpha_2^4 + \alpha_2^4\alpha_3^4 + \alpha_3^4\alpha_1^4)$$

and $$K_4\,\alpha_1^2\alpha_2^2\alpha_3^2(\alpha_1^2\alpha_2^2 + \alpha_2^2\alpha_3^2 + \alpha_3^2\alpha_1^2).$$

It will prove necessary to make use of the first of these higher order terms, K_3, later on in section 6.2.1.

1.3. Methods of Measurement of Anisotropy Energy Constants.

There are three main methods for measuring the anisotropy constants of ferromagnetic materials:

(i) from magnetisation curves;

(ii) by ferromagnetic resonance experiments;

(iii) by torque magnetometry.

The first two methods are of rather more limited usefulness and may be less accurate than the third, and so will only be treated briefly.

It should, however, be pointed out that both the first two methods are capable of a very high order of accuracy if performed carefully using the most modern techniques. This is evidenced by the classic measurements of K_1 and K_2 for nickel

by Krause and Patz[K1], using the magnetisation curve method, and by Rodbell[R1], using a resonance method.

1.3.1. Magnetisation Curves.

It has been pointed out in the introduction to anisotropy that the anisotropy energy is a measure of how much less energy is required to magnetise the specimen in an easy direction than in a hard direction. It thus follows directly that if the work done in magnetising the specimen to saturation in different directions can be measured, i.e., $\int_0^{M_s} H.dM$, then the value of the anisotropy constants can be obtained.

The example of a cubic anisotropy is worked out in detail in the various textbooks (e.g., Anderson[A1] pp. 126-128), and the result obtained is:

$$K_1 = 4(A_{110} - A_{100})$$

$$K_2 = 27(A_{111} - A_{100}) - 36(A_{110} - A_{100})$$

where A_{hkl} is the area under the M-H curve for saturation in the /hkl/ direction. Examples of such single crystal magnetisation curves are given below in Fig. 1.1. (from Bozorth[B1], p. 478):

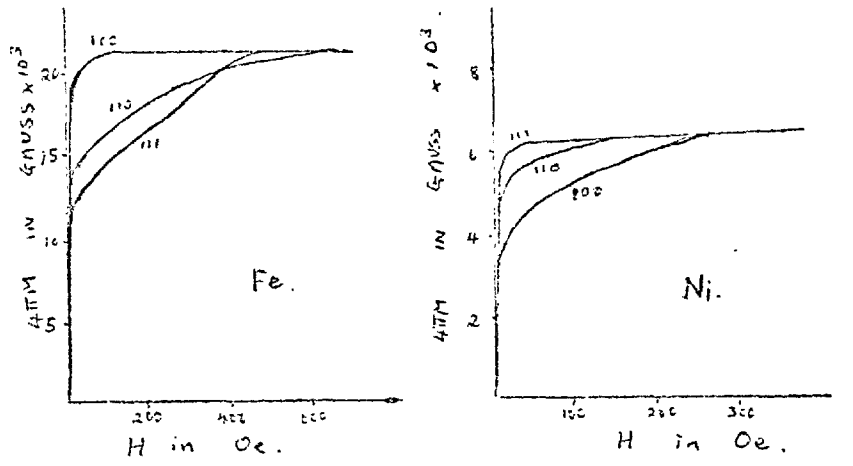

Fig. 1.1.

For a uniaxial anisotropy, the magnetisation curve for tilt of M_s from easy to hard direction is simply a straight line reaching saturation at the anisotropy field $H_k = \pm \frac{2K_u}{M_s}$, as described below in section 2.2. The area then enclosed by the curve in any one quadrant is simply $\frac{1}{2} \times M_s \times \frac{2K_u}{M_s} = K_u$, as expected by simply putting $\theta = 90^\circ$ in the uniaxial anisotropy energy expression.

1.3.2. Ferromagnetic Resonance.

The resonant frequency in a ferromagnetic resonance measurement depends on the total internal field acting on the spin system in the sample. This will be the sum of the applied field, H_a, corrected for demagnetisation by the specimen, and

any anisotropy field, H_k, present. Thus, the resonance condition in its simplest form becomes $\omega = \gamma (H_a + H_k)$. The anisotropy field, and hence the anisotropy constants, can thus be obtained from the shift in resonance field as the applied field is rotated from hard to easy direction.

An alternative and elegant method is to induce spin resonance in the anisotropy field itself by the application of a suitable small alternating driving field. This is known as internal ferromagnetic resonance, and has been described and reviewed by Anderson[A2] and so need not be elaborated further here.

1.3.3. Torque Magnetometry.

The most unambiguous and a standard method of deducing the angular dependence of the magnetic anisotropy, E_k (θ), and hence the anisotropy constants is by use of the torque magnetometer at high fields. This was first used by Weiss[W1] in 1905, and has been developed by numerous investigations ever since. It will be dealt with in detail in section 3.4 .

CHAPTER 2.

General Properties of Thin Magnetic Films.

2.1. Introduction.

The method of fabrication of thin films has a profound influence on their properties. In particular, for films produced by vacuum evaporation or sputtering, the structural properties are affected by the substrates on which they are deposited, its temperature, the rate of deposition, and the residual gas atmosphere, which can give rise to inclusions and surface oxidation. All these factors must be born in mind when considering any intrinsic properties of the film, such as magnetisation, as these will be strongly influenced by the film structure.

The main properties of magnetic films in general will now be very briefly discussed to assist in understanding the terminology used, and as a prelude to a more detailed review of one particular property - the induced anisotropy.

2.2. Single Domain Behaviour and Consequences Thereof.

A ferromagnet reduces its bulk magnetostatic energy by forming magnetic domains, which are formed in greater and greater number until the creation of additional domain walls requires the expenditure of more energy than is gained by the further reduction of magnetostatic energy. The wall energy is governed

by the exchange and anisotropy energies of the material and is a surface energy. The stray field magnetostatic energy arising from the domain walls is negligible by comparison with these energies.

In 1930, Frenkel and Dorfmann[F1], and subsequently also Kittel[K2] (1946) predicted that if a sample of bulk ferromagnet were to reduce in size in any one dimension, there would come a point when it became energetically favourable to do away with domain walls, the whole sample becoming a single domain. This is because the total wall energy, being a surface energy, could become comparatively more important than the magnetostatic energy, which is a volume effect. In particular, for a thin film, a domain wall would imply a row of free poles on either surface. (The Bloch wall, in which the magnetisation tilts out of the plane of the two antiparallel domain magnetisations in crossing the wall, was the only wall model known at the time of Kittel's calculation.) This would give rise to a very considerable magnetostatic demagnetising energy because of the closeness of the two film surfaces. The results of Kittel's calculation, which assumed a uniaxial anisotropy perpendicular to the film, showed that the critical thickness for single domain behaviour was around 5000 Å, which is of the right order of magnitude when compared with experimental results.

The first "modern" experiments, using electronic detection techniques to give sufficient sensitivity to the flux-detecting mechanics of B-H loop plotters, thus enabling them to be used on the 10^{-4}cc. or less of thin film samples, were reported by Crittenden et al.(C1) in 1951. Some two years later, they reported the results of some work on nickel films using their loop-plotter(C2). The films behaved as Kittel had predicted. They were single domain, and the direction of M could be re-orientated, by the application of an applied field, into any direction equally easily. They were thus isotropic as far as Crittenden could see. In addition, they responded to magnetic annealing if cooled from above the Curie temperature in an applied field, in exactly the same way as some bulk ferromagnetic materials, though the direction and magnitude of the resulting uniaxial anisotropy was rather unreliable. It was unfortunate that Crittenden chose nickel for his experiments, because the intrinsic anisotropic properties of the film were too small comparatively for him to detect on his apparatus.

It was not until two years later that the crucial experiment which initiated the flood of work on thin magnetic films was performed by Blois(B2). He evaporated permalloy (81% Ni, 19% Fe) films onto substrates situated in a magnetic field during deposition, and found that a strong anisotropy existed in the

plane of the film. The anisotropy was immediately characterised by observing hysteresis loops as being uniaxial, with an easy axis along the direction of the applied deposition field. Since the films were also single domain, it was expected that the prediction of Kittel should be applicable, i.e., that such a sample should reverse its magnetisation by coherent spin rotation rather than domain wall motion. The hysteresis loops of single domain uniaxial samples in which only coherent rotation could occur were first calculated in a classic paper by Stoner and Wohlfarth[S1]. Though the details of the calculation need not concern us here, two of the results are of particular interest and will be used later in connection with measurement techniques. These are the hysteresis loops observed in the hard and easy directions:

a) Hard direction -

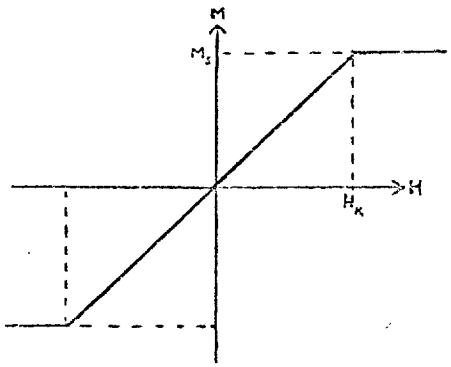

Fig. 2.1.

The equation of the loop, shown in Fig. 2.1., is:

$$M = \frac{M_s^2}{2K_u} . H_y \quad \text{for} \quad |H| < \left|\frac{2K_u}{M_s}\right|$$

$$\text{and } M = M_s \quad \text{for} \quad |H| > \left|\frac{2K_u}{M_s}\right|$$

b) Easy direction -

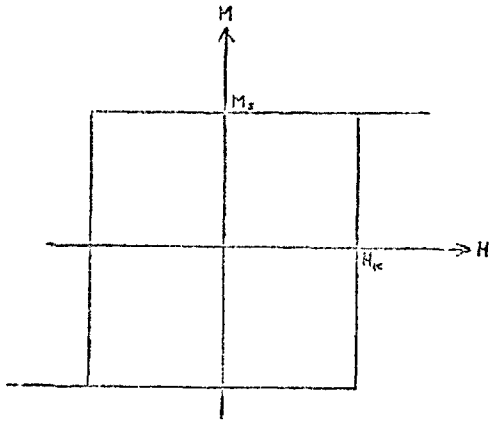

Fig. 2.2.

The equation of the loop is simply (Fig. 2.2.):

$$M = +M_s \quad \text{for} \quad H > -\frac{2K_u}{M_s}$$

$$\text{and } M = -M_s \quad \text{for} \quad H < +\frac{2K_u}{M_s}$$

The uniaxial anisotropy can be considered phenomenologically as an internal field keeping the magnetisation in the preferred direction, and has a magnitude $H_k = \frac{2K_u}{M_s}$. This is known as the

anisotropy field, and is of the order of a few oersteds typically in permalloy films. As shown in the easy direction loop, (Fig. 2.2.), it would be expected that a field just equal to H_k applied along the easy axis would be sufficient to switch the film from one stable M_s state to the other by coherent spin rotation. It is for this reason that the thin magnetic film was recognised as having such potential for use as a computer storage element. It has two distinct stable states capable in theory of being switched from one to the other by fields of the order of a few oersteds in a time of the order of a few nanoseconds, this being the time taken for a coherent rotation process to take place. With present-day techniques, ferrite cores are switched by a non-coherent rotation process which can be completed in as short as a microsecond. The coherent rotation process possible in films thus represents an improvement over cores of over two orders of magnitude in switching speed. Furthermore, lower fields would be required for switching films. Another potential advantage of the use of thin films for manufacturing stores was the great reduction in physical size possible, planar layers of thin films being capable of a very high packing density. The estimated cost of production was also lower than for comparative ferrite core stores.

Very soon after Blois' first experiments on permalloy films, the hysteresis loops were compared by Smith(S2) with those

expected by a single domain coherent rotation model and found to be substantially the same for "good" permalloy films. This showed the assumptions to be approximately correct. The word approximately is used because it was found that there were some important departures from the ideal single domain model and these severely affected the switching process.

2.3. Departures from Single Domain Behaviour.

Since the first experiments of Blois and of Smith mentioned above, work on the properties of thin magnetic films has proceeded broadly along two distinct lines. In the first place, much research has gone into understanding the mechanisms and origins of the deviations from ideal behaviour mentioned above, since it is these aspects which ultimately limit the switching speed and versatility of any practical film store. The other course of research has been directed at trying to find the origin of the uniaxial anisotropy itself. The aim here is to affect the switching properties of a thin film store by being able first to control the anisotropy before considering the details of the reversal process itself.

It is now proposed to outline the deviations from ideal single domain behaviour, since these are relevant to anisotropy

measurements. These deviations are all caused by a breakdown in the assumption that the film remains a single domain throughout.

2.3.1. Reverse Domain Nucleation.

In the first place, the statement has been made that the film should change its M-direction by coherent rotation under the influence of a field H_k or more. This has assumed that the coercive field for domain wall movement, H_c, is larger than H_k. In most cases, however, H_c is smaller than H_k. As the easy axis switching field is increased, the magnetisation then prefers to reverse by the nucleation and growth of reverse domains from the film edges. This was demonstrated very strikingly by Middelhoek[ML] using the Bitter colloid technique. The energy required for the establishment of these domain walls comes from the applied field. The M-H loop is still, however, approximately rectangular, but for a different reason. The small nuclei of reversed magnetisation at the film edges grow only very slowly in the increasing reverse field, until H_c is reached. Beyond this point, the domain walls move very freely through the film and the reversal process is completed with very little increase in the field.

When the field is applied at some other angle to the easy axis, reversal begins by coherent rotation, but after turning

through a certain angle, reverse domains are nucleated and the reversal proceeds from then by domain wall motion.

2.3.2. Ripple.

In principle, therefore, if H_c were greater than H_k, magnetisation reversal should take place only by coherent rotation. This is not, however, so in practice, because of an effect known as magnetisation ripple, or dispersion. This allows the creation of a multidomain state spontaneously throughout the film, rather than just from reverse nuclei at the film edges.

The ripple is a wavelike deviation of $\underline{M}$ from the mean direction of $\underline{M}$ across the film. Its origin is thought to be in the local magnetocrystalline anisotropy of the separate randomly orientated crystallites of the film. These local anisotropies can be considered as being small perturbations on K_u. K_u, though much smaller than the crystal anisotropy, still predominates because of the strong magnetostatic coupling between neighbouring crystallites. In a very large field the ripple falls to zero since all the local anisotropies are overcome by the field energy, and the magnetisation points in the field direction everywhere. Now, to visualise the effect of the ripple on the switching properties, consider a film saturated by a hard direction field. As the field is slowly reduced, each local M-vector is no longer

so strongly aligned with H, and so tilts slightly towards its own local easy axis. The ripple thus increases, and as the field becomes less and less, the film separates into distinct regions having different M-directions, with neighbouring regions rotating in opposite senses towards the mean easy axis, as shown in Fig. 2.3.

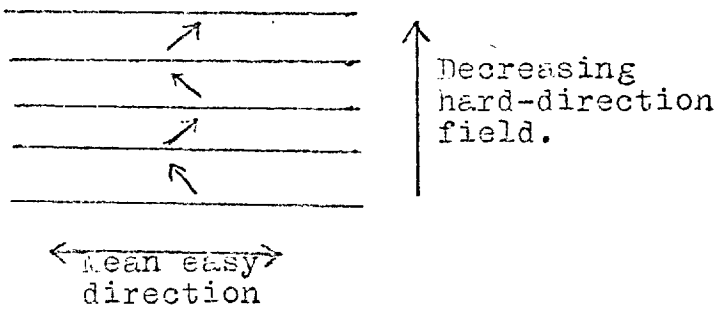

Fig. 2.3.

These regions eventually become clearly differentiated magnetic domains separated by domain walls - a direct consequence of the ripple. This sort of mechanism in fact applies for reversal along other directions in the film plane also. It has a profound effect on the M-H loops if dispersion is sufficiently large. There comes a point in the reversal procedure when the ripple amplitude has become so big that magnetostatic interaction between neighbouring areas of different M-alignment can no longer be neglected. When the energy calculations of these interactions are performed it is found that they act in such a way as to

oppose further growth of the ripple, and hence further reversal. The structure is then said to be "locked", and it requires a much larger reversing field to overcome these interactions and complete the switching.

Thus the uniaxial anisotropy of the film only governs the switching properties provided that the dispersion is not too prominent. It is for this reason that great care must be taken in the evaluation of the methods of measuring the anisotropy, as will be discussed below in chapter 3.

2.3.3. Anomalous Films.

Both the above-mentioned deviations from single domain behaviour occur in what are comparatively called "good" films. These are films usually deposited under reasonable evaporation conditions, i.e., at several hundred Å per minute, onto clean substrates heated to about 200-350° C, and in about 10^{-6} mm. Hg. residual pressure. Such films have H_k and H_c values of a few oersteds (for permalloy) and a low easy-axis dispersion of the order of a degree or so.

There also exists, though, a large class of films, termed anomalous films, where deviations from the Stoner-Wohlfarth model are even more drastic. Such films are usually formed when one or more of the production criteria for good films is broken, so

that the dispersion and H_k rise from their optimum values. Such films tend to have isotropic hysteresis loops, and observation shows that very little of the flux rotates coherently in the Stoner-Wohlfarth mode, but that non-coherent rotation and wall motion predominate. Such films have been subclassified by Cohen[C10] and subsequent workers, and include the so-called rotatable initial susceptibility films, mottled films, inverted films, rotatable anisotropy films and negative H_k films. Because such films show virtually no switching by the Stoner-Wohlfarth model, their M-H loops can often provide very little meaningful data about the anisotropy; indeed, the M-H loops of R.I.S. films are almost exactly the same in all directions in the film. The only way then of learning about the nature of the anisotropy of such films is by performing torque magnetometry measurements in a range of fields, both low and high compared with H_k.

2.4. Single Crystal Films.

Single crystal films arise from the use of single crystal substrates for their preparation. If conditions are correct the phenomenon known as epitaxy occurs and the magnetic film grows in a single crystal to a greater or lesser degree of perfection. The term "single crystal" is used loosely here, since the film

in almost all known cases grows as a series of very large crystallites, with very slight mutual misorientation. The effect of the separate crystallites can usually be neglected. This contrasts with films grown on amorphous substrates, which have a polycrystalline form with much smaller crystallites, of the order of hundreds of Å across, and whose effects are thought to be of premier importance in theories of the origin of anisotropy dispersion. The anisotropy, though, not involving crystallite size in its theories of origin, is surprisingly independent of substrate material so long as it is amorphous and reasonably smooth.

If the films are single crystal, they also have the magnetocrystalline anisotropy characteristic of single crystals. This will be superimposed on the uniaxial anisotropy normally present in polycrystalline films. It is not generally true to say, as have Wilts and Humphrey[W2] in a recent review paper, that "the development of epitaxy completely obscures the normal uniaxial anisotropy". Methods for separating and extracting these two components are given in the sections on measurement and torque magnetometry in chapter 3.

2.4.1. The Effects of Stress on Monocrystalline Films.

As discussed above in section 1.1.3., the application of an externally applied stress to a magnetised ferromagnet will

produce an extra contribution E_λ to the total anisotropy energy. When a single crystal is stressed, this magnetoelastic energy takes a particularly interesting form. E_λ has been rigorously derived by Baltzer[B9] for cubic crystals:

$$E_\lambda = -\sigma h_1(\alpha_1^2\beta_1^2 + \alpha_2^2\beta_2^2 + \alpha_3^2\beta_3^2 - \tfrac{1}{3})$$
$$- 2\sigma h_2(\alpha_1\alpha_2\beta_1\beta_2 + \alpha_2\alpha_3\beta_2\beta_3 + \alpha_1\alpha_3\beta_1\beta_3)$$
$$-\sigma h_3\ (S - \tfrac{1}{3})$$
$$-\sigma h_4\ (\alpha_1^4\beta_1^2 + \alpha_2^4\beta_2^2 + \alpha_3^4\beta_3^2 + \tfrac{2}{3}S - \tfrac{1}{3})$$
$$- 2\sigma h_5(\alpha_1\alpha_2\alpha_3^2\beta_1\beta_2 + \alpha_2\alpha_3\alpha_1^2\beta_2\beta_3 + \alpha_1\alpha_3\alpha_2^2\beta_1\beta_3)$$

where σ is a linear stress applied at direction cosines β_i, and the h_i, α_i and S have their usual meaning in magnetostriction theory. Now, thin films as deposited on their substrates are usually in a state of high isotropic planar stress, and Freedman[F5] has calculated what contribution such an isotropic planar stress would make to the total anisotropy energy of a (100) single crystal magnetic film. He regarded the isotropic stress system in the plane of the film as a combination of two orthogonal stresses acting along the cubic axes. Thus for:

$$\sigma[100],\quad \beta_1 = 1,\quad \beta_2 = \beta_3 = 0$$

and for: $\sigma[0\bar{1}0]$, $\beta_2 = 1$, $\beta_1 = \beta_3 = 0$

Substituting these values into Baltner's expression and adding gives:

$$E_\lambda = \sigma(\tfrac{2}{3}h_4 - 2h_3)\alpha_1^2\alpha_2^2 - \sigma(\tfrac{1}{3}h_1 + \tfrac{1}{3}h_4 - \tfrac{2}{3}h_3)$$

The first term has the same angular dependence in the (100) plane as the magnetocrystalline anisotropy. Thus, the effective crystalline anisotropy constant becomes:

$$K_1 + \sigma(\tfrac{2}{3}h_4 - 2h_3)$$

where K_1 is the normal constant for unstressed bulk material. The second term in the E_λ expression is a constant and so does not contribute to the anisotropy energy.

2.5. The Uniaxial Anisotropy.

To quote from Wilts and Humphrey[W2] again, "with over ten years of concentrated effort, the uniaxial anisotropy is still unexplained, and hence one of the more interesting areas of investigation in ferromagnetism." Since uniaxial anisotropy is the major subject of study in the experimental programme described in this thesis, it is now proposed to consider in detail its supposed origins.

2.5.1. Introduction.

This topic has been regularly and extensively reviewed

during the past few years in several books and individual review articles, e.g., in exclusive chapters by Prutton[P1] and Soohoo[S5] in their respective books; in sections of chapters on magnetic thin films by Cohen[C6] and Pugh[P2] in books on thin films in general; and in individual review articles by Prutton[P3,P4] (1962, 1964), Methfessel[M2] (1966), Wilts and Humphrey[W2] (1968) and Slonczewski[S6] (1968). For this reason, it is considered unnecessary to reproduce here an extensive review of the subject. It is proposed, instead, to review, firstly, some of the latest work which has not yet had full coverage in the published reviews; secondly, many of the more obscure mechanisms based on impurities and imperfections in the films, as these too have not been very fully treated in the review literature. Only those aspects and conclusions of the major theoretical models which are specifically required for the analysis of the experimental results will be dealt with in detail, the remaining points being merely mentioned for the sake of completeness.

There are four major sources postulated for uniaxial anisotropies observed in films under various conditions.

2.5.2. Oblique Incidence Anisotropy.

This arises when the vapour beam strikes the substrate at an angle of incidence, and appears even without the presence of an aligning field. Its origin has been attributed[S7,C7] fairly

conclusively by electron microscopy to a geometric effect in the structure of the resulting film, and so the anisotropy is a pure shape anisotropy. Since, by the term "induced uniaxial anisotropy" is usually meant the M-induced anisotropy, i.e., that induced by the magnetic effects of the orientation of M during the deposition, oblique incidence anisotropy need not be considered further.

2.5.3. Magnetostrictive Constraint Mechanism.

When the film is deposited in the presence of a field at a temperature T_d it deforms because of magnetostriction, and, in the simplest formulation of the theory by Robinson, suffers a strain of magnitude λ_{T_d} in the direction of M. At the high substrate temperatures usually used, this strain has no accompanying stress because of the mobility of the atoms. As the film cools, there comes a temperature T^1 at which the atoms are no longer sufficiently mobile to allow the strain to continue to follow the changes in λ with temperature. An anisotropic stress of magnitude $Y\lambda_{T^1}$ (where Y = Young's modulus) is thus formed in the film at lower temperatures. This stress will be tensile or compressive according as λ_{T^1} is positive or negative. As discussed above in section 1.1.3, such an anisotropic stress defines a uniaxial anisotropy, first proposed by Becker and Döring[B7],

$$E = -\frac{3}{2}\lambda_o \sigma \sin^2\theta$$

where λ_o is the value of λ at the measuring temperature and σ is the stress. For this mechanism, therefore,

$$E = -\frac{3}{2}\lambda_o\lambda_{T1} Y \sin^2\theta$$

There have been various refinements of this basic theory. Ignatchenko[I1], for instance, took into account the contraction in the direction perpendicular to M because of Poisson's ratio, ν. He therefore used an effective stress $Y\lambda_{T1}/(1+\nu)$.

The most accurate formulation of the constraint theory is due to West[W5]. He explains that it is incorrect in all the above-mentioned derivations to use a mean λ to evaluate the constraint energy E. In polycrystalline cubic films, for example, the mean value of λ is given by the usual expression:

$$\lambda = \frac{2}{5}\lambda_{100} + \frac{3}{5}\lambda_{111}$$

Thus, if λ_{100} and λ_{111} are of opposite sign, it is possible that the mean value of λ is small, and yet the constraint energy could be quite large because of the large stress, tensile or compressive, in individually orientated parts of the film. He therefore performed a rigorous derivation of the constraint energy using the correct averaging procedure for individual crystallites, and produced for the anisotropy constant of a random polycrystalline array the result:

$$K_{constraint} = \frac{9}{10}\left[(C_{11} - C_{12})\lambda_{100}(T_o)\lambda_{100}(T^1) + 3C_{44}\lambda_{111}(T_o)\lambda_{111}(T^1)\right]$$

where the C's and λ's are the standard elastic and magnetostrictive constants. Both West in his original paper, and Slonczewski[S6] since, have compared the experimental results of several investigators with the above constraint term, and have found that the experimental values of $K_{constraint}$ are almost always equal or less than the theoretical value. This West explained in terms of the dependence of the constraint energy on the substrate-film bond, the constraint term only reaching its theoretical value when the bond strength is at its maximum value.

Recent, and so far unreviewed work by Baltz and Drew[B8] has illustrated a magnetoelastic constraint term clearly. They deposited permalloy films of various compositions on single crystal quartz and observed abnormally large uniaxial anisotropies. This they eventually traced to the large difference in the thermal expansion coefficients of quartz in the [0001] and [11$\bar{2}$0] directions. This caused large anisotropic stresses in the films as they cooled whilst constrained to the substrates, so giving anisotropy contributions over and above the normal magnetostrictive self-constraint term.

With the sole qualification of the microstress theory proposed by Kneer and Zinn[K6], the constraint term as derived by West is now firmly established as describing correctly an important source of uniaxial anisotropy.

2.5.4. Directional Ordering of Atom Pairs.

From the fact that a significant uniaxial anisotropy is present even in films of zero-magnetostrictive composition, which would give a zero (or very small according to the West derivation) constraint anisotropy, it is concluded that there is at least one other major source of anisotropy. A theory first proposed independently by Neel[N3] and Taniguchi[T3] to account for some annealing properties of bulk ferromagnetic alloys involves the directional ordering of atom pairs, and this could apply to alloy thin films. Expressed simply, this stated that since the spin-coupling coefficients between different constituent atom pairs in an alloy are different, pairs of like atoms would tend to diffuse in the annealing field at high temperature into such a position as to minimise their energy with respect to the magnetisation direction. Thus, on cooling to room temperature, this short range directional order is frozen into the alloy lattice, and so the magnetic energy varies with the direction of $\underline{M}$. Analysis shows that this variation is in fact a uniaxial anisotropy. The anisotropy constant for a concentration C of one constituent of the alloy is given by:

$$K_{pair} \propto C^2(1 - C)^2 \omega \, \omega^1 / T^1$$

where the ω are the interaction energy constants at measuring (T) and annealing temperatures (T^1), introduced by Néel to include

the possible coupling schemes between neighbouring atom pairs. Experiments by Ferguson[F3] on bulk alloys of Ni-Fe showed good agreement with the pair-ordering theories, but it was difficult to predict the magnitude of the pair-ordered anisotropy in thin films. From Ferguson's results on bulk alloys, the characteristic time for establishment of an equilibrium pair-ordered state in 82/18 permalloy is of the order of 10^4 seconds at 450° C corresponding to an activation energy of the ordering process of about 3eV. Films, on the other hand, are grown in times of the order of tens of seconds at temperatures as low as room temperature, giving an activation energy of the order of only $1 \sim 1\frac{1}{2}$eV. In addition, with the notable exception of Methfessel et al's[M3] work on U.H.V. films, the values of the K_{pair} so produced in films is always well below that predicted from the bulk values. Another difficulty with the pair theory is that the derived concentration dependence $C^2(1 - C)^2$ is only strictly valid for dilute solutions, yet it is necessary for want of a more rigorous theory, to use the theory throughout the whole of the composition range of Ni-Fe films.

Despite these problems, a number of workers have tried to account for the whole of the uniaxial anisotropy in Ni-Fe films over a broad composition range by a combination of the constraint release term and a pair-ordering type of term. The magnitude of

the latter was empirically decided on by using one variable parameter adjusted to fit experimental values of K_u at the non-magnetostrictive composition where the whole of K_u is supposedly due to pair-ordering. Reference to the relevant papers by Robinson[R2], West[W5], Siegle and Beam[S9], Telesnin et al.[T4], and Wilts[W6], or in the latter two cases, to the deductions drawn from them by Slonczewski[S6], shows that the fit so obtained is reasonably satisfactory.

These fits of K_u data to the strain-pair model are, however, only semiquantitative, because of:

i) lack of knowledge of the true constraint temperature,

ii) lack of knowledge of the true temperature dependence of the atom-pair interaction energy constants, even after arbitrary values for the ω have been chosen by using a proportionality constant in the K_{pair} expression which forces a good single-point fit at one composition and temperature,

iii) lack of knowledge of the true concentration dependence of K_{pair}.

Serious doubts about the validity of the model also arose from the data obtained by Suzuki and Wilts[S10] in 1967 on the Fe-rich end of the Ni-Fe composition range. They showed that in this region, the presence of an α (BCC) phase gave a

substantially lower contribution to K_u than would have been obtained if these compositions still existed in the δ (FCC) phase, as for higher Ni content alloys. If the value of K_u is calculated below 50% Ni by extrapolating back from the δ phase results, it is found that the characteristic maximum of K_u at about 50% Ni predicted by the strain-pair theory no longer appears. This, they deduced indicated that pair-ordering was not a significant contribution to K_u. Since this deduction was based on only a single point extrapolation below 44% Ni, and also assumed that the variation in K_u over a wide compositional and substrate temperature range was due primarily to variation of K_{pair}, their results are not conclusive evidence against the existance of pair-ordering.

Nevertheless, the above doubts, and those presented within the experimental work to be described in section 2.5.5. below, have led to the conclusion that there must be further significant contributions to K_u besides the simple strain-pair terms.

2.5.5. The Role of Impurities and Imperfections.

2.5.5.1. Introduction.

In this section contributions to K_u are considered from the following sources:

i) Impurity atoms in the lattice,

ii) Vacancies, self-interstitials, dislocations etc. in the lattice,

or iii) The special effects of oxygen.

Historically, the effects of lattice imperfections and impurities on K_u in bulk ferromagnetic alloys have all been interpreted by variations of the directional ordering theories mentioned in section 2.5.4., and have been well reviewed by Graham[G1] pp. 297-306. It is important to point out that these effects can contribute to K_u either directly by their own directional order, or by enabling pair-order of the alloy atoms to proceed more easily. The latter, for instance, is particularly the case for the anisotropy induced by cold rolling of permalloy, where it is thought that the diffusion of atoms into ordered pairs is enhanced by dislocations moving during deformation. This interaction between the possible effects of impurities and imperfections leads to some difficulty in the interpretation of experimental results.

The first direct evidence that lattice imperfections alone could produce a uniaxial anisotropy was from neutron irradiation experiments, first performed in 1959. Magnetic annealing of bulk samples of the pure metals Fe, Co, Ni produced no uniaxial anisotropy. If, however, the samples were first neutron irradiated and then annealed, or, were irradiated in a magnetic field, an

anisotropy appeared[B10][F6]. Since neutron irradiation produces vacancies, interstitials, and their complexes, it was deduced that these defects were responsible for the induced anisotropy. This type of experiment was first extended to thin film samples by Williams and Schindler[W7]. They found that K_u of permalloy films deposited in the absence of a field but subsequently neutron irradiated showed similar composition dependence to that of a simple strain-pair theory as discussed above. This was attributed to the fact that the directional short range order could occur by radiation-enhanced diffusion even at the fairly low temperatures of their experiments. ($< 60^\circ$ C). This, therefore, constituted an example of a defect mechanism contributing to K_u indirectly, by allowing the normal pair-ordering mechanism to proceed. Their peak in K_u around 55% Ni was about $2\frac{1}{2}$ times higher than expected from strain-pair theory, but this they said could well be due to a long range order of the composition Ni Fe. Such ordering, with a concomitant increase in K_u, had been observed by Pauleve et al[P5]. It is also feasible that directional defect ordering itself was contributing to this peak.

Sorohan[S11] has performed a series of experiments in which Ni films were bombarded with 1·9 kV argon ions. The resulting changes in K_u could be quantitatively accounted for

by a Néel-Taniguchi-type ordering of the divacancies produced by the impact of the incident ions.

The most recent neutron and ion bombardment experiments - those of Roth et al.[R3] on 81/19 permalloy films - produced values of rotational activation energies for the annealing of K_u comparable with Ferguson's bulk pair-ordering values. The effect of the bombardment was, as for Williams and Schindler, to induce the evolution of pair-ordering. At the same time, it was noticed that a reduction in K_u occurred as the radiation proceeded, probably due to the onset of the long-range order of Ni_3Fe. They also found an additional component to K_u present in films deposited at 150° C, but not in 300° C depositions. This was attributed to the ordering of lattice imperfections, which had a much higher density in the lower temperature depositions.

2.5.5.2. Static Annealing Experiments.

All the above procedures have demonstrated the effects on K_u of lattice imperfections artificially introduced. However, there is a high concentration of defects in thin films simply as a result of the growth process itself. The usual way of separating out different contributions to K_u is by observing the kinetics of the change of K_u with time and temperature during a magnetic annealing experiment. As mentioned above in section 2.5.4.,

activation energies for the annealing of K_u in permalloy films are usually much lower than those expected from the auto-diffusion of the Ni and Fe atoms as obtained from bulk measurements. Additionally, under certain conditions, annealing effects can be observed at temperatures as low as 300° K, at which practically no diffusion of the metal atoms is expected to occur. These observations suggest that part of K_u is caused by structural defects in the film. These have much higher mobilities than the lattice atoms themselves. For example in bulk Ni, interstitials are clearly mobile at 100° C, vacancies at 250° to 300°, and dislocations only at 400° C. Divacancies, on the other hand, are mobile even well below 100° C(J1).

Historically, the first worker to invoke imperfection ordering to explain the results of annealing experiments was Takahashi(T5). He could fully account for the changes in K_u in his films by assuming a two-component model: i) a pair-ordering term which could not be rotated below 300° C, as expected from bulk activation energies, and ii) an annealable component with activation energy of about 1eV, - of the correct order for vacancy migration.

Metzdorf(M4) has performed a comprehensive series of annealing experiments on 81/19 permalloy films. Like Takahashi, his results fitted a two-component model. One of these was more

easily re-orientable and constituted about $\frac{1}{3} K_u$ provided $T_{anneal} < T_{deposition}$. For $T_a > T_d$, however, increasing T_a rotates an increasing fraction of K_u, until at 400° C, a complete re-orientation could be achieved in 1 hour. Metzdorf therefore assumed that these conditions had established the ordering mechanism for K_u in a state of complete thermal equilibrium. Since the values of K_u achieved were, however, considerably below the expected bulk pair-ordered equilibrium values, he concluded that pair-ordering was not a significant contribution to K_u, at least for depositions and anneals at up to 400° C. He quoted the results of Methfessel et al.(M3) mentioned in section 2.5.4. to show that there was nothing intrinsic in the structural imperfection peculiar to thin films which would prevent the bulk values of K_{pair} from being achieved. Metzdorf therefore concluded that the primary source of K_u in his films was the effects of impurity atom ordering or vacancy ordering, the former being the preferable origin.

Metzdorf's arguments are, however, open to considerable criticism because of his equating his own films with those of Methfessel. Methfessel's films were probably exceptionally free of defects and impurity interstitials. (They were deposited at a high rate, in U.H.V., on to well outgassed (1000° C), carefully prepared quartz or saphire substrates, and were then subjected

to a high temperature anneal.) Metzdorf considered that the bulk values of K_{pair} in Methfessel et al's films were probably due to the high temperatures used (400° - 525° C), but did not consider that it could have been the structure of their films which was really instrumental in allowing the expected bulk K_{pair} to be achieved. Films such as Metzdorf's own, grown under normal technical conditions could be expected to have a much lower K_{pair}, because the high density of interstitial atoms present may well only allow a much smaller degree of pair-ordering.

In the light of these qualifications of Metzdorf's conclusions, it seems likely that his two-component model is similar to that of Takahashi, i.e., pair-ordering as the main constituent to K_u, with imperfection or impurity ordering constituting a smaller, more easily annealable part.

Even Siegle and Beam[S9], as mentioned above in section 2.5.4., found it necessary to propose that their K_{pair} was modified by the presence of "local regions of structural abnormalities", i.e., imperfections. This they assumed since K_{pair} had a "distribution of annealing times and/or activation energies" rather than a single discrete value. The possibility of direct ordering of the imperfections themselves was thought less likely because of the good $C^2(1 - C)^2$ compositional dependence of K_{pair}.

Smith and Weiss[S12], by a sequential annealing and measure-

ment procedure, were able to separate five contributions to such a K_u spectrum in 81/19 permalloy films:- one component, unannealable in 2 hours at 400° C, attributed to pair-ordering (which has 3eV activation energy); 2 components, locked by exposure to O_2, $E \leq 0{\cdot}2eV$, attributed to lattice vacancies which allowed re-orientation of anisotropic vacancy clusters or iron pairs; two components, $E \approx 1eV$, perhaps due to self-interstitials or carbon impurity atom interstitials.

2.5.5.3. Dynamic Annealing Experiments.

A very fruitful approach in investigating the distinct contributions to K_u excited by anneal has been to analyse the resulting H_K isotherms into the sum of a number of separate simple exponential processes of order one. Then, for n annealing processes, after time t,

$$H_k(t) = \sum_{j=1}^{n} H_{K_j}(0)\left[2e^{\left(\frac{-t}{\tau_j}\right)} - 1\right]$$

where τ_j is the j^{th} relaxation time with activation energy E_j, given by the Arrhenius relation:

$$\tau_j = \tau_{oj}\, e^{\left(\frac{E_j}{KT_a}\right)}$$

By using a slight variant of this analysis procedure, Lesnik, Levin and Nedostup[L4] were able, in an ingenious analysis, to account for the whole of the anisotropy in 82/18 permalloy films

by means of a model based only on the relative number of ordered vacancies, disordered vacancies and interstitials in the film lattice. They assumed H_K to be proportional to the number of ordered vacancies. The activation energies of the two diffusion processes postulated - migration of vacancies to ordered positions, and of interstitials to undergo recombination with vacancies - were practically identical with values obtained by Neel[N4] on bulk Ni samples.

Less surprising results using this sort of H_K analysis have been obtained by the two main groups - that of Kneer and Zinn[K6,K7], and that at the M.I.T. Lincoln Laboratory.

The former found that for 81/19 Ni Fe, iron pair-ordering could be the mechanism for the main contribution. This constituted 60% H_K with E_j = 1·5eV in the as-produced films, rising to 85% H_K with E_j = 2·1eV after a high temperature anneal. This latter figure was approaching E_j values for bulk materials. Three other faster processes were also found. In pure Ni films, these three fast processes accounted for the whole of H_K, though the wider scatter of the data made it impossible to determine distinct E_j values. One important outcome of Kneer and Zinn's work on Ni has been a suggested modification to the West constraint term as mentioned in section 2.5.3. Because the H_K isotherms for the Ni films were not smooth curves, but showed small discontinuous

jumps, Kneer and Zinn suggested that this behaviour was not compatible with a constraint arising from the film-substrate bond. They proposed that the constraint was caused by the anisotropic stressfield associated with imperfections, impurities or dislocations, frozen into individual crystallites during deposition. The measured isotherms were therefore a result of the orientation kinetics of these microstress origins. Their $K_{constraint}$ had the same functional form as that of West, but with the addition of a proportionality factor, f, dependent on the thermal history of the sample. Thus, the different level of constraint found by different observers was attributed by them to differences in the density of origin centres for the microstresses, rather than in variation of film-substrate bond, as suggested by West.

Smith, Weiss and Harte[S13] of the M.I.T. group found 3 and perhaps 5 processes accounting for $\frac{1}{2} H_K$ in 81/19 Ni Fe. They could not relate any of these processes to the oxygen locked vacancy mechanism of their previous paper, but one process matched one of Kneer and Zinn's fast processes. This group subsequently developed a new rotating anneal method which only excited one component of the anisotropy at a time[H5]. In previous experiments, all processes had been annealed simultaneously, making interpretation difficult and ambiguous. Preliminary

results using this method gave imperfection processes with similar relaxation times to those of Kneer and Zinn and of their own previous work, but with activation energies one order lower.

It is apparent from two major problems that none of the above imperfection processes can be attributed to the action of point defects alone:

i) why all the τ are several orders of magnitude greater than the Debye relaxation time for point defects (10^{-13}sec.), and

ii) why the E are at least $\frac{1}{2}$eV too low for point defect diffusion.

The latest suggestions of this group (H6) explain these two anomalies and the differences between the rotating anneal and the previous annealing experiments. They use a model involving the diffusion of interacting single and divacancies to oriented grain boundaries.

Another method which is shedding light on the role of lattice defects in K_u is that of observing the annealing kinetics of defects artificially introduced into the film during production. This was first done by Andrä and Steenbeck (A5) on 96/4 Ni Co and pure Ni films, electrolytically charged with hydrogen during deposition. They found that besides the anisotropy caused by the directional ordering of hydrogen interstitials, there also existed an additional component which they explained either by the action of Ni interstitials in the dumb-bell configuration or

by divacancies. Luborsky[L5] has applied annealing kinetics analysis as explained above to investigate the effects on K_u of increasing concentrations of sulphur (up to 6%) in electro-deposited 81/19 Ni Fe films. His low temperature isothermal anneals (at up to 90° C) gave an activation energy of 0·74 eV for the processes affected by the sulphur. After stabilisation at 150° C, E fell to $\approx$ 0·4 eV. He proposed from his results that the inclusion of sulphur in his films produced vacancies, defects, strain fields and other structural damage which allowed pair-ordering to proceed even at the low temperature used. A $(\frac{t}{\tau})^{\frac{1}{2}}$ dependence in the rate equation for anneal suggested, after Slonczewski[S14], that the diffusion of vacancies or defects to a sink such as the grain boundaries was the operable mechanism. The stabilisation treatment completely anneals out these imperfections.

In conclusion, it must again be stated that imperfections can contribute to K_u either by direct self-ordering, e.g., Lesnik's work, or indirectly by permitting one of the more basic mechanisms to act, e.g., Luborsky's work. It therefore remains undecided as to whether such components of K_u are distinct origins of equilibrium anisotropy energy in their own right, or whether they are simply different relaxation paths leading ultimately to the same energy dictated by the two more basic mechanisms of pair-ordering and constraint release (Slonczewski[S6]).

2.5.5.4. Impurities.

To illustrate the effects on K_u of even very low levels of contamination in permalloy films, it is only necessary to mention the quite independent results of Astwood and Prutton(A6), and of Hodges(H7) concerning contamination from refractory source crucibles. This has not been confirmed, however, in subsequent experiments by Wilts(W8).

In a number of experiments, the effects of gas, in particular oxygen, absorbed in the film have been studied. Possible mechanisms by which oxygen impurity atoms could act as a source of uniaxial anisotropy have been subdivided by Prutton(P3) into three categories:

i) a ferromagnetic-antiferromagnetic exchange mechanism from Ni O inclusions,

ii) a magnetostrictive effect in the ferromagnetic film resulting from the strain in ordered Ni O,

iii) (111) plane faulting due to absorbed oxygen atoms, (Heidenreich model(H8)).

The most systematic study of the effects of gases on the properties of magnetic films has been performed by Paul and Hanson(P6). Summarising their results for H_k, no noticeable change was observed for p_{O_2} from just below 10^{-9} torr to around 1×10^{-5} torr, where H_k began to rise fairly rapidly. Other

inert gases had no noticeable effects up to a few x 10^{-4} torr. Paul and Hanson have also given a fairly full literature survey of gas effects on magnetic films, so this will not be reproduced here. A critical analysis of this past work and the interpretation of all the effects found in terms of Frutton's three mechanisms will be given in chapter 6 , when discussing the results of the present experiment.

2.5.6. Experimental Programme.

In view of the discussion in sections 2.5.1 to 2.5.5. above, it is clear that insight into the origins of the uniaxial anisotropy in thin magnetic films requires experiments to be performed under reproducible and rigorously clean conditions. Given these it becomes possible to perform the following definitive experiment. If a defect-free film of a pure ferromagnetic element is grown in a magnetic field under ultra high vacuum conditions, and is then released without straining from its substrate, it should display no uniaxial anisotropy, since all the above proposed mechanisms will have been eliminated. Should an anisotropy nevertheless appear, it will then be possible either to postulate new mechanisms, or to explain its appearance in terms of departure from the ideal conditions envisaged for the experiment.

To facilitate the achievement of these conditions, the

following details of the experiment were fixed. In the first place, nickel was chosen as the material to be used both because of its comparative freedom from massive oxidation, and because of the vast body of published work on it from which various constants and properties could be reliably used. Secondly, only single crystal films were to be studied since such films

i) make the analysis of any magnetic data simpler and more meaningful, and

ii) do not have the high density of grain boundaries of polycrystalline films, making for simpler structural analysis.

The use of soluble substrates for the epitaxial growth would also enable the magnetic influences of the stress system in the films to be studied. The use of U.H.V. was necessary not only to ensure a low partial pressure of oxygen, but also to increase the structural perfection of the resulting films. Baltz(B11) has shown that permalloy films grown epitaxially by fairly rapid deposition in U.H.V. (10^{-9} torr) exhibited a very high degree of crystallographic orientation and a very low defect density when compared with similar depositions performed in ordinary high vacuum (10^{-5} torr).

CHAPTER 3.

Anisotropy Measurements on Thin Films.

3.1. Introduction.

The methods available for making anisotropy measurements on thin film samples are broadly speaking the same as those available for general anisotropy measurements, as specified in section 1.3. Because of some special properties peculiar to films, however, these three methods have to be modified somewhat, whilst on the other hand, other novel techniques present themselves. These are now briefly considered as a prelude to demonstrating which method seemed the most suitable for the project in hand.

3.2. Magnetisation Curve Measurements.

In practice, the method outlined above of measuring the area between magnetisation curves is not used to find H_k. (One of the very earliest workers did use this method, but the validity of its applicability to any other than "perfect" uniaxial films is very doubtful.) Use is made, however, of the hard and easy axis loops (as magnetisation curves for thin films are usually called).

According to the Stoner-Wohlfarth model of single domain

uniaxial behaviour mentioned above in section 2.2., the hard axis loop (Fig. 2.1.) reaches saturation at $H_K = \frac{2K_u}{M_s}$, so that H_K, and hence K_u if M_s is known, is easily found. In practice, however, most films do not show the closed straight line hard direction loop which follows from the Stoner-Wohlfarth model. As H is increased towards saturation, the loop opens up showing hysteresis. For films with a low $\frac{H_c}{H_K}$ ratio, the single domain model holds true for drive fields of less than about $\frac{H_K}{2}$, if the film has been previously saturated along an easy direction. The procedure then adopted is to extrapolate the low drive hard axis loop to saturation. The saturation level is obtained by displaying on the curve tracer the easy axis loop, which is square and saturates at the same level M_s, as shown in Fig. 3.1.

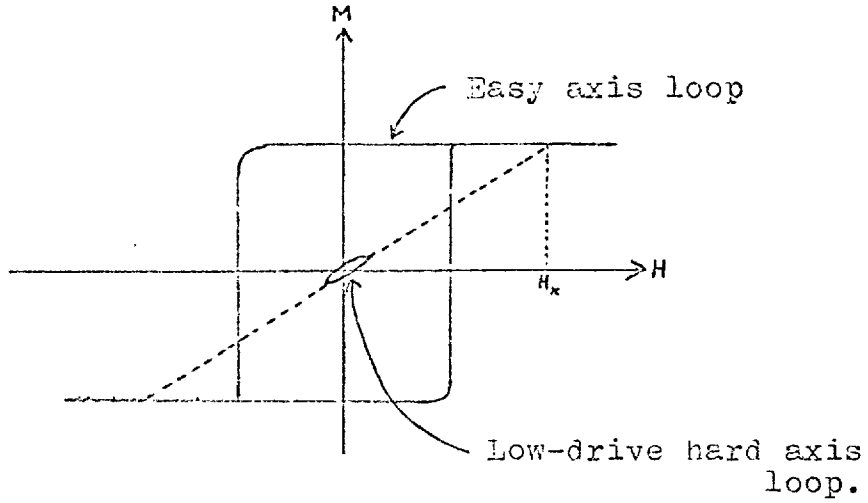

Fig. 3.1.

Deviations from the single domain model occur because of the effect of the magnetisation ripple, which increases with increasing $\frac{H_c}{H_k}$ ratio. The ripple hinders the rotation of the magnetisation, as explained in section 2.3.2. This produces a smaller slope of the hard axis loop than the true single domain model would give, so yielding values of H_k which are too large. The hard axis loop slope also varies with the drive field for high $\frac{H_c}{H_k}$ films, besides the opening of the line with increasing drive.

For these reasons, the use of hysteresis loop plotter in this way is not considered a "reliable" method of determining anisotropy constants because of its very high dependence on the validity of the single-domain model of rotation.

Besides these objections, the hysteresis loop plotter only gives simple results for unmixed anisotropy, i.e., a single order. With mixed anisotropies, switching analysis becomes almost impossibly complicated, thus debarring this method on a second count.

There have been several modes of operation of the loop plotter proposed, which overcome the difficulties arising because of the ripple. These methods are essentially susceptibility methods, and so will be considered after the next method.

3.2.1. Susceptibility Method.

This was first proposed by Torok et al.[T1] and Feldtkeller[F2] and uses the same sort of coil system as does the hysteresis loop plotter.

The basic measurement of Feldtkeller plots the transverse A.C. susceptibility as a function of an applied saturating D.C. field, H_{11}, for H_{11} in the easy and hard directions respectively. From the single domain theory, the expressions obtained for χ in terms of H_{11} as the field is slowly reduced are:

$$\chi = \frac{M_s}{H_{11} - H_k} \quad \text{for } H_{11} \text{ in the hard direction}$$

and $$\chi = \frac{M_s}{H_{11} + H_k} \quad \text{for } H_{11} \text{ in the easy direction.}$$

The two curves are thus congruent but displaced by an amount $2H_k$ along the H_{11} axis. The reason for this is that χ is proportional to $\frac{d^2E}{d\theta^2}$, and for any particular quadrant of the critical switching astroid introduced by Stoner and Wohlfarth, $\frac{d^2E}{d\theta^2}$ has the same value for $H_{11} = H_o - H_k$ along the easy axis as for $H_{11} = H_o + H_k$ along the hard axis. The actual value of the susceptibility measured is affected by the ripple in exactly the same way as for the loop plotter. However, the value of H_k measured is not affected because the ripple will have the same effect on the M rotation whether in the hard or the easy direction. This assumes that the orientation of stray anisotropies which cause the

ripple are distributed in a manner that causes symmetrical ripple along the easy and hard axes for the same value of $\frac{d^2E}{d\theta^2}$. Subject to this assumption, which for crystallographically symmetrical films seems to hold, the susceptibility method is a "reliable" method for H_K measurement in that it is unaffected by the ripple. On the other hand, for high $\frac{H_c}{H_K}$ ratio films, the absolute value of χ falls, so that it becomes difficult to measure the separation of the χ versus H_{11} curves accurately. The method is thus rather inaccurate for such films.

In the method of Chambers, Pomfret and Prutton(C3), the flux detection is performed by making use of the Kerr magneto-optic effect acting on a light beam reflected from the film surface. The modulation of the light beam by the M oscillation is detected by a photoresistor feeding a phase-sensitive detector tuned to the A.C. field frequency, so providing a direct output of the susceptibility as the saturating field is rotated. Thus, a curve of $\frac{d^2E}{d\theta^2}$ against θ can be obtained on an X-Y plotter.

The methods of Kobelev(K3) and of Beam and Siegle(B3) are magnetically very similar in principle. Beam and Siegle's method is particularly convenient to use as their Kerr magneto-optic detection system gives a null output when, according to their analysis, the relationship $MH_{11} = \frac{\partial E_k(\theta,H)}{\partial \theta}$ is satisfied.

H_{11} is the small controllable D.C. field which they use to achieve a zero flux change in their particular configuration. The null output could then be automatically coupled to control the value of H_{11}, and a plot of H_{11} against the orientation of the film sample would give a $\frac{\partial E_K}{\partial \theta}$ versus θ curve. From this, $E_K(\theta)$ and the anisotropy constants could be obtained. This will be discussed in section 3.4.2.

In all susceptibility measurements, the sensitivity falls as the static saturating field increases, e.g., in Beam and Siegle's magnetometer, the sensitivity is proportional to $\frac{1}{H_1^2}$. This therefore limits the saturating field that can be applied. This could have serious consequences, as will be discussed more fully in the analysis of the torque magnetometer below.

Of the various susceptibility methods, those of Prutton, and of Beam and Siegle, because of their automatic plot-out facilities, are capable of dealing with mixed anisotropies. The other methods need rather complicated manipulation to separate various anisotropy contributions of different order.

It seems appropriate to mention here another flux-change method of measuring anisotropy, that of Hagedorn[H1], though this is not a susceptibility method. This method has been called a "pseudo-torque" method by Humphrey[H2], because the observation of flux change is such as to make the measurement very similar to

the measurement of torque.

In his method, a field H_o rotates at a frequency f in the plane of the film. For $H \gtrsim 5\ H_k$, M is also rotated in the film plane at a frequency of f but is modulated at multiples of f by the anisotropy. The signal induced in a balanced pick-up coil at the film is measured with a lock-in detector, enabling voltage measurements at frequency f and its harmonics to be obtained. These are related in a simple way to the coefficients in the expression $E_k(\theta)$, regardless of how complicated $E_k(\theta)$ may be.

There are two limitations to this method. Firstly, the applied orthogonal drive fields used to produce H_o must have extremely low harmonic content - a criterion not easy to achieve with commercially available power amplifiers - if the higher order anisotropies are to be accurately measured; and secondly, Hagedorn's analysis shows the sensitivity to be inversely proportional to H_o, so that measurements in very high fields are difficult.

The complementary method to that of Hagedorn, i.e., detecting flux changes whilst the sample is rapidly rotated in a static field, has been described by Flanders[F4] recently. Its biggest disadvantage is that the sensitivity falls as $\frac{1}{H}$, where H is the applied field. The fact that it involves mechanically moving parts, when compared with purely electronic flux-change measurements as described above, also gives it some of the disadvantages of

standard torque magnetometers.

3.3. Ferromagnetic Resonance. (Soohoo(S5), pp. 187-196)

The resonance condition for a thin film sample depends on the direction of application of the static field. For a field applied in the plane of the film, the resonance condition can only be worked out analytically for H in the easy or hard directions:

$$\omega_{11} = \gamma \sqrt{4\pi M(H \pm H_k)}$$

Thus, in principle, if the separation of the absorption lines is measured, $2H_k$ can be found since the other constants are known independently. In practice, a resonance measurement is also performed with the field perpendicular to the film plane, when the resonance condition becomes:

$$\omega_{\perp} = \gamma (H_{\perp} - 4\pi M)$$

H_k can then be found without assuming values of M and γ.

In assessing this method for the current project, the considerable expense of a U.H.F. bridge or a microwave spectrometer, as well as the lack of experience in resonance techniques made the method unsuitable even before its merits could be considered. That aside, there are, in fact, two important drawbacks to resonance measurements. In the first place, the analysis of mixed

anisotropies becomes difficult. Secondly, being a dynamic method, it would be quite conceivable that the anisotropy constants, when measured dynamically would produce quite different results from when performed quasi-statically. This is because the latter are performed isothermally under conditions of constant stress whilst the former are adiabatic measurements under effectively constant strain conditions[A3]. A detailed examination by Birss and Wallis[B3] of some data obtained by different workers using different methods for K_2 of nickel has not fully borneout this premise. The latest anisotropy work on nickel[A4], which represents the most rigorous torque measurement work yet performed, does however conclude that there is a distinct difference between the results of static and dynamic measurements.

The effects of ripple on resonance measurements is another quite unknown factor weighing against this method.

3.4. Torque Measurements.

The method of torque magnetometry may be applied directly to the measurement of anisotropy in films. The only drawback is the high mechanical sensitivity required because of the low values of torque produced. In all the other respects mentioned above,

the torque magnetometer is satisfactory in operation. Thus, it can handle samples with mixed anisotropies without any change in operating mode, and the separation of these components is a fairly routine operation. It also operates best at high fields, where the single domain theory is definitely valid since the ripple amplitude is then very small. Indeed, it is this aspect which gives it its unquestionable superiority over all the other methods. For this reason, the torque magnetometer method was selected for the anisotropy measurements on the films to be produced.

This method is, therefore, now discussed in more detail.

3.4.1. Theory of Torque Measurements.

The torque acting on the $\underline{M}$-vector of a ferromagnetic sample in an applied field $\underline{H}$ is given by:

$$\underline{L} = \underline{M} \times \underline{H} \qquad (1)$$

If the sample is mechanically constrained, then $\underline{M}$ will swing from the easy direction in which it lay before application of $\underline{H}$, to a position somewhere between it and $\underline{H}$. This equilibrium position of $\underline{M}$ will be attained when the torque given by equation (1) is exactly counterbalanced by the torque due to the anisotropy "spring". It is this anisotropy "spring" which transfers the magnetic torque on $\underline{M}$ into a mechanical torque acting on the sample.

To be able to utilise this phenomenon, it is necessary to determine the exact relationship between the anisotropy energy and the torque $\underline{L}$. The following treatment follows that of Kouvel and Graham[K4].

Let the total energy per unit volume be:

$$E = E_H + E_K \tag{2}$$

where E_H and E_K are the magnetostatic and anisotropy energies respectively, both taken per unit volume. At equilibrium, E must be minimal, i.e.:

$$\frac{\partial E}{\partial \theta} = 0 \ , \quad \frac{\partial^2 E}{\partial \theta^2} > 0 \ , \tag{3}$$

where θ is the angle between $\underline{M}_S$ and an easy direction, as shown in Fig. 3.2. $\underline{M}_S$, the saturation magnetisation, is defined as the

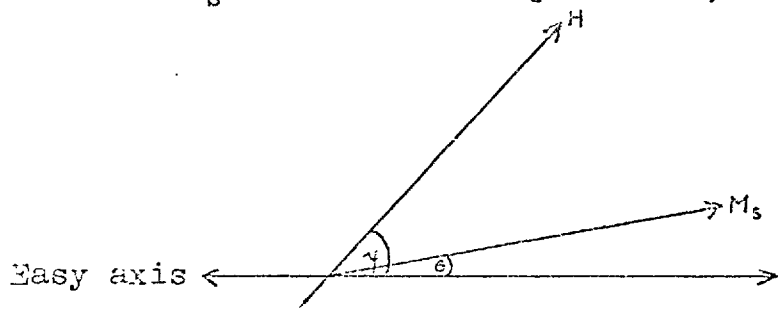

Fig. 3.2.

magnetic moment per unit volume at infinite field, and this implies perfect technical saturation, i.e., that the field $\underline{H}$ is large enough to make $\underline{M}$ at any point in the sample parallel to $\underline{H}$ at any other point.

In general, referring to Fig. 3.2.,

$$E = E(\theta, \psi) = E_K(\theta) + E_H(\psi - \theta) \tag{4}$$

$\therefore$ At equilibrium, $\frac{\partial E}{\partial \theta} = 0$

$$\therefore \frac{\partial E_H}{\partial \theta} + \frac{\partial E_K}{\partial \theta} = 0 \tag{5}$$

Now, the torque per unit volume acting on the magnetisation is, by definition of torque:

$$L = -\frac{dE}{d\psi} \tag{6}$$

where ψ, as shown in Fig. 3.2., is measured for convenience from the easy axis. Since the E_K part of E is not an explicit function of ψ, (6) can be written:

$$L = -\frac{\partial E_H}{\partial \psi}$$

Adding and subtracting $\frac{\partial E_K}{\partial \theta}$:

$$L = -\frac{\partial E_K}{\partial \theta} - \left(\frac{\partial E_H}{\partial \psi} - \frac{\partial E_K}{\partial \theta}\right) \tag{7}$$

Now, since we have assumed saturation,

$$E_H = -M_S H \cos(\psi - \theta)$$

$\therefore$ From (5), $\frac{\partial E_K}{\partial \theta} = +M_S H \sin(\psi - \theta)$ (8)

But $\frac{\partial E_H}{\partial \psi} = +M_S H \sin(\psi - \theta)$ (9)

$\therefore$ From (8) and (9):

$$\frac{\partial E_H}{\partial \psi} = +\frac{\partial E_K}{\partial \theta}$$

Substituting back into (7), the term in brackets disappears.

$$\therefore \underline{\underline{L = -\frac{\partial E_K}{\partial \theta}}} \tag{10}$$

Experimentally, it is difficult to obtain values of θ since the direction of M_s cannot be directly observed. However, if a very high field is applied, M_s becomes aligned with H so that θ becomes very nearly equal to ψ. ψ can, of course, be measured. Thus, the torque on the sample becomes $-\frac{\partial E_k}{\partial \psi}$ per unit volume.

In practice, the sample is suspended in the high field by a torsion wire, and the torque exerted by the specimen can then be measured by the rotation of the torsion head necessary to bring the sample back to its equilibrium position. The magnetic field is rotated slowly and the torque can then be measured as a function of magnetisation orientation with respect to a reference direction in the sample. From this curve, known as a torque curve, the form of the anisotropy energy, $E_k(\theta)$, and the anisotropy constants, K, can be reproduced.

3.4.2. Torque Curve Analysis.

In order to use the $L = -\frac{\partial E_k}{\partial \theta}$ relationship, the form of $E_k(\theta)$ must now be specified.

A simple case will first be considered to illustrate the way in which the torque curve is used. This will be followed by the more complicated practical cases which require complex analysis to solve.

Consider a cubic single crystal posessing only crystalline anisotropy. For this case:

$$E_k = K_1(\alpha_1^2\alpha_2^2 + \alpha_2^2\alpha_3^2 + \alpha_3^2\alpha_1^2) + K_2\alpha_1^2\alpha_2^2\alpha_3^2 + \ldots \qquad (11)$$

In the (100) plane:

$$\alpha_1 = \cos\theta$$

$$\alpha_2 = \sin\theta$$

$$\alpha_3 = 0$$

$\therefore$ Equation (11) becomes:

$$E_k = K_1 \cos^2\theta \sin^2\theta = \frac{K_1}{4}\sin^2 2\theta$$

$$\therefore L = -\frac{\partial E_k}{\partial \theta} = -\tfrac{1}{2}K_1 \sin 4\theta$$

Thus, the torque curve for a measurement made with $\underline{H}$ always in the (100) plane has a 4θ dependence, with maxima and minima of $\pm \frac{K_1}{2}$. It crosses the zero-torque axis along easy and hard directions as shown in Fig. 3.3. The first order anisotropy constant, K_1, is thus simply obtained.

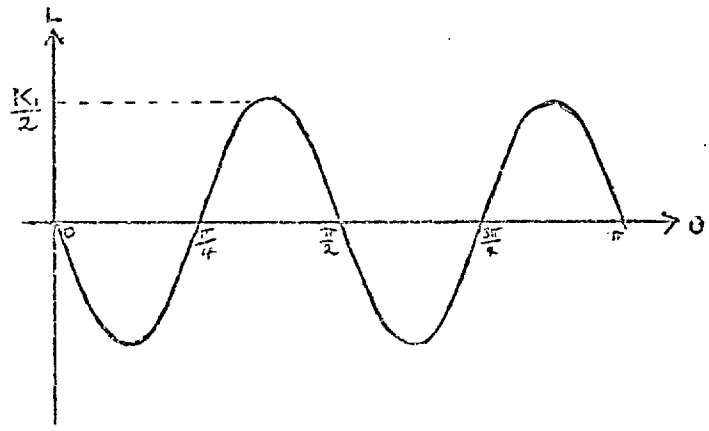

Fig. 3.3.

For the problem in hand, it is necessary to evaluate the torque curves resulting from measurements in the (100) plane of a cubic crystal, with a superimposed uniaxial anisotropy which need not be specifically aligned relative to the crystal axes. The magnetocrystalline anisotropy expression has to be considered up to third order approximation.

$$E_a = K_o + K_u \sin^2(\theta + \phi) + K_1(\alpha_1^2\alpha_2^2 + \alpha_2^2\alpha_3^2 + \alpha_3^2\alpha_1^2) + K_2\alpha_1^2\alpha_2^2\alpha_3^2 + K_3(\alpha_1^4\alpha_2^4 + \alpha_2^4\alpha_3^4 + \alpha_3^4\alpha_1^4) + \ldots\ldots \quad (12)$$

where ϕ is the angle which the uniaxial anisotropy makes with a cube edge. Substituting the values of direction cosines for a (100) plane:

$$\alpha_1 = \cos\theta\,, \quad \alpha_2 = \sin\theta\,, \quad \alpha_3 = 0\,,$$

equation (12) becomes:

$$E_a = K_o + K_u \sin^2(\theta + \phi) + K_1 \sin^2\theta \cos^2\theta + K_3 \sin^4\theta \cos^4\theta + \ldots\ldots$$

$$= K_o + K_u \sin^2(\theta + \phi) + \frac{K_1}{4}\sin^2 2\theta + \frac{K_3}{16}\sin^4 2\theta$$

$$\therefore \frac{\partial E_a}{\partial \theta} = 2K_u \cdot \sin(\theta + \phi) \cdot \cos(\theta + \phi) + \frac{K_1}{4} \cdot 2 \sin 2\theta \cdot 2 \cos 2\theta + \frac{K_3}{16} \cdot 4 \sin^3 2\theta \cdot 2 \cos 2\theta$$

which, when simplified algebraically becomes:

$$\frac{\partial E_a}{\partial \theta} = K_u \sin 2(\theta + \phi) + \frac{K_1}{2} \cdot \sin 4\theta + \frac{K_3}{8} \cdot \sin 4\theta - \frac{K_3}{16} \cdot \sin 8\theta + \ldots\ldots$$

$$\therefore L = -\frac{\partial E_a}{\partial \theta} = -K_u \sin 2(\theta + \phi) - \left(\frac{K_1}{2} + \frac{K_3}{8}\right) \cdot \sin 4\theta + \frac{K_3}{16} \cdot \sin 8\theta$$

The torque curve now contains 2θ, 4θ and 8θ components, and in order to separate them to obtain the values of the anisotropy constants, it is necessary to perform a Fourier analysis. Details of the method used for the analysis are given in appendix (1). The result of the analysis is to produce L as a series expansion of sine and cosine terms, thus:

$$L = a_o + a_1 \cos 2\theta + a_2 \cos 4\theta + \ldots\ldots + b_1 \sin 2\theta + b_2 \sin 4\theta + \ldots\ldots \quad (13)$$

Now, the expression obtained for E_a which must be compared with the above L expression is in the form:

$$E_a = a_o + A \sin 2(\theta + \alpha) + B \sin 4(\theta + \beta) + C \sin 8(\theta + \beta) + \ldots\ldots \quad (14)$$

since it is not known what relation the arbitrary origin of θ for the analysis bears to the crystal axes. The angle between these two "zeros" of θ is set as β, in which case $\phi = \beta - \alpha$.

A is here equal to $-K_u$

B is here equal to $-\left(\frac{K_1}{2} + \frac{K_3}{8}\right)$

C is here equal to $+\frac{K_3}{16}$

Equation (14) is expanded thus:

$$\begin{aligned} E_a = a_0 &+ A \sin 2\alpha . \cos 2\theta + A \cos 2\alpha . \sin 2\theta \\ &+ B \sin 4\beta . \cos 4\theta + B \cos 4\beta . \sin 4\theta \\ &+ C \sin 8\beta . \cos 8\theta + C \cos 8\beta . \sin 8\theta \\ &+ \ldots\ldots \end{aligned} \qquad (15)$$

Comparing coefficients of cos 2θ, sin 2θ, cos 4θ, sin 4θ, etc. in (15) and (13):

$$\left.\begin{aligned} a_1 &= A \sin 2\alpha \\ b_1 &= A \cos 2\alpha \end{aligned}\right\} \quad \text{whence} \quad A = \sqrt{a_1^2 + b_1^2}$$

and

$$\alpha = \tfrac{1}{2} \tan^{-1}\left(\frac{a_1}{b_1}\right)$$

Similarly:

$$\left.\begin{aligned} a_2 &= B \sin 4\beta \\ b_2 &= B \cos 4\beta \end{aligned}\right\} \quad \text{whence} \quad B = \sqrt{a_2^2 + b_2^2}$$

and

$$\beta = \tfrac{1}{4} \tan^{-1}\left(\frac{a_2}{b_2}\right)$$

and

$$C = \sqrt{a_4^2 + b_4^2} \quad \text{with} \quad \beta = \tfrac{1}{8} \tan^{-1}\left(\frac{a_4}{b_4}\right)$$

and so on.

Hence, the values of K_u, K_1, K_3 and ϕ may be obtained from the analysis. When the angular origin for the analysis is not known relative to the $\theta = 0$ position of the anisotropy function,

this method of utilising the data is rather simpler than that proposed by Sato and Chandrasekhar[S3]. They performed the Fourier analysis many times on each curve, moving the origin of analysis every time and assuming that $\beta = 0$ always. They then plotted the coefficient of the term they were extracting against the origin taken for each analysis. The maximum value of coefficient from the curve thus obtained was the true coefficient required. At this position, the origin of analysis and the origin of the torque relationship were concurrent. One of the advantages which such a method brings is a reduction in the errors inherent in performing a Fourier analysis using only a fininte number of terms, since the analysis is done several times using a different set of data point on each occasion. This advantage is incorporated to the same effect in the analysis method used in this experiment, as explained in the appendix.

Unless proper precautions are taken, there are two limitations to the torque magnetometer method, one of an experimental nature, and the other theoretical. These will now be discussed in turn.

3.4.3. The Stability Condition for Torque Curve Measurements.

It was first pointed out by Webster[W3], that a magneto-torsional system consisting of a non-linear deflecting couple - such as the anisotropy torque - opposed by a linear restoring

couple - such as the suspension wire in the simple torque magnetometer - will be unstable in some configurations unless the restoring couple has sufficient stiffness. The treatment outlined here is due to Harrison[H3].

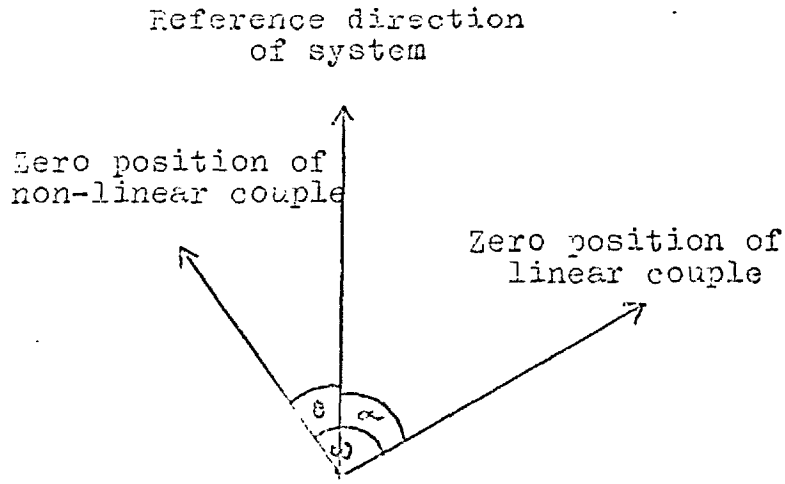

Fig. 3.4.

The instability can arise if the non-linear deflecting couple, expressed as a function of the angle of deflection, posesses a maximum at some point, which is so for anisotropy torque. It then becomes possible for an increase in the angle of deflection from certain equilibrium positions just below that maximum to produce a decrease in the deflecting couple which is larger than the decrease provided by the linear restoring couple in moving through a similar deflection. At this point, the anisotropy torque "takes control", so to speak, of the suspension system and "runs away" with it, causing the instability. The restoring

couple only "catches up" the anisotropy torque when the torque curve approaches a minimum value. Of course, if the linear restoring couple per unit deflection is sufficiently large, it will always "keep control" of the suspension system, and will not allow the anisotropy torque to take over, regardless of its rate of change with angle.

The stability condition is determined by minimising the total energy of the system.

Referring to Fig. 3.4 the work done against the anistropy torque in producing the deflection θ is given by:

$$E_k(\theta) = V\int_0^{\theta} -L(\theta) \cdot d\theta$$

where V is the volume of sample and $L(\theta)$ is the torque curve function. That done against the suspension wire is:

$$\int_0^{\alpha} k\alpha \cdot d\alpha = \tfrac{1}{2}k\alpha^2$$

where k is the torsional constant of the suspension. The total energy is then:

$$\begin{aligned} E_T &= E(\theta) + \tfrac{1}{2}k\alpha^2 \\ &= E(\theta) + \tfrac{1}{2}k(\omega - \theta)^2 \end{aligned}$$

For a specific equilibrium setting, i.e., ω fixed, the equilibrium is stable if $\frac{dE_T}{d\theta} = 0$ and $\frac{d^2E_T}{d\theta^2}$ is greater than 0.

$$\frac{dE_T}{d\theta} = \frac{dE(\theta)}{d\theta} - k(\omega - \theta), \quad = 0$$

$$\frac{d^2E_T}{d\theta^2} = \frac{d^2E(\theta)}{d\theta^2} + k, \quad > 0$$

or, since $E(\theta) = V\int_0^{\theta} -L(\theta)d\theta$, $-V \cdot \frac{dL(\theta)}{d\theta} + k > 0$,

$$\text{i.e.,} \quad k > V \cdot \frac{dL(\theta)}{d\theta} ,$$

$$\text{i.e.,} \quad \frac{k}{V} > \frac{dL(\theta)}{d\theta} \tag{16}$$

Thus, for the measurement to be performed under stable conditions, k must be chosen so that $\frac{k}{V}$ is greater than the maximum positive slope of the torque curve.

It is interesting to note the limitation set on angular deflection of the suspension system as a result of this analysis. If $L_{max.}$ is the maximum torque in the $L(\theta)$ expression to be plotted, then $k\theta_{max.} = L_{max.}V$. For stability, k must be greater than $V(\frac{dL}{d\theta})_{max.}$

At the maximum torque point, therefore,

$$\frac{L_{max.}\,V}{\theta_{max.}} > V(\frac{dL}{d\theta})_{max.}$$

$$\text{i.e.,} \quad \theta_{max.} < \frac{L_{max.}}{(\frac{dL}{d\theta})_{max}}$$

This implies that the angular sensitivity of the torque magnetometer cannot be increased simply by increasing the volume of specimen used.

The value of $\theta_{max.}$ is now evaluated for the (100) plane torque curve in a cubic crystal. For this case,

$$L(\theta) = -\tfrac{1}{2}K_1 \sin 4\theta$$

$$\therefore \quad \frac{dL}{d\theta} = -2K_1 \cos 4\theta$$

$$\therefore \quad L_{max} = +\frac{K_1}{2}$$

$$\text{and} \quad \left(\frac{dL}{d\theta}\right)_{max} = 2K_1$$

$$\therefore \quad \theta_{max} < \frac{\frac{K_1}{2}}{2K_1} \qquad (17)$$

i.e., less than $\frac{1}{4}$ radian.

Thus, for a pure (100) cubic anisotropy, if the maximum deflection from the zero position is greater than about 14°, the torque measurement will go unstable on the steepest positive parts of the curve.

The consequences of this are discussed further in section 4.2. where the experimental aspects of the torque magnetometer are treated.

3.4.4. The Field Dependence of Torque Curve Measurements.

In the derivation of the relationship between torque and anisotropy energy, (Equation (10)), it has been assumed that the saturation magnetisation $\underline{M}_s$ is defined as the magnetic moment per unit volume at infinite field, under which condition, $\underline{M}$ at any point in the sample is parallel to $\underline{M}$ at any other point in the sample. In fact, even for perfect samples, this condition is more rigorous than is necessary in theory, since all that is required is that the sample is in a single domain state. By the simple domain theory of magnetisation, this occurs for an

applied field of only $M + \frac{2|K_1|}{M}$ for a (100) plane measurement on a cubic crystalline disc, where N is the demagnetising factor of the disc. (Derived from Lawton and Stewart[L1] - footnote (2) of Kouvel and Graham[K4]). The infinite field condition is only specified to ensure single domain conditions in real samples.

Since measurements of torque are never in practice done in infinite fields, it becomes necessary to investigate the effect of the use of finite fields. The results of such an investigation show that there are two quite separate corrections to be applied to the torque curves, and these are now considered, though both are not always necessary in practical cases, as indicated below in section 4.7.

3.4.5. M-Deviation Correction.

Even after the sample has attained a single-domain state so that the $L = -\frac{\partial E_k}{\partial \theta}$ relation applies, experimental arrangements only allow γ and not θ to be measured. Here γ is the angle $\underline{H}$ makes with the sample reference direction, and θ the angle $\underline{M}_s$ makes with the specimen. It therefore becomes necessary to correct for the deviation of $\underline{M}$ from $\underline{H}$. This deviation is very simply stated[B5, B6], since the torque on the sample, $-\underline{M}_s \times \underline{H}$, only exists whilst $\underline{M}_s$ and $\underline{H}$ are non-parallel,

$$\text{i.e.,} \qquad L = -MH \sin\alpha$$

where α is the angle by which M deviates from $\underline{H}$ towards the

nearest easy direction to $\underline{H}$. For small α, therefore, the deviation is proportional to the torque.

$$\alpha = - \frac{L}{MH} \tag{18}$$

This applies regardless of the functional form of L with respect to θ. The actual shape of the torque curve as measured is then simply obtained by replacing θ by $(\theta - \alpha)$ in the expression of $L(\theta)$.

This will now be illustrated by two examples, firstly the pure uniaxial case, and then the mixed uniaxial and biaxial case.

For a uniaxial anisotropy, $E_k = K_u \sin^2\theta$,

$$- L = K_u \sin 2\theta \tag{19}$$

in infinite field. Therefore, the M-deviation angle, α, at lower fields is $- \frac{K_u \sin 2\theta}{MH}$. Therefore, θ in equation (19) must be replaced by $\theta + \frac{K_u \sin 2\theta}{MH}$.

$$\therefore - L = K_u \sin\left(2\theta + \frac{2K_u \sin 2\theta}{MH}\right)$$

$$= K_u \sin 2\theta \cdot \cos \frac{2K_u \sin 2\theta}{MH} + K_u \cos 2\theta \cdot \sin \frac{2K_u \sin 2\theta}{MH} \tag{20}$$

It is now assumed that $\frac{K_u}{MH} \ll 1$. This assumption is implicit in equation (19) above, and must be so if the sample is even only a little way above the single domain state, where $\frac{K}{MH}$ is

about $\frac{1}{2}$ depending on the demagnetising factor of the sample. The sine and cosine expressions involving $\frac{K_u}{MH}$ in equation (20) can then be expanded to give:

$$-L = K_u \sin 2\theta \left[1 - \frac{2K_u^2}{M^2H^2} \sin^2 2\theta\right] + \frac{2K_u^2}{MH} \cos 2\theta \cdot \sin 2\theta$$

$$= K_u \sin 2\theta + \frac{K_u^2}{MH} \sin 4\theta \qquad (21)$$

neglecting the $(\frac{K_u}{MH})^2$ term in $\sin^3 2\theta$ as of second order of $\frac{K}{MH}$ only.

Thus, it is seen that the torque curve now contains a biaxial term $+ \frac{K_u^2}{MH} \sin 4\theta$ because of the lack of complete alignment of $\underline{M}_s$ with $\underline{H}$.

This result is of some importance in the phenomenon known as "torque reversal". This was first observed by Nesbitt, Williams and Bozorth[N1] who found that the fourth order torque of single crystals of Fe_2NiAl decreased and changed sign as the measuring field was increased. This same phenomenon was observed for Alnico 5 by Nesbitt and Williams[N2], and for Co ferrite by Williams, Heidenreich and Nesbitt[W4], the latter associating the phenomenon only with materials which respond to magnetic annealing.

They all explained the biaxial torque by the specific model of uniaxial anisotropy employed to account for the results

obtained. Chikazumi[64] showed thereafter that this result is quite general for any anisotropy mechanism randomly distributed along three orthogonal axes of the sample. He derived an expression for the effective biaxial anisotropy constant then appearing, $\frac{8K_u^2}{3M_sH}$. This had to be added to any cubic crystal anisotropy present, to give the resultant fourth order anisotropy.

Comparing the torque expression derived in equation (21) above with Chikazumi's result for a uniaxial anisotropy along one axis only of the crystal (equation (3) in his paper), there appears to be a discrepancy of a factor of 2. From Chikazumi, $E_x = -M_sH - K_u\beta_1^2 - \frac{4K_u^2}{M_sH}(\beta_1^2\beta_2^2 + \beta_1^2\beta_3^2)$ where β is the applied field direction. Putting $\beta_1 = \sin\theta$, $\beta_2 = \cos\theta$, $\beta_3 = 0$ for a (100) plane measurement, and differentiating to obtain the apparent torque: $-L = K_u \sin 2\theta + \frac{2K_u^2}{MH}\sin 4\theta$. The reason for this discrepancy is that his energy expression, E_x, is expressed in terms of the β's, the field direction, whilst to obtain the torque, the differential of E with respect to the α's, i.e., the M direction has to be taken.

Calling $\alpha_1 = \sin\theta'$, $\alpha_2 = \cos\theta'$

and $\beta_1 = \sin\theta$, $\beta_2 = \cos\theta$

where the unprimed θ refer to magnetisation directions, and the

primed quantities, θ^1, to measurement directions; Chikazumi's energy relationship then becomes:

$$E = -K_u \sin^2 \theta^1 - \frac{K_u^2}{MH} \sin^2 2\theta^1$$

$$\text{Now } L = -\frac{\partial E}{\partial \theta} = -\frac{\partial E}{\partial \theta^1} \cdot \frac{\partial \theta^1}{\partial \theta}$$

$$\text{and } \theta = \theta^1 + \frac{K_u}{MH} \sin 2\theta^1 \quad \text{approximately}$$

$$\therefore \frac{\partial \theta}{\partial \theta^1} = 1 + \frac{2K_u}{MH} \cos 2\theta^1$$

$$\therefore -L = \frac{(K_u \sin 2\theta^1 + \frac{2K_u}{MH} \sin 4\theta^1)}{(1 + \frac{2K_u}{MH} \cos 2\theta^1)}$$

$$\approx (K_u \sin 2\theta^1 + \frac{2K_u^2}{MH} \sin 4\theta^1 - \frac{K_u^2}{MH} \sin 4\theta^1 + \ldots\ldots)$$

$$\left(\text{for small } \frac{K}{MH}\right)$$

$$= K_u \sin 2\theta^1 + \frac{K_u^2}{MH} \sin 4\theta^1$$

i.e., exactly as obtained by the calculation here.

It is important to note, however, that it is not correct to say, as Chikazumi does, that the torque reversal occurs at the field given by making the biaxial energy term zero. Torque reversal and energy reversal are <u>not</u> directly equivalent unless both are expressed in terms of magnetisation directions, and

not field directions, simply because $L = -\frac{\partial E}{\partial \theta} \neq -\frac{\partial E}{\partial \theta^1}$.

Test of the Theory.

Some figures are now inserted into the derived expressions for L to test the validity of the result. The results of Nesbitt and Williams[N2] on single crystal samples of Alnico 5 are used for simplicity, since their results showed that Alnico 5 has zero magnetocrystalline anisotropy. Figure 10 of their paper shows the uniaxial anisotropy induced along one [100] axis only by heat treating a (110) disc in a field perpendicular to its face:

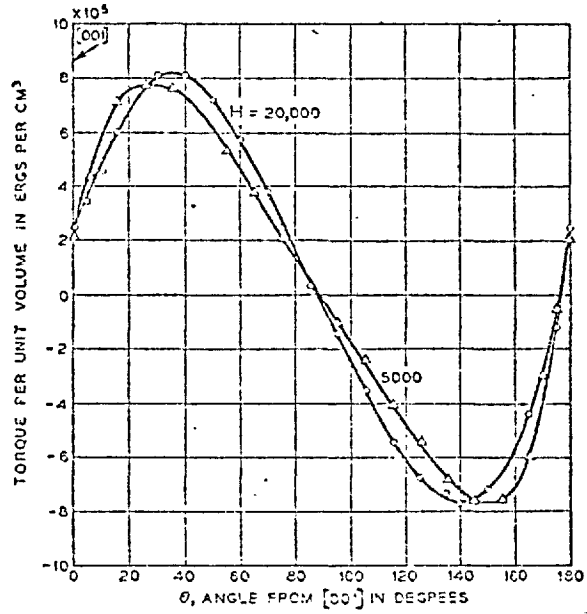

Fourier analysis of their torque curves on an IBM 7094 computer yields the following results:

	Coeff. of 2θ	Coeff. of 4θ
H = 20,000 oe.	$7{\cdot}9 \times 10^5$ erg/cc.	$1{\cdot}1 \times 10^5$ erg/cc.
H = 5,000 oe.	$7{\cdot}4 \times 10^5$ erg/cc.	$2{\cdot}1 \times 10^5$ erg/cc.

Using the accepted value of $4\pi M_s$ of 14,000 gauss for Alnico 5, the coefficient, $\frac{K_u^2}{MH}$, of the 4θ component of L, is found to be $\frac{0{\cdot}72 \times 10^4}{H}$ for $K_u = 8 \times 10^5$ erg/cc. Inserting the values H = 20,000 oe. and H = 5,000 oe., the 4θ coefficients in their Fig. 10 come to $0{\cdot}36 \times 10^5$ erg/cc. and $1{\cdot}44 \times 10^5$ erg/cc. respectively, which are in good agreement with the values obtained from the Fourier analysis if two factors are taken into account:

i) the poor accuracy of the extraction of a small 4θ component from a large 2θ component for the data presented;

ii) that the assumption that there is no crystalline anistropy present in the data of Fig. 10 is valid.

More impressive is the agreement with their results on a (100) disc, also heat treated in a field applied perpendicular to the disc face. In this case, the uniaxial anisotropy is induced equally into both perpendicular [100] directions of the disc. The torque expression becomes:

$$-L = K_u \sin 2\theta + K_u \sin 2(\theta + \tfrac{\pi}{2}) + \frac{K_u^2}{MH} \sin 4\theta + \frac{K_u^2}{MH} \sin 4(\theta + \tfrac{\pi}{2})$$

Expanding, this becomes:

$$-L = \frac{2K_u^2}{MH} \sin 4\theta$$

i.e., the 2θ component is supressed and only the pseudo-4θ component appears in the torque curve. Assuming the same value of K_u as in the (110) disc (and since the magnitude of the K_u induced, ceteris paribus, depends only on the direction of field during heat treatment, which was the same in the two cases), the expected values of the 4θ coefficient of torque, as in Fig. 7 of their paper, can be calculated for the various H.

e.g., At 7,000 oe.,

$$\frac{2K_u^2}{MH} = 2.05 \times 10^5 \text{ erg/cc. compared with}$$

2.25×10^5 from their experimental curves.

Similarly, at 20,000 oe.,

$$\frac{2K_u^2}{MH} = 0.72 \times 10^5 \text{ erg/cc. compared with}$$

0.80×10^5 from their curves.

The theoretical 4θ component versus $\frac{1}{H}$ plot in fact shows a remarkable fit to their experimental curve as shown in Fig. 8, taken from their paper:

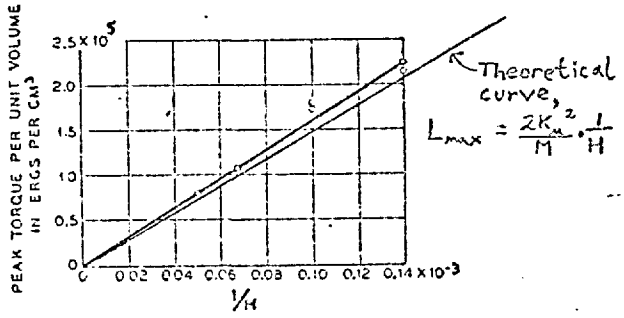

FIG. 8. Peak torque *vs* 1/*H* for Alnico 5 crystal (100) heat treated in a field perpendicular to its face. Maximum value of ordinate scale is 2.5×10^5.

The result derived above in equation (21) thus furnishes a simple explanation for the results of Nesbitt and Williams. The method of derivation shows, however, that this spurious fourth order torque is only a special instance of the higher order torques which always arise when torque measurements are done in "non-infinite" fields. The method of derivation, though less basic than that of Chikazumi, since he deals with energy relationships whilst this method uses the torque relationships as starting point, is more easily applied to practical cases in torque magnetometry. It enables the higher order components to be evaluated analytically for any conceivable case of anisotropy.

To illustrate this, the second example - of mixed uniaxial and biaxial anisotropies is evaluated in appendix A.2. The treatment is rather more complicated algebraically, but is performed in an exactly analogous manner. The result obtained for the torque is:

$$-L = K_u \sin 2\theta + \frac{K_1}{2} \sin 4\theta - \frac{K_u K_1}{2MH} \sin 2\theta + \frac{K_u^2}{MH} \sin 4\theta + \frac{3K_u K_1}{2MH} \cos 6\theta + \frac{K_1^2}{2MH} \sin 8\theta \qquad (22)$$

where the first two terms represent the normal expression. As expected, extra terms in sin 4θ and sin 8θ arise from the original sin 2θ and sin 4θ terms, but the new feature of this mixed

anisotropy case is the appearance of cross product $(\frac{K_u K_1}{MH})$ cosine terms of order 2θ and 6θ. The latter is of particular interest since the normal anisotropy expression for a (100) plane measurement of a cubic crystal specifically excludes a 6θ term, $K_2 \alpha_1^2 \alpha_2^2 \alpha_3^2$ being the only term in E_k which could give a 6θ term to L (θ) , and one of the direction cosines always being zero in a (100) plane. The significance of these additional terms will be further discussed in the experimental results section below.

The torque reversal found by Nesbitt et al.(N1) and by Williams et al.(W4) is now simply explained by the $\frac{K_u^2}{MH}$ sin 4θ term of equation (22) being added to the $\frac{K_1}{2}$ sin 4θ term of the same equation, the actual field at reversal being where:

$$\frac{K_u^2}{MH} + \frac{K_1}{2} = 0$$

$$\text{i.e.,} \qquad H = -\frac{2K_u^2}{MK_1}$$

In practice, the constants of the expression (22) only apply if K_u is aligned along a [100] direction. If this is not so, the anisotropy expression:

$$E_k = K_u \sin^2(\theta + \phi) + K_1 \sin^2\theta \cos^2\theta$$

must be used where ϕ is the misalignment of K_u from the cube edge. This leads to amendments of some of the coefficients by

factors of sin ϕ and cos ϕ, and also to extra terms in for instance cos 4θ. The form of the result is not, however, radically changed.

3.4.6. The H-Dependence of K Correction.

Even if the M-deviation correction is applied, it has been experimentally found that the coefficients obtained from torque curves are field dependent and grow with increase of measuring field. For this reason, the practice was initiated (first by Schlechtweg[S4] in 1936) of measuring the anisotropy constants at several increasing fields, and plotting the curve of apparent anisotropy constant against $\frac{1}{H}$. This usually gave a straight line, whose extrapolation to $\frac{1}{H} = 0$, i.e., $H = \infty$ was supposed to give the true anisotropy constant. (See Bozorth[B1], p. 566).

Tarasov[T2] was the first to suggest a mechanism for this, in that the discs used for the measurements were not completely saturated, reverse domains existing at the edges to very high field values. This he deduced from the fact that the constant "a" in his empirically-found expression:

$$K_{1_{measured}} = K_{1_{true}} \left(1 - \frac{a}{H}\right)$$

decreased with decreasing thickness - to - diameter ratio of his specimens of iron-silicon. The maximum fields he used were 3·5 kOe.

The experiments of Tarasov were repeated by Kouvel and Graham[K4] up to 20 kOe., and they found that their data fitted a relationship of the form:

$$K_{1_{measured}} = K_{1_{true}} \left(1 - \frac{c}{\sqrt{H}}\right)$$

first proposed by Langford[L2]. This again they ascribed to a small variation of M with θ arising from a reverse domain structure persisting to fields well above the theoretical saturation limit.

That both these empirically discovered relationships of K with field were not the full story was first proposed by Veerman, Franse and Rathenau[V1]. Their experiments, which were performed on nickel spheres, showed a steady linear increase of the apparent anisotropy constant with field, by about ½% per kOe. from fields of about 8 kOe. to 33 kOe. Below 8 kOe, the increase was rather steeper, and this they attributed to the lack of technical saturation which the previous workers had found. They therefore concluded that the magnetocrystalline anisotropy "constants" were not constants at all, but were a function of the applied field H. They suggested that the functional relationship arose because K_1 could be completely described as a function of M, which itself is a function of H and T, the temperature. This result was also connected by

them with the well-known anisotropy of M, introduced by Callen and Callen[C5].

Recent results of Flanders[F4] on (100) discs of nickel have shown a much smaller intrinsic field dependence of K_1. Between 2 and 20 kOe., he obtained a value of $\frac{1}{K_1} \cdot \frac{dK_1}{dH}$ of less than 0·04% per kOe., i.e., more than one order of magnitude less than Veerman's result.

The latest series of anisotropy measurements on nickel by Aubert[A4] have taken this approach to the problem to an even finer stage. He has shown the impossibility of making really accurate anisotropy measurements simply by means of extrapolation procedures to infinite field.

3.4.7. Instrumental Sources of Error Torques.

If the applied field is regarded as being homogeneous over the whole of the sample volume, the measurement will be relatively insensitive to small linear displacements of the centre of the specimen from the axis of the torquemeter suspension. For the special case of thin film torque measurements, the measurement will be very sensitive to tilt of the specimen from the horizontal plane of rotation of H. The effective torque due to tilt of the specimen is, therefore, now calculated, by a method due to Leaver[L3].

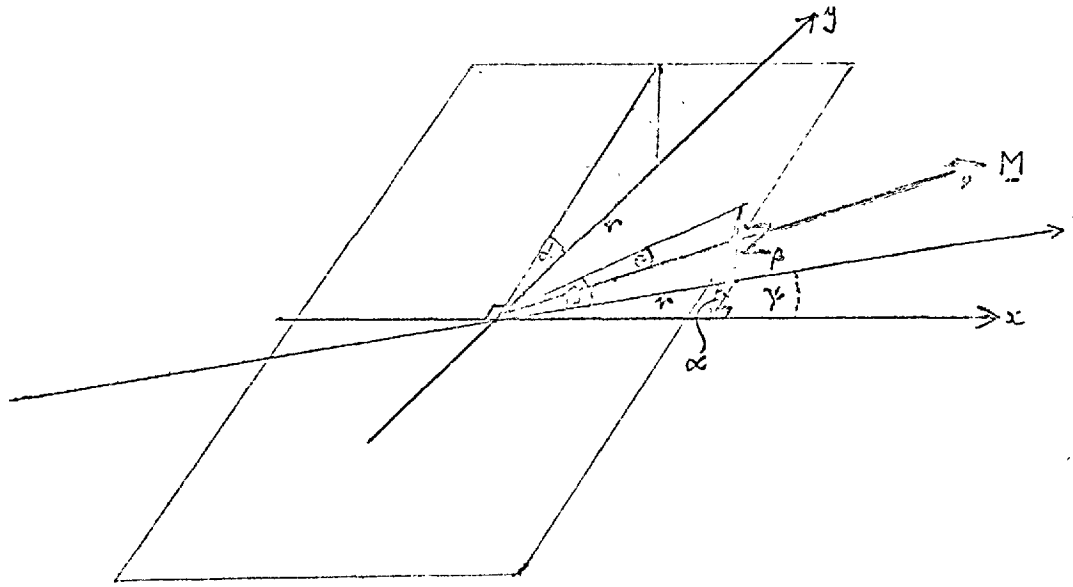

Fig. 3.5.

Referring to Fig. 3.5., let the plane of the film along the y-axis, have an inclination α from the plane of rotation of H. Then the effect of H will be to attempt to pull $\underline{M}$ out of the plane of the film against the torque exerted by the perpendicular anisotropy $K_\perp$ of the film which tries to keep $\underline{M}$ in the film plane. The extent to which $\underline{M}$ lifts from the film plane varies with γ, the angle of application of H, and it is this variation which gives rise to the effective tilt anistropy.

It is first necessary to find how the angle, β, between the component of H in the film plane and the plane of rotation

of H (the x-y plane) varies with γ.

Using the two vertical black shaded triangles with Z_β as their common side:

$$Z_\beta = r \tan\beta$$

and $$Z_\beta = r \sin\gamma . \tan\alpha$$

$$\therefore \quad r \tan\beta = r \sin\gamma . \tan\alpha$$

For small tilt angles, the tan terms may be approximated by the angles.

$$\therefore \quad \beta = \alpha \sin\gamma \tag{23}$$

The extent to which M is pulled down in a vertical plane towards H is given by equalising the torques on M due to i) the film's perpendicular anisotropy and ii) the field H.

$$\therefore \quad MH \sin(\beta - \theta) = K_\perp \sin 2\theta$$

where $K_\perp$ is the perpendicular anisotropy constant, and equals $2\pi M^2$ for a stress-free polycrystalline film, or $2\pi M^2 + K_1$ for a (100) plane cubic single crystal film.

Therefore for small tilt angles,

$$MH(\beta - \theta) = 2K_\perp \theta$$

$$\text{i.e., } \theta = \frac{\beta}{1 + \frac{2K_\perp}{MH}} \tag{24}$$

The additional energy given the film by the M tilt is therefore the sum of the magnetostatic and perpendicular anisotropy terms:

$$E = K_\perp \sin^2\theta - MH \cos(\beta - \theta)$$

which, for small tilt angles becomes:

$$E = K_\perp \theta^2 - MH\left[1 - \frac{(\beta-\theta)^2}{2}\right]$$

Substituting for θ and $(\beta-\theta)$ from (24),

$$E = K_\perp\left(\frac{\beta^2}{1+\frac{2K_\perp}{MH}}\right) + \frac{MH}{2}\cdot\frac{4K_\perp^2}{M^2H^2}\cdot\frac{\beta^2}{\left(1+\frac{2K_\perp}{MH}\right)^2} - MH$$

Using equation (23) to eliminate β:

$$E = \frac{K_\perp \alpha^2}{\left(1+\frac{2K_\perp}{MH}\right)^2}\sin^2\gamma + \frac{2K_\perp^2\alpha^2}{MH\left(1+\frac{2K_\perp}{MH}\right)^2}\sin^2\gamma - MH$$

The first two terms represent a uniaxial anisotropy as γ is varied, i.e., as H is rotated. The effective anisotropy constant is:

$$K_{eff.} = \frac{K_\perp\alpha^2}{\left(1+\frac{2K_\perp}{MH}\right)^2} + \frac{2K_\perp^2\alpha^2}{MH\left(1+\frac{2K_\perp}{MH}\right)^2}$$

$$= \frac{K_\perp\alpha^2}{\left(1+\frac{2K_\perp}{MH}\right)^2}\cdot\left(1+\frac{2K_\perp}{MH}\right)$$

$$= \frac{K_\perp\alpha^2}{\left(1+\frac{2K_\perp}{MH}\right)} \qquad (25)$$

The effect of this anisotropy on the torque curves and the precautions thereby needed are discussed in the experimental section.

CHAPTER 4.

The Torque Magnetometer - Design Considerations and Performance.

4.1. Introduction.

When considering what sort of design to use for the torque magnetometer, three factors had to be taken into account initially:

a) It would be useful to have an instrument which could produce torque curves in a minimum of time, firstly to minimise the problem of maintaining a constant temperature at the sample - the anisotropy constants being very strongly dependent on temperature - and secondly so that curves could be rapidly plotted at several fields on the same sample, in order to perform the infinite field extrapolation procedure.

b) The instrument should have an accuracy which is a minimal function of operator skill and fatigue.

c) It should most desirably be capable of taking samples of widely different thicknesses and composition without loss of sensitivity, in order to be of most universal application in the laboratory.

For these reasons, work was initially commenced on an automatic recording magnetometer. In this sort of instrument, a restoring couple equal and opposite to the torque being measured is applied to the sample by an electrostatic or

electromagnetic torque generator. The null position is detected by a beam of light shining on a split photocell, whose output is amplified by a high-gain servo-amplifier, and then applied to the torque generator. This output signal, proportional to the measured torque, can then be used, together with a signal proportional to the magnet rotational angle, to provide an automatic plot-out of the complete torque curve. Thus, the first two requirements above are fulfilled, but more important is the way in which is the third. Since the "stiffness" of the suspension is dependent on the feedback characteristics of the amplifier, it can be made as high as is desired. The limit is set by the necessity of having a tiny sample deflection to maintain the off-balancing current from the photocells. The stability requirement considered in section 3.4.3. then becomes quite trivial, for the suspension can be made effectively almost infinitely stiff, thus maintaining stability for large torques. Also, since the feedback can be simply changed by means of switching in or out resistors, it is possible to maintain full sensitivity of the instrument over a large range of torques. This advantage of the automatic force-balancing mode of operating a torque magnetometer is not always fully appreciated.

Unfortunately, the particular design chosen, that of Humphrey and Johnston[H4], proved to be a little overambitious

for the constructional facilities available for the project, and when it had become imperative to commence magnetic measurements, the electromagnetic torque-balancing unit was still not successfully operational. The instrument therefore had to be passed over for use in this experimental programme.

It was, therefore, decided to construct a classical type of magnetometer in the minimum amount of time, but nevertheless, some interesting features were incorporated to facilitate the taking of measurements. The system is shown in Fig. 4.1.

4.2. Suspension System.

As regards the stiffness of the suspension wire, a criterion for the range of films to be measured had to be adopted to enable only one suspension to be used. This saved having to change suspension from film to film. In the first place, only nickel films were to be measured, thereby restricting any variation in the order of magnitude of torque per unit volume from film to film. Secondly, it was decided to try to make all measurements on films of similar thickness and area and an arbitrary 1000Å thickness and 1 cm. diameter were selected as standard. This was regarded as being a good compromise between a sufficiently thick film to:

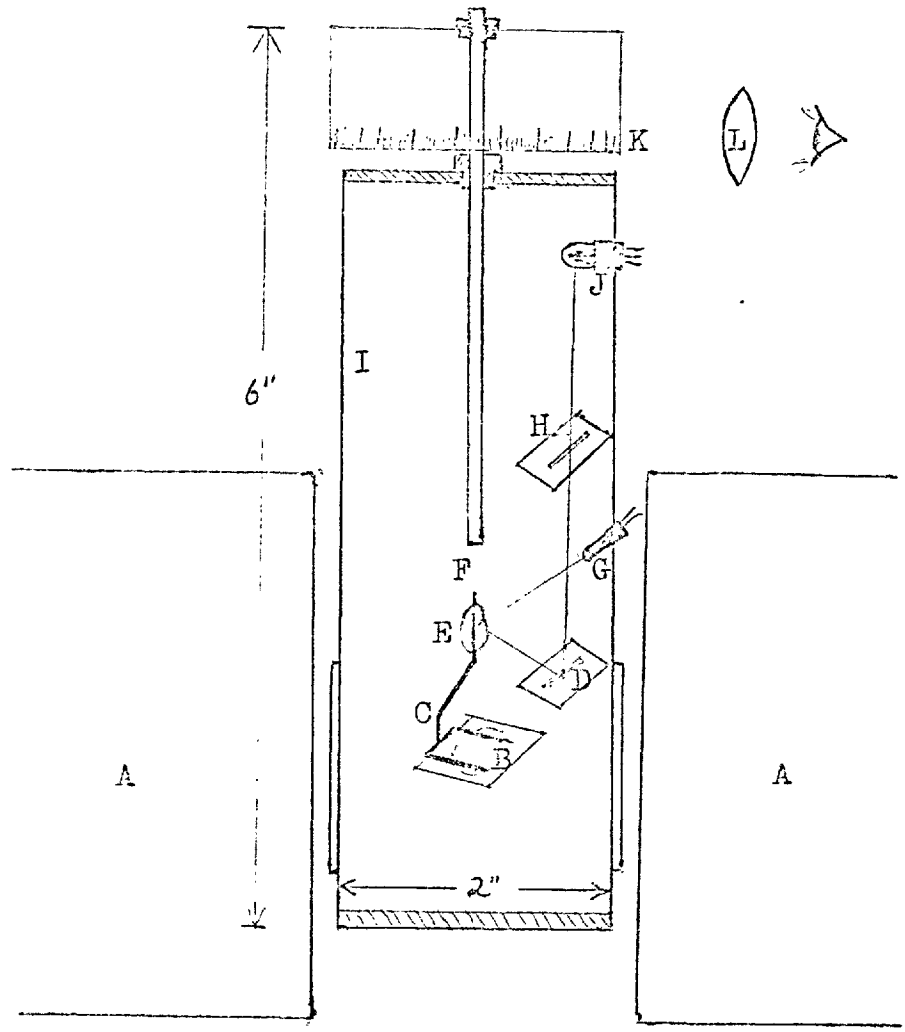

Key.

A	Pole pieces.	G	Microlamp.
B	Sample.	H	Defining slit.
C	Quartz sample holder.	I	Perspex tube.
D	Slit shaped mirror.	J	OCP71 photo-transistor.
E	Mirror.	K	Torsion head scale.
F	Torsion fibre.	L	Lens.

Fig. 4.1.(a). Torque Magnetometer.

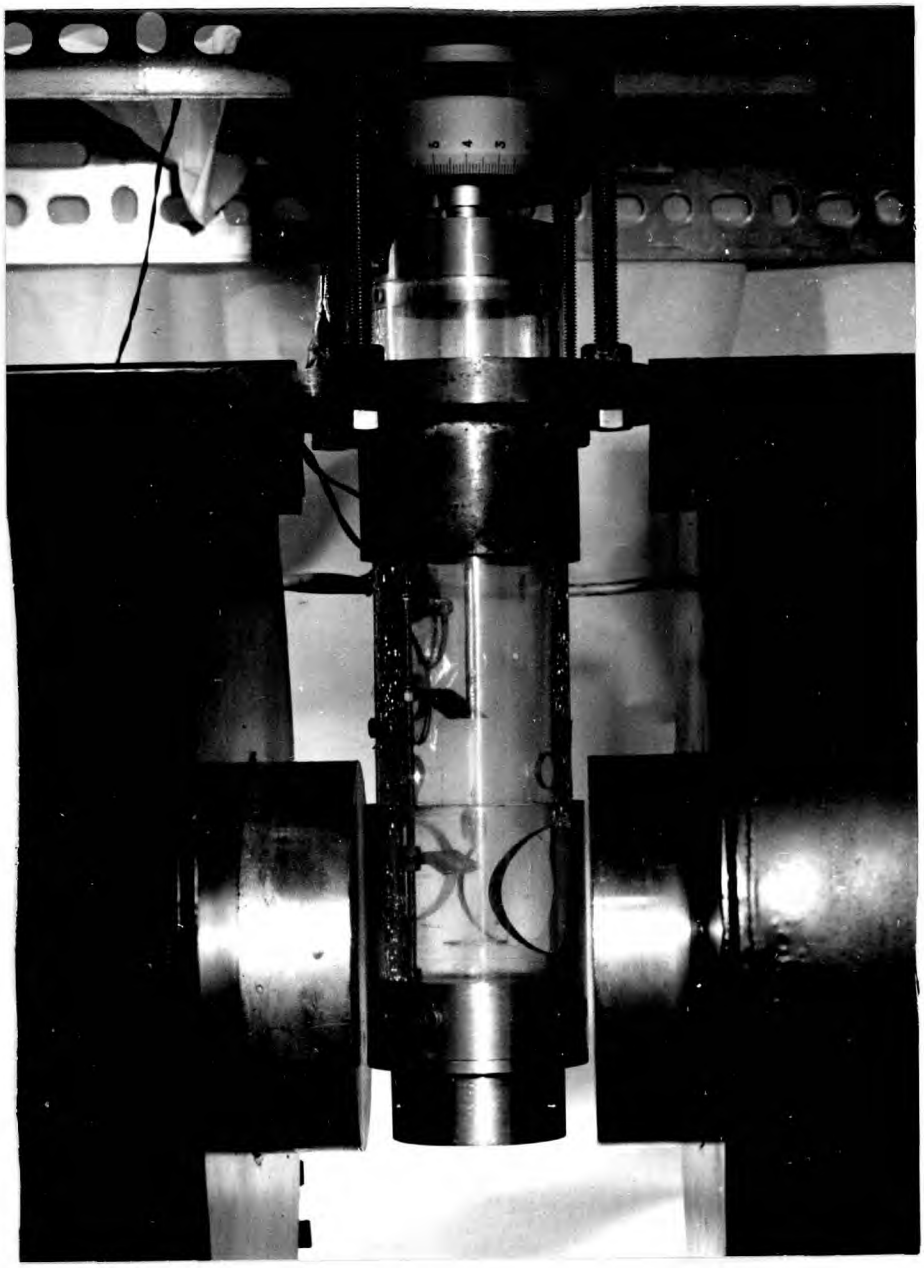

Fig. 4.1.(a) Torque magnetometer.

a) reduce the relative effects of surface oxidation, and

b) increase the volume of magnetic material on which to make measurements; and a film not so thick as either to:

a) make electron microscopy investigations difficult, or

b) risk the magnetisation lifting from the plane of the film.

It was expected that a thickness of 1000Å could be easily achieved to within ± 200Å. The maximum torque then expected would therefore come from a 1200Å biaxial film attached to its substrate, with a maximum of internal stress. This would set an upper limit to the torque to be measured with that suspension. The lowest torque expected would then be from a stress-free biaxial film of about 800Å. Since the effect of the maximum expected intrinsic stress was estimated to produce an increase in effective K_1 of less than 50%, the result of this thickness limitation was to produce a range of torques differing from film to film at most by a factor of 2. If the shapes of the torque curves are now regarded as being pure biaxial to a first approximation, then their maximum positive slopes, which is the quantity which determines their stability for a specific suspension, can be regarded as being proportional to their torque maxima. Thus, if a suspension constant was chosen stiff enough just to keep the largest amplitude torque curve from going unstable, the sensitivity of this suspension would only

be reduced by one half for the smallest amplitude torque curves to be dealt with. An estimate of the torsional constant required was therefore made:

Maximum effective K_1 for stressed film of nickel

$$\approx 7{\cdot}5 \times 10^4 \text{ erg/cc.}$$

From equation (17) in section 3.4.3.,

$$\left(\frac{dL}{d\theta}\right)_{max} = 2K_{1_{eff.}} \approx 1{\cdot}5 \times 10^5 \text{ erg/cc.}$$

Maximum film thickness $\approx$ 1200Å

$\therefore$ Maximum volume V $\approx \pi \times (0{\cdot}5)^2 \times 1200 \times 10^{-8}$ cc.

$$\approx 10^{-5} \text{ cc.}$$

$\therefore$ From equation (16), maximum torsional constant

$$k = V \left(\frac{dL}{d\theta}\right)_{max} \approx 1{\cdot}5 \times 10^5 \times 10^{-5} \text{ dyne.cm./rad.}$$

$$\approx 1{\cdot}5 \text{ dyne.cm./rad.}$$

Having obtained this critical value of torsional constant required for the suspension, there was a choice of several materials and even several sizes of the same material. The deciding factor was a consideration of what would be the most desirable length of suspension to use. For that particular length selected, the cross-section of the material had to be sufficiently large for it to withstand the inevitable rigours of loading and unloading specimens. Now the torsion head would constantly be adjusted by hand during the course of a curve plot,

and this process would inevitably give small mechanical shocks to the suspension, which would then set the sample swinging. It was therefore decided that the suspension length should be chosen to minimise the time taken for these lateral oscillations to die away. Since most of the damping of the suspension would be due to air friction, the higher the frequency of the swing the more rapidly it would die away. The suspension length was therefore chosen to be as short as possible. This criterion also had the advantage of keeping to a minimum any sideways movement of the specimen if the field were at all inhomogeneous. This follows since the work done against gravity in moving the sample sideways, and hence raising it, is directly proportional to the suspension length.

The limit to the minimum length of suspension was set mainly by the ability of the suspension to withstand the weight of the sample and holder, and any mechanical shocks they may be subjected to. A secondary consideration was that the suspension length must be a well defined and unchanging quantity. With extremely short suspensions, the end regions where the wire is attached to the support post and sample holder, and where the restoring couple may not therefore be linear with angle, would constitute too great a percentage of the total suspension length to ensure an accurately linear torsional characteristic. Bearing

these two limitations in mind, a suspension made of 0·0065" x 0·0005" phosphor bronze was selected from the available materials, and a length of about 1·7 cms. gave the required torsional constant. The "breaking stress" of this material was quoted as about 40 gms. wt., which gave a very generous safety margin, the sample and holder being less than 2 gms.

The suspension was calibrated in the following way. Three lengths of $\frac{1}{8}$" brass rod were cut, about $1\frac{1}{2}$ cm., 2 cm. and $2\frac{1}{2}$ cms. respectively, to provide three accurately known moments of inertia. These were placed in turn on the sample holder, and the torsional oscillations of the system were timed. An absolute measure of k was thus possible. (In fact only two test pieces were necessary to eliminate I_o, the moment of inertia of the sample holder, but a third was included to increase the accuracy of the calibration.)

4.3. Optical Detection System.

A compact optical system, with an optical path length of only $4\frac{1}{2}$ inches, driving an OCP 71 photo-transistor was used for detecting the zero-position of the sample. The beam of light was produced by a subminiature bronchoscope lamp* of 1 mm. diameter

---

* Obtained from Rimmer, Bros., 18, Aylesbury Street, E.C.1.

with an integral lens for producing a parallel beam. As shown in Fig. 4.1., the beam was reflected from the mirror mounted on the sample holder, on to a long slit mirror, $\frac{1}{2}$ mm. wide. About $1\frac{1}{2}$" above the mirror was a defining slit also $\frac{1}{2}$ mm. wide and carefully aligned to be exactly parallel to the slit mirror. $1\frac{1}{2}$" above the defining slit and co-linear with mirror and slit was the phototransistor, whose current was monitored on a very fast-response moving coil microammeter. The torsion head was adjusted to give maximum deflection on the meter. In practice, the swinging of the light beam either side of the phototransistor caused regular double-kicks of the meter needle, one as the beam flashed across the detector in one direction, and another when it returned in the other direction. By adjusting the torsion head to produce meter kicks at equal intervals, it was possible to get extremely close to the zero position even before the suspension had come to rest, and in this way a great deal of time was saved. It was found possible to adjust any particular null setting reproducibly to within $\frac{1}{10}$ mm. on the torsion head, the limit being set by the ability to read off or move the torsion head by a smaller increment. This corresponded to an angular deflection of $0{\cdot}15^{\circ}$, or a torque of 4×10^{-3} dyne cm. with the c. 1·5 dyne cm./rad. suspension used for the instrument.

4.4. Spurious Instrumental Torques.

Initially a number of spurious torques caused considerable difficulty. The major component was simple to eliminate, being the background torque arising from the sample holder and mirror. The exact origin was quite unknown, since care had been taken in the construction of the sample holder to use only non-ferromagnetic materials of very high purity:- quartz rod, a piece of quartz cover-slip for the mirror backing, pure evaporated aluminium for the mirror surface, and "durofix" for attaching the mirror to the sample holder itself. This no-sample torque curve remained quite constant in time and so was simply subtracted out of each set of torque figures before plotting. The acceptability of this procedure was checked by turning all films through 90° on the sample holder, and replotting the curve. After subtraction of the no-sample torque, the results always exactly superimposed on the original curve to within the experimental accuracy.

The only other component which gave spurious torques on the curves was far more difficult to find and may never have been discovered had it not been for the accidental failure of the magnet power supply on one occasion whilst the sample holder was resting on its support. It was noticed that, as the field collapsed, the detector current changed, despite the fact that

the sample holder could not have moved. An induction effect was rapidly eliminated as the source of this, and it was discovered that application of the field actually appeared to bend the beam of light! In fact, this effect was traced to the lamp, whose filament was a single loop of tungsten wire driven by a D.C. current. This therefore suffered a translational force in the field. Thus as the field rotated around the sample, the beam of light moved its origin and direction, and so the effective zero-position of the suspension shifted. The solution was simply to drive the lamp filament with an A.C. current so that its mean position remained unaltered with applied field direction. Mains frequency proved useless as the filament vibrated with such an amplitude that it hit the bulb walls and broke. Higher audio and ultrasonic frequencies did not help since although the movement of the filament was no longer visible above a few kc/s, the filaments always suffered some sort of fatigue failure in a very short time. This applied even at 50 kc/s. It was therefore necessary to drive the bulb with an R.F. current, and a 1 Mc/s signal was fed into an R.F. power amplifier to provide sufficient current to light the lamp. It has since functioned for several hundred hours without failure.

4.5. Magnet System and Temperature Control.

A four inch Newport magnet was used to provide the field, with the pole-pieces set at a $2\frac{1}{2}$" gap. This gave a maximum field inhomogeneity of 1% at 5 koe over a 1 cm. cube at the centre of the gap around the sample.

Two major faults in the magnet were discovered, one of which proved to advantageous and the other the opposite. In the first place, the water cooling system for the magnet coils was so poorly designed that even with a flow rate of 1 gallon per minute, at which the temperature rise of the outlet water was less than 1 degree, the cheeks and pole-pieces became almost too hot to touch at full power. At half-power, $7\frac{1}{2}$ A., which gave 5·1 koe, the pole-pieces still reached about 40° C. The magnetometer itself was enclosed in an airtight perspex tube, and the effect of the radiation from the pole-pieces at this current was to raise the temperature of the inside of the tube, and hence of the sample, to a very uniform 31° C, independent of the room temperature around (within reasonable limits of fluctuation). Now, the magnetocrystalline anisotropy constants are extremely fast functions of temperature. The variation with T for K_1 of nickel is theoretically expressed by Carr[C8] as:

$$\frac{K_1(T)}{K_1(0)} = (1 - 1{\cdot}74\,\frac{T}{T_c})(\frac{M}{M_o})^{10}$$

although in practice, a much higher power of $(\frac{M}{M_o})$ is obtained. For this reason, it is essential to have close temperature control of the sample during measurement, and the constant heating effect of the magnet pole-pieces at constant current provided this, without any need for elaborate screening from draughts and temperature fluctuations in the room.

The experimental procedure adopted was to turn on the magnet at least one hour before the measurements were to be commenced to enable the whole magnetometer to reach the equilibrium temperature. The dark current of the phototransistor was used to measure the temperature to within $\frac{1}{2}$ degree C. It was calibrated against a thermocouple in the magnetometer. The dark current at constant voltage, was just under 50μA at a room temperature of 22° C, rising exponentially to just over 360μA at the operating temperature of 31° C. The torque measurement was not commenced until the system had stabilised for some time at its equilibrium temperature.

The other magnet fault lay in the calibration of the turntable. The appearance of unexpectedly large odd Fourier components in the analysis led, after elimination of all other known causes, to the suspicion that the turntable scale was not regularly divided. A check was therefore made, using a travelling microscope, of the angular intervals on the engraved scale, and

it was discovered that there was a random cumulative error in the engraved angular scale which amounted to as much as $0{\cdot}9^{\circ}$ from the true angular position at the worst point. This sort of error probably arose from worn locating pegs on the engraving machine used in the factory. A correction table was drawn up and the true angular position always obtained by reference to it.

4.6. Specimen Tilt.

The specimen holder was so designed as to present a horizontal plane for the sample when it is symmetrically placed relative to the axis of the suspension fibre, and the holder hung from its single support point. This was achieved during construction by tiny manipulations of the angles of the arms of the holder with a micro oxy-hydrogen torch. The holder was hung with a sample in position and slowly rotated by means of the torsion head whilst a beam of light was reflected from the surface of the sample at a glancing angle. From the movements of the reflected light spot, it was estimated that the sample was then well within $\frac{1}{2}^{\circ}$ of the horizontal, the exact angle being difficult to specify more precisely because of the swing of the sample during rotation. During measurements, it was found that because of slight variations in shape of the substrates, in order

to reduce the tilt angle to zero the sample required very small adjustments from the position which put the centre of the film on the axis of suspension. The method used was to observe a reflection in the film at an almost glancing angle as the film was rotated.

Substituting values into equation (25) of section 3.4.7. to obtain some idea of the order of error torque expected:

$$K_\perp \approx 2\pi M^2 + K_1$$

where $2\pi M^2$ is the shape anisotropy and K_1 the magnetocrystalline anisotropy.

Let $\alpha = \frac{1}{2}^o \approx 10^{-2}$ rad.

and $H = 5$ koe $\quad M = 500$ gauss

$\therefore K_\perp = 2\pi . (500)^2 - 5 \times 10^4$ erg/cc.

$\approx 1{\cdot}5 \times 10^6$ erg/cc.

$$\therefore K_{tilt} = \frac{K_\perp \alpha^2}{(1 + \frac{2K_\perp}{MH})}$$

$$\approx 75 \text{ erg/cc.}$$

This represents about $1{\cdot}5 \times 10^{-3}$ of K_1 for Ni , and so will not interfere with the measurements, as such a fraction of K_1 appearing as a uniaxial component could not be detected. It is worth while noting, however, that because of the square-law dependence of K_{tilt} on α, if the tilt were as little as 2^o the uniaxial torque appearing would correspond to an anisotropy

constant of about 1000 ergs/cc. This would be a very serious error in many of the measurements.

4.7. Field Dependence of Measurements.

With the magnetometer (and operator) working well, it was found possible to perform a complete torque curve plot at intervals of 5° over 180° in about 2 hours. Because of the time involved, the question of making several plots at different fields to obtain "infinite-field" corrected values for the K's as discussed above in section 3.4.6. had to be seriously considered.

Since $K_1 \gg K_u$ for all the samples measured, to a first order of approximation the M-direction was determined only by the magnetocrystalline part of the combined anisotropy. It is thus only necessary to consider how close the applied field was to infinite field conditions for K_1 measurements on the samples. The room temperature value of H_{K_1} for nickel comes to about 200 oe. Thus, at the field used, 5·1 koe, the measurements were being done at about 25 H_{K_1}. Therefore, even if the $\frac{1}{\sqrt{H}}$ correction of Kouvel and Graham is used - which gives a severer dependence of K on H than the more usually used $\frac{1}{H}$ correction - and the same value of constant for the slope of their curve is substituted, the present experimental conditions would give a

K value within 7% of K at infinite H. In fact, the situation could well be even better than this, since the thinness of film samples as compared with their discs would make the occurrence of reverse domains at the edges of the sample even less likely to occur. The qualifications of Veerman et al. and of Flanders mentioned above do not affect these conclusions, since according to their work, it is only meaningful to ascribe a specific value to K_1 accurately if the field at which that measurement is made is specified.

The only check that could conveniently be applied with the magnet used with the magnetometer was to increase the field from the 5·1 koe used, to the maximum field possible, 6·7 koe. At that input power, the heating effect from the pole-pieces was so considerable that it was impossible to plot a full torque curve without the temperature of the sample rising appreciably. For this reason, only a rough check on any increase in K_1 was possible from spot torque values taken at the curve peaks. The result showed a negligible increase in the K_1 peaks for the samples used, estimated at 2% $\pm \frac{0}{1}$ %. Though not a very comprehensive test it was sufficient to show that any technical H-dependence of K_1 was complete at 5 koe. Since, in any case, the main feature of the experiment was to extract $\frac{K_u}{K_1}$ ratios, rather than to make accurate K_1 measurements, the use of a fixed

field value as high as 5 koe was thought to be justified without field extrapolation procedures.

4.8. Magnetometer Accuracy.

As mentioned above in section 4.3., the optical null-detection system was found to be capable of resolving an angular position of the sample to within $\pm$ 0·1°, i.e., $\pm$ 0·05 mm. on the torsion head. It should be pointed out, however, that this resolution was only maintained over the steep negative-going slopes of the torque curve where the system sensitivity was high. The reason for this is that on these sections, the composite suspension system - consisting of magnetic and elastic torques - is closest to instability, with the magnetic torque exercising its greatest effect. Thus, only a tiny rotation of the torsion head led to a comparatively large rotation of the sample away from the null position, so giving a high angular sensitivity. On the positive-going slopes, the situation was reversed. The torsion head had to be moved more appreciably to effect a noticeable shift of the sample from the null position. It was thus more realistic to put a resolving limit of $\pm$ 0·1 mm. on the positive-going parts of the curves.

It is thus stated with confidence that the accuracy of

any point on a torque curve as plotted is within $\pm$ 0·1 mm. This represents a torque of $\pm$ 4 x 10^{-3} dyne cm. with the suspension used. This is the reproducibility limit of the instrument itself, and inspection of, for instance, the linearity of the almost straight slopes of the torque curve fully supports this estimate.

CHAPTER 5.

Design and Performance of Vacuum System.

5.1 Introduction.

The usual method currently adopted to achieve ultra high vacuum in evaporation plants is to use titanium ion pumps combined with titanium sublimation pumping. The latter provides extra speed during the evaporation itself. Since no small 6" ion pumped U.H.V. system was commercially available at the time this work was begun, it was decided to construct the system in the laboratories from standard parts available. Since an ion pump operates by "storing" all the gases it pumps and in view of the large amount of gas evolved in the course of the high temperature bake-out of a vacuum system, it was decided not to instal a second ion pump for use during bake-out, as is usual commercial practice. Instead, a well trapped U.H.V. oil diffusion pump was chosen for this purpose, as this pumps indefinitely without change in performance, subject to regular oil changes.

5.2. The Vacuum System.

The vacuum system is shown in Fig. 5.1. Only stainless steel components were used, sealed to each other with aluminium

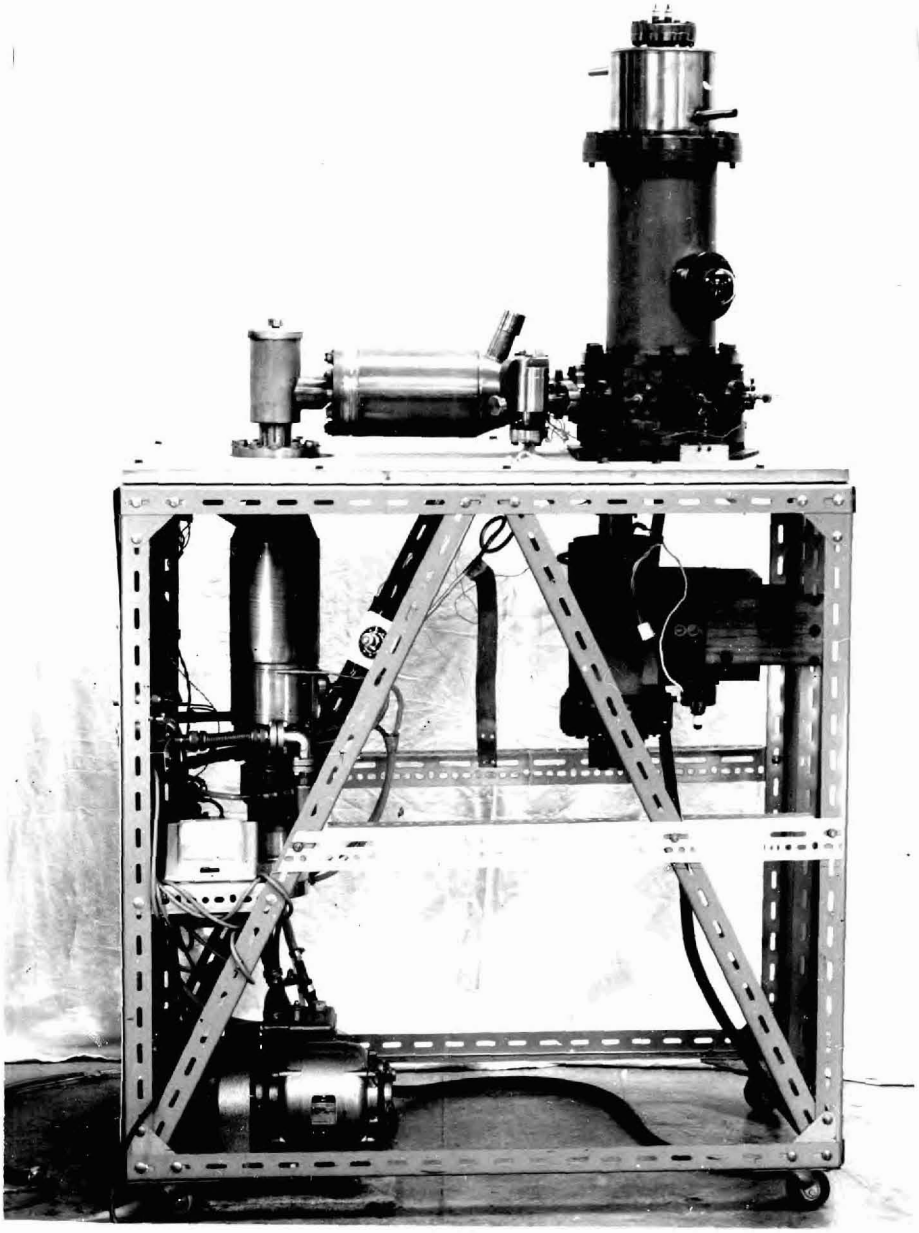

Fig. 5.1. (a) View of vacuum system.

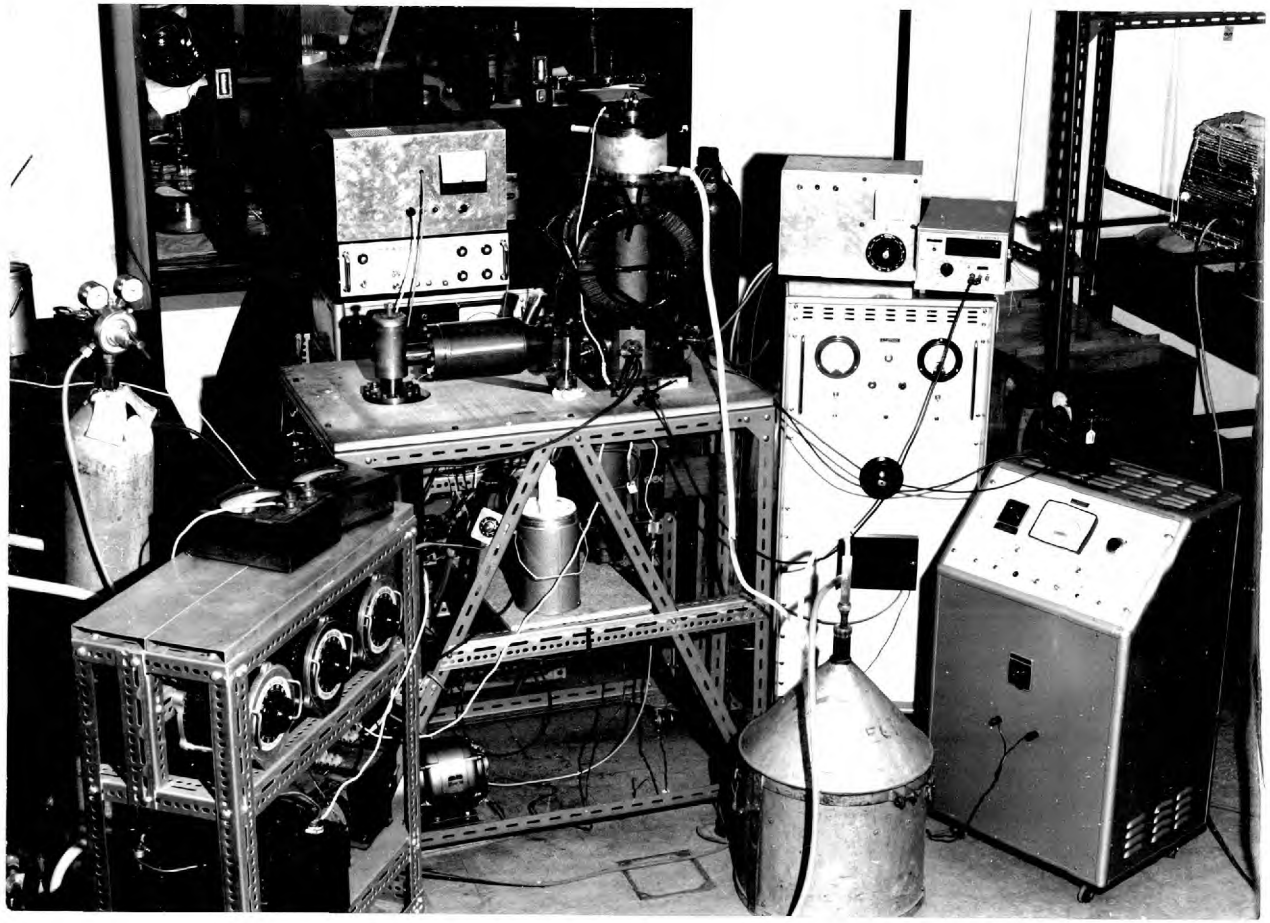

Fig. 5. 1. (b). View of vacuum system with evaporation in progress.

wire rings. The 3" Edwards diffusion pump, type E02, surmounted by the water cooled baffle and liquid nitrogen trap could achieve the 10^{-10} torr range when charged with Convalex-10 oil. This testified to the very low level of contamination produced by it, so justifying its use in place of a second ion pump. Its pumping speed was only 25 l/s. at the chamber, after allowing for the main isolating valve and a second cold trap. The main pumping was performed by a 25 l/s. Ultek ion pump mounted below the baseplate. On top of the chamber was bolted a 6" titanium sublimation pump, water or liquid N_2 cooled, manufactured by Vacuum Generators, Ltd. to the author's design. The base-collar was machined in the Departmental workshops, and A.E.I. type 570 vacuum lead-through electrodes were sealed to it. A Vacuum Generators type M 6 bakeable leak valve was also installed. Two ovens were constructed in the laboratories, one of 4 KW for the top half of the system, and one of 1 KW for the ion pump below the working level. These enabled all parts of the system on the U.H.V. side of the main valve to be baked at over 400° C. The total cost of the system, including the evaporation source, was less than £1000.

Evolution of the system during operation led to a high degree of automation in the pumping cycle. For the overnight bake-out, the power level to the furnaces was initially set with thermostatic switches. Secondary control was effected by

an Edwards relay unit actuated by the backing pressure. This interrupted the bake-out whenever the pressure rose above 150μ of mercury. At the end of the bake-out time, a time switch was installed to turn the furnaces off. This was arranged for two hours before the operator's arrival in the morning to save part of the delay during the cooling time.

The liquid nitrogen level in the diffusion pump cold trap was maintained automatically overnight with a dispenser designed and built by the author. One arm of a Wheatstone bridge composed of four 10Ω carbon resistors rested in the cold trap near the top. The other three arms were maintained in a reference Dewar of liquid nitrogen. A fall in the cold trap liquid nitrogen level unbalanced the bridge. The resulting imbalance voltage was D.C. amplified and used to activate a magnetic valve which admitted nitrogen gas into the liquid nitrogen reservoir forcing more liquid nitrogen into the cold trap, so rebalancing the bridge. The arrangement is shown in Fig. 5.2. The D.C. amplifier is a Mullard[M5] design, with the output meter replaced by the actuating relay as shown.

When the system had cooled to below 200° C after bake-out, the main valve was shut and the ion pump switched on. From this moment, the system was operated like any normal ion pumped U.H.V. system. The ultimate pressure was below 1×10^{-10} torr as detected on a Mullard IOG 12 ionisation gauge.

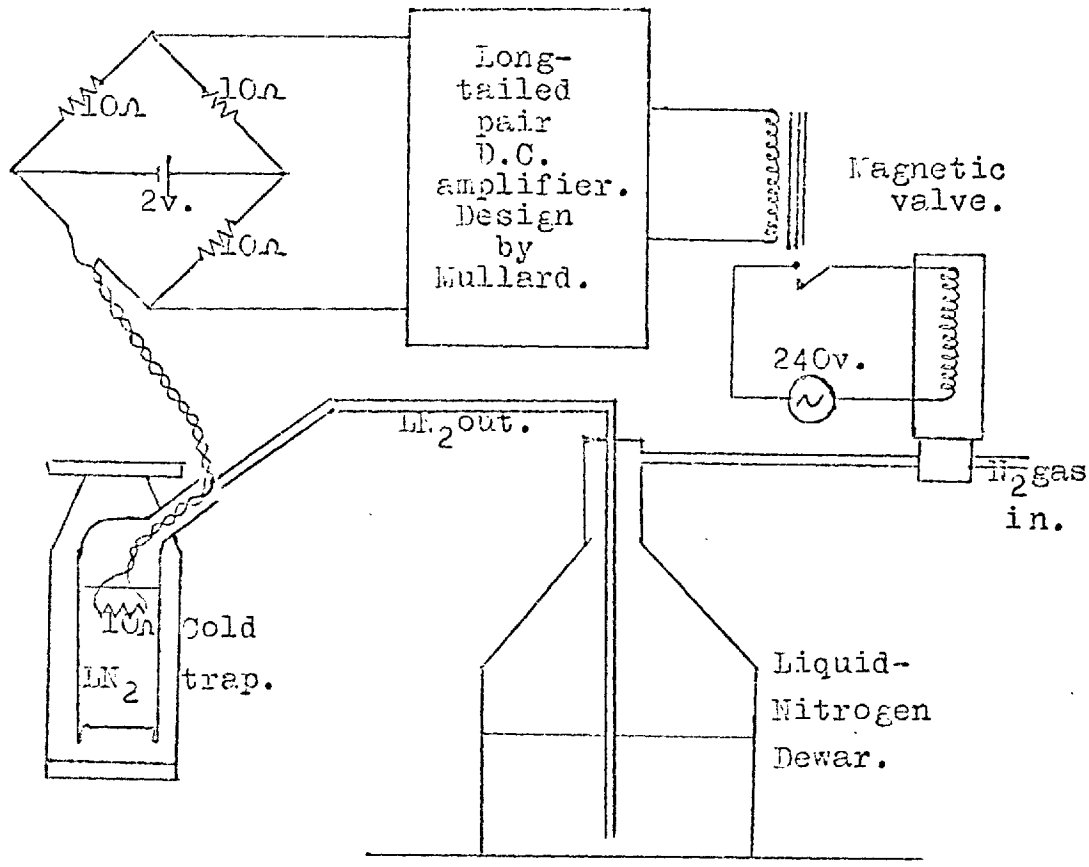

Fig. 5.2.

The quality of an evaporation depends, however, not on the ultimate pressure the system can attain, but on the degree of limitation of the pressure rise during the evaporation. To this end, all the contents of the vacuum chamber were designed to be capable of thorough outgassing.

5.3. Evaporation Furnace.

To comply with the stringent conditons for cleanliness, a

cold-hearth electron bombardment furnace was used, in which the substrate "sees" only the molten top of the ingot. The design by Unvala[U1] was used with a number of alterations to make the furnace more suitable for U.H.V. It was made entirely of stainless steel in the laboratories.

The main feature was the isolation of the 0·020" tantalum filament from the body of the furnace, using ceramic insulators in the base to hold the nickel filament supports in place. By applying an accelerating voltage to the body with respect to the filament, the inside of the furnace could be outgassed by electron bombardment. The top and outside of the furnace were similarly outgassed using four filaments supported by a nickel structure around the furnace. During outgassing, 100 watts was used to heat the inside until the hearth temperature reached 500° C through radiation from the hot furnace. This took about 20 minutes. At this stage, the collar of the furnace was around 1200° C, whilst the base was around 750° C. 250 watts was sufficient to outgas the outside walls to 1000° C.

The cold hearth was turned out of O.F.H.C. copper, and vacuum brazed at 950° C to a stainless steel flange using gold-nickel eutectic wire (81% Au.). The nickel ingot, supplied by Metals Research, Ltd., was of 5N multiplely zone-refined material, the

last pass having been in vacuum. It was found possible to put up to 650 watts into a 2 - 3 mm. spot in the centre of the ingot, this producing a deposition rate of up to 10Å/sec. 20 cm. from the ingot. Because of the good thermal conductivity of Ni at high temperatures, it was necessary to have a large ingot length-to-diameter ratio (2 to 1), and the comparatively large room temperature clearance of 0·0015" between ingot and hearth, in order to maintain a sufficient temperature gradient just to melt the whole of the top surface of the ingot.

5.4. Substrate Heating.

This is one of the most difficult aspects of film production technique and yet is extremely important since the constraint temperature and film structure depend crucially on the substrate temperature. (See for instance ref. S16). The design of the substrate heater was, therefore, the subject of considerable thought.

The requirements were for i) a very low outgassing-rate heater, ii) producing a uniform temperature across the substrate, with iii) the temperature of the substrate itself accurately monitored. Contact heaters were, therefore, excluded, being i) gassy, and ii) so dependent on the degree of so-called

contact between substrate and conduction plate. Black body enclosures, as recommended by Wilts[W6], were considered to be of doubtful value, since they only ensure that the substrate temperature is the same as the black body temperature when a complete thermal equilibrium has been reached. On Wilts' own admission, his substrate temperature rise during deposition was of the order of 1° C per sec., i.e., over 50° C per minute. This is considered to be extremely high, since the response of black body heaters is much too slow to allow for correction of this by turning down the heater power as the evaporation proceeds. The origin of this temperature rise is very unlikely to be found in the thermal energy incident on the substrate by radiation and the evaporant, as suggested by Wilts. The calculations shown in Appendix A3 indicate that the maximum possible temperature rise from these two sources in the present author's system were about 10^{-2} deg. C/sec. and $1{\cdot}4 \times 10^{-3}$ deg. C/sec. respectively. Even allowing for the smaller thermal capacity of Wilts' substrates, the expected temperature rise from these two sources is about an order of magnitude short of that observed by Wilts.

A radiation heater was therefore used. It consisted of a resistively heated 0·002" molybdenum strip, 1" wide clamped a few mm. behind the substrate support. The advantages of such

a heater were several. Its low mass made for very rapid response to changes in input power. The heating uniformity was excellent. The field at the substrate due to such a strip was extremely uniform (See Appendix A 4). Its closeness to the substrate necessitated using a comparatively low radiating temperature. This had advantages as will be evident below.

The use of a radiant heater on alkali halide substrates led however to a number of potential difficulties. Sodium chloride crystals, on which the majority of the evaporations were performed, is substantially transparent to radiation of from about 0·2μ to somewhat over 15μ. Black bodies with radiation temperatures around that possessed by the substrate heater during normal usage (1000-1400° K), have little of their radiant energy below 0·2μ or above 15μ, as shown in Fig. 5. 3.

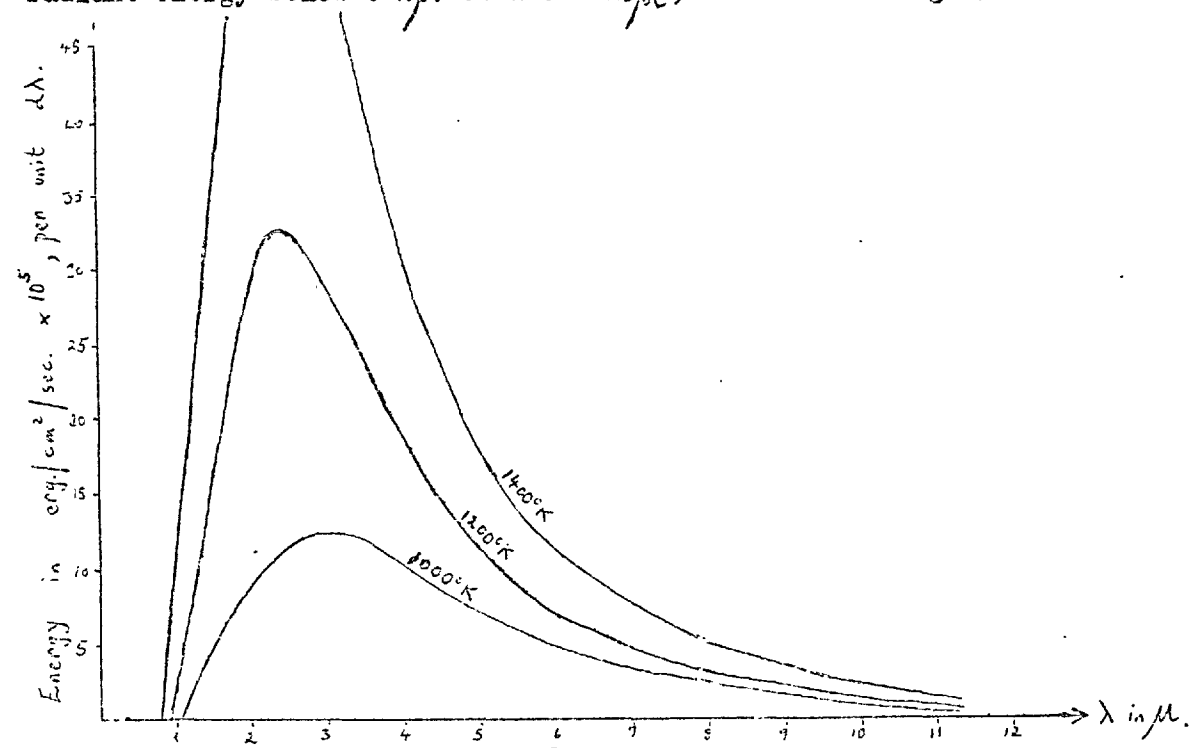

Fig. 5.3.

The substrates therefore absorb very little of the incident heat and the heating efficiency is low, but, nevertheless, adequate heating can be achieved. (This is sometimes overcome by coating the back surface of the rock-salt with an absorber such as colloidal graphite paste, but this was excluded here on the grounds of contamination.)

A second problem was that the substrate support should not absorb appreciably more of the radiation than the substrate itself. This was to ensure as uniform a heat flow as possible across the substrate, thus keeping its temperature uniform right up to the edges of the mask. From the choice of materials available for the mask, fused quartz was the most suitable, becoming fairly opaque below $0{\cdot}12\mu$ and beyond about 6μ. From the tabulated data for the Planck radiation integral (American Inst. of Physics Handbook, chapter 6 K), the following ratios of integrated radiation are obtained:

At 1000° K, $\dfrac{\int_{\lambda}^{\infty} W d\lambda}{\int_{0}^{\infty} W d\lambda} = \begin{cases} 0.26 \text{ for } \lambda = 6\mu \\ \\ 0{\cdot}03 \text{ for } \lambda = 15\mu \end{cases}$

At 1400° K, $\dfrac{\int_{\lambda}^{\infty} W d\lambda}{\int_{0}^{\infty} W d\lambda} = \begin{cases} 0{\cdot}13 \text{ for } \lambda = 6\mu \\ \\ 0{\cdot}01_3 \text{ for } \lambda = 15\mu \end{cases}$

i.e., at 1000° K, there is about 9 times as much integrated

radiation between 6μ and ∞ as there is between 15μ and ∞. The corresponding ratio for 1400° K is about 10 times. Since the quartz mask was only $\frac{1}{10}$ the thickness of the substrate, its absorbtion was thus about the same as that of the substrate. It was therefore presumed that the quartz support did not seriously affect the uniformity of heating of the rock-salt substrate.

5.4.1. Substrate Temperature Measurement.

The best method of measuring the surface temperature of the substrate is by means of a thin film thermocouple evaporated on to that surface. There are, however, a number of disadvantages to this method. Firstly, it is difficult to produce a durable thin film thermocouple on such a water soluble material as NaCl. Secondly, because the thermocouple has to monitor the temperature of the substrate as the deposition proceeds, the dummy block of NaCl with the thermocouple on it must be exposed to exactly the same conditions as the substrate itself. Thus, before evaporation even commenced, it would show a higher reading than a clean substrate because of the disturbing effect of the thermocouple on the heat flow. Then again, during the course of the evaporation, it must become coated with evaporant and so would cease to function. A thin protective layer, such as Si O, would be useful in this respect, but would still demand

the employment of a fresh temperature sensor for each evaporation, as the evaporant could not be removed without damaging the thermocouple.

Wire thermocouples pressing against the substrate surface are also unsuitable as they are never in equilibrium with the substrate itself because of the variability of the thermal contact achieved.

It was therefore decided to use a very fine wire thermocouple (44 s.w.g.) embedded in a 0·018" diameter hole drilled in the side of a blank of rock-salt. This was placed on the quartz mask next to the substrate, as shown in Fig. 5.4.

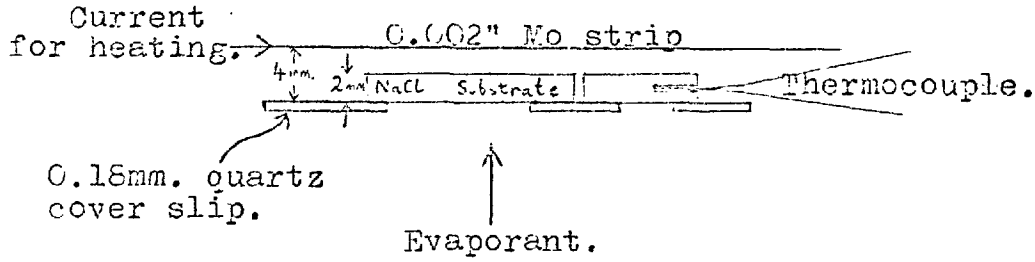

Fig. 5.4.

It proved to have the following advantages:

i) The very small mass of the thermocouple tip gave it a very short time constant for equilibrium with the massive NaCl block around it. The NaCl in fact acted as a black body radiator with respect to the thermocouple embedded in it.

2) The wires were too small to upset the thermal conditions of such a large piece of NaCl.
3) The NaCl blank reacted during the deposition in exactly the same way as the substrate itself, being covered by evaporant at the same rate and so reflecting or absorbing radiation in the same way. In this respect, conditions within the blank were identical to those of the substrate itself.
4) A simple wipe-over with a moist filter paper was sufficient to remove all the evaporant and leave the sensor ready for the next deposition.

A simple experiment was performed to test the effectiveness of the thermocouple. An Fe-Ni thermocouple was deposited on to the front face of a blank of rock-salt containing a 44 s.w.g. chromel-alumel wire thermocouple. The embedded thermocouple showed a temperature about 12° C lower than that of the thin film at 300° C, but this was not necessarily significant since the Fe-Ni thermocouple could only be calibrated in wire form, the thin film form being much too fragile. Errors of 10 degrees are quite common when such an extrapolation to a thin film thermocouple is made. (The expected temperature difference between the centre of the substrate and its surface due to the thermal flux across the substrate is only about 3 deg. C. This assumes that the radiant heat flow from the substrate heater, typically at 1200° K, is ½ cal./cm.^{2}/sec., as obtained from the radiation integral tables and the known emissivity of Molybdenum. Using the given value of thermal conductivity for NaCl, - 0.02 cal./cm./sec./deg. C - the temperature difference across 1mm. of the substrate comes to 3 deg. C. This is about one order lower than for a similar glass substrate.)

More significant was the comparison of the responses of the two thermocouples to a step function in the heater power. Unfortunately, though detailed graphs could not be plotted

through the inability to collect the data sufficiently rapidly, from the points taken it was evident that the initial response of the wire thermocouple to a 25 degree step function was within a few seconds of that of the thin film one. The asymptotic approach to the higher temperature was rather slower for the wire than for the thin film, but the longer time scale (15 minutes) of this section may well explain this. Even if this delay effect is real, since changes during evaporation take place very rapidly, this temperature sensor was regarded as being entirely satisfactory.

In use during an evaporation, the thermocouple showed no significant change when the shutter was opened, in agreement with the calculations in section 5.4. As the evaporation proceeded a small gradual rise in temperature was observed until, when the film became visible to the eye ($400 \sim 500\text{Å}$), the temperature would shoot up if the input power were untouched. This was probably the effect of reflection of the radiation from the film surface back through the substrate, thereby doubling its heating effectiveness. As the film became completely opaque (1000Å), the temperature rise decreased to a very slow rate, this probably being the exponential tail to the temperature change effect. If unattended, this temperature rise was over 100° C from 300° C. It was this effect which had caused many of the films grown

previous to the development of this temperature sensor to be ruined through overheating, since a wire thermocouple touching the front surface of the substrate, as initially used, had not shown this large rise. In practice, the input power of the heater was turned down as the evaporation proceeded, keeping the temperature constant.

5.5. Ratemeter and Magnetic Field.

The ratemeter was simply a semicircular plate in the upper part of the chamber which collected the resultant plasma current from the vapour stream. This current was read on an AVO meter and was found to be electronic in origin. The ratemeter had to be calibrated against pressure and furnace emission current, as the current collected was a function of both of these. In one run, for example, for fixed furnace conditons,

$$I_{ratemeter} = 21\mu A \quad \text{at } 8 \times 10^{-9} \text{ torr}$$

$$\text{and } I_{ratemeter} = 72 \sim 75\mu A \text{ at } 1{\cdot}5 \times 10^{-6} \text{ torr.}$$

The ratemeter current was independent of pressure below about 10^{-7} torr. In practice, fixed furnace operating conditions made rate-monitoring very straightforward. The nature of the ratemeter current is discussed further in the section on structure

and colour centres below, section 6.1.2.

As derived in Appendix A 4, the magnetic field at the substrate due to the heater strip is given by

$$H = \frac{4I}{W} \tan^{-1} \frac{W}{2d}$$

For the conditions of this experiment, this gave a field of 11 oe for 50 A heater current (a typical value). The heater current return to earth was taken through a pair of single turn Helmholtz "coils" made of thick copper strip on either side of the substrate. They were positioned in such a way as to exactly counteract the heater field. The field due to substrate heating was thus reduced to less than 1 oe at all times.

Any externally applied field required was produced from a large Helmholtz pair situated outside the chamber and providing up to 175 oe at the substrate. The substrate heater had to be driven by D.C. from large accumulators to prevent it from vibrating in this externally applied field.

The substrate heater arrangement is visible in Fig. 5.6.

5.6. Evaporation Procedure.

The furnace was outgassed whilst the system was still hot from its bake-out. The substrate was outgassed, at not more than 400° C for NaCl, for up to ½ hour. It had been found that the rock-salt already sublimed noticeably at about 415°~420° C

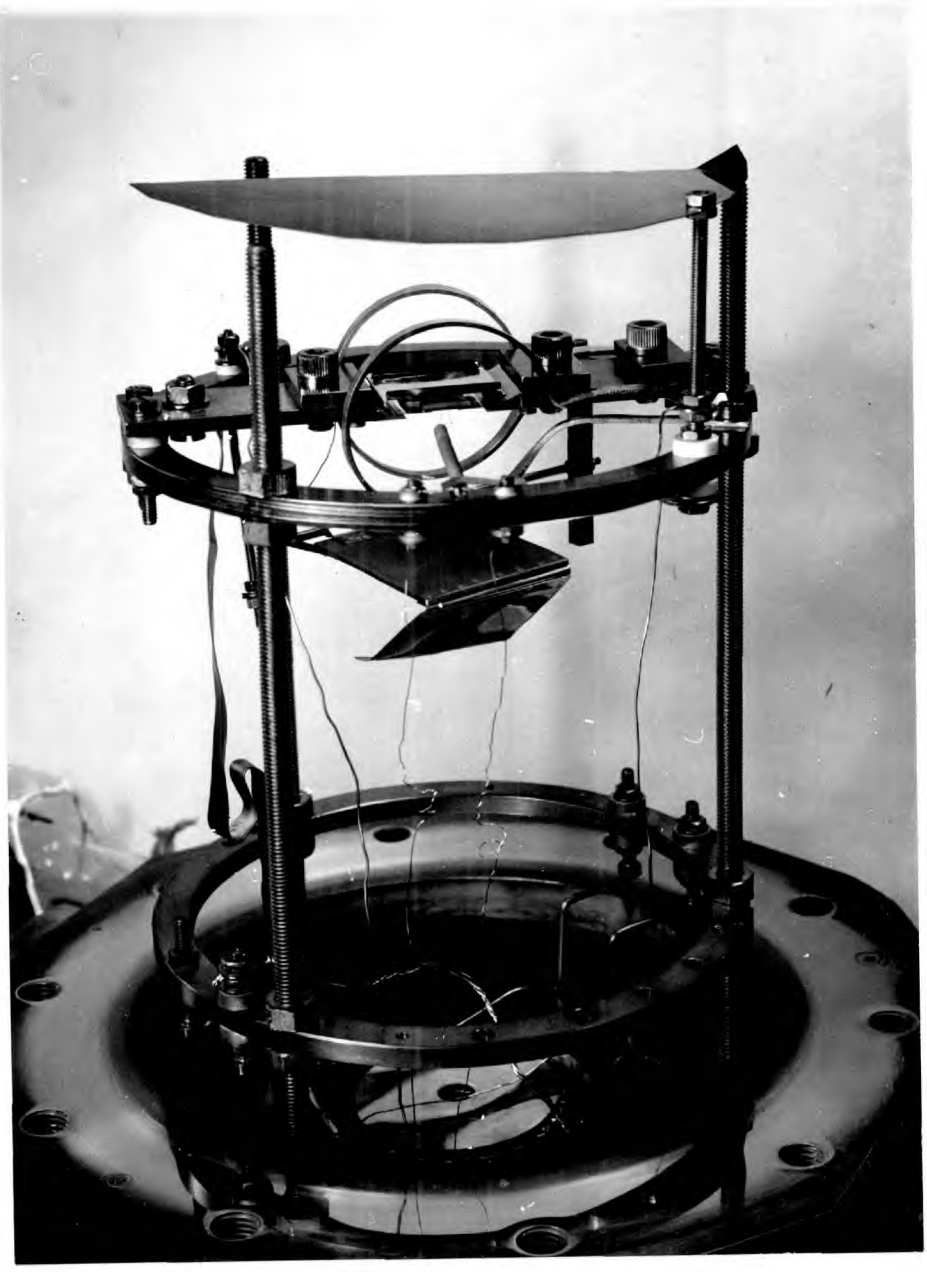

Fig. 5.6. Interior of vacuum chamber, showing substrate heater and temperature probe at top, furnace at bottom.

resulting in a ruined surface if a bake-out were attempted near this temperature. This finding is compatible with the results of Sella and Trillat[S15]. The shutter release wire was also outgassed, and the substrate temperature was dropped to the desired value. The furnace was started and when the initial pressure rise was over, the leak valve was opened if it was desired to admit any gas. The shutter could then be dropped to commence the evaporation. The best pressure held during evaporation was 5×10^{-9} torr at 5Å/sec. deposition at 20 cm. A more usual pressure was $8 \sim 9 \times 10^{-9}$ torr at 6~7 Å/sec. The films were allowed to cool in the field, if applied, and needed about 15 minutes to fall below 100° C from 350° C.

The quartz mask had a small 2 mm. hole near the corner of the substrate position to produce a specimen for electron microscopy. This was performed in a JEM-7 model at 100 KV.

After the magnetic measurements, the film thickness was determined by X-ray fluorescence. The method was doubly calibrated using five standards. In the first place, these standards had been weighed on production to within $\pm$ 1μg. Secondly, the standards were analysed by the Imperial College analytical services laboratory staff by using a micropolarography method. The accuracy of the straight line produced, Fig. 5.5,

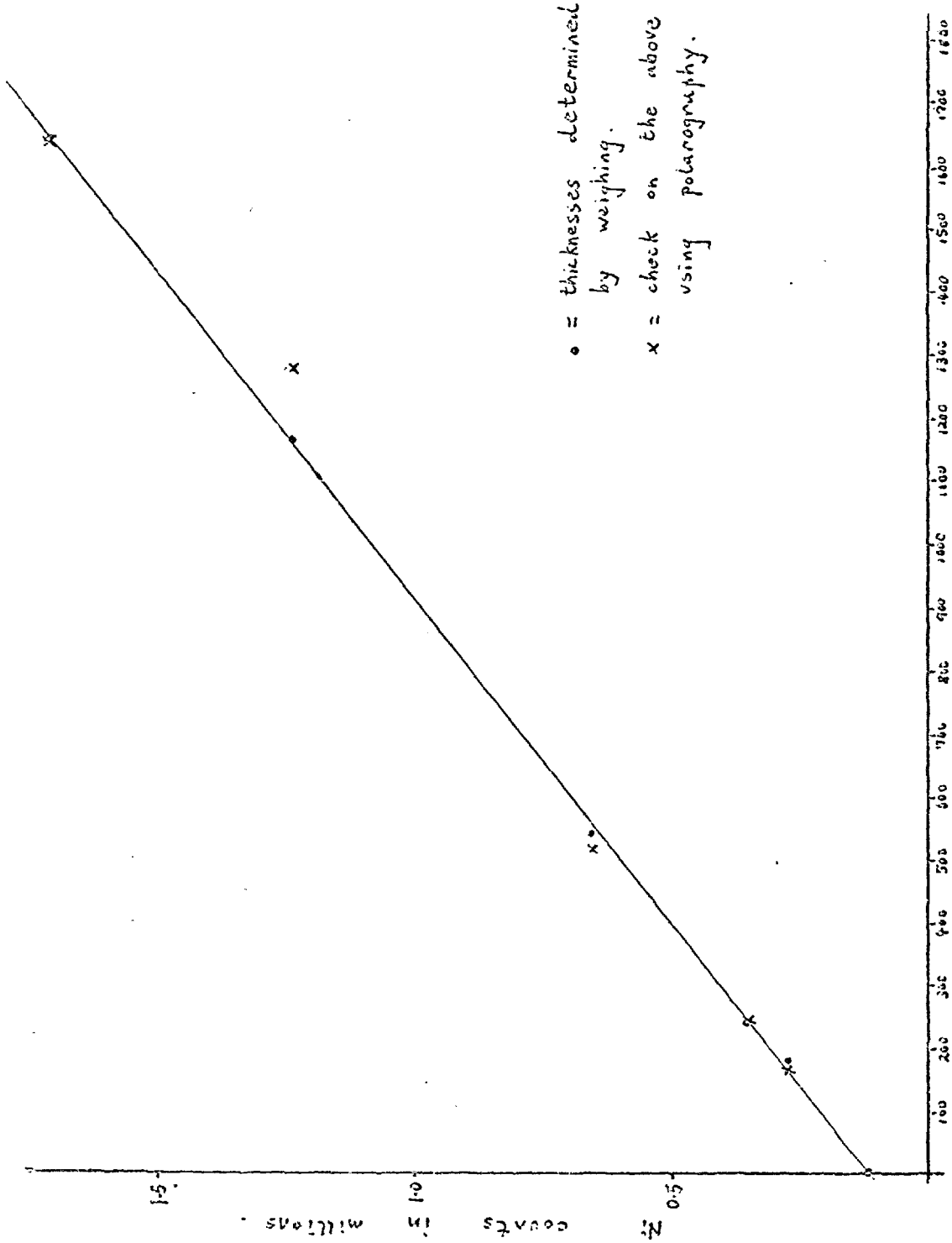

Fig. 5.5. Thickness calibration curve.

shows that the X-ray fluorescence method should be capable of producing film "thicknesses" to within $\pm$ 10Å. The "thickness" so determined is in fact proportional to the mass of metal present, independent of density, and so is ideal for magnetics work.

CHAPTER 6.

Magnetic and Structural Results and their Interpretations.

6.1 General Properties of the Films.

After the initial trial period, in which most of the major operational features of the vacuum plant and of the evaporation procedure were mastered, about forty serious attempts were made to produce films for investigation, from which only about 30 were actually produced. Of these some were eliminated by visual inspection as being unlikely to give meaningful magnetic data. The usual cause for this rejection procedure, particularly amongst the early films before substrate temperature control had been adequately understood, was a cloudiness of the film surface. This indicated that the substrate had been allowed to get too hot, either during pre-heating or during evaporation. One or two films were also rejected on the grounds of gross variations in thickness across them, probably a result of substrate contamination. This left 22 films which were actually measured on the torque magnetometer.

6.1.1. Film Growth and Structure.

Many of the features of the film production technique described in this section were in fact only adopted as a result of identifying the causes of failures in previous films. Three

types of substrate were used in the main. In the first place, following the suggestions of Heavens et al[H9], polished rock-salt substrates were used. The polishing agent was a suspension of tin oxide in saturated sodium chloride solution. This technique produced very flat surfaces on the rock-salt, albeit with a high density of microscopic scratch marks. Since these were random in direction, and, being invisible to the eye, certainly smaller than cleavage steps, they were not thought to influence the magnetic properties of the films. It was not found possible to take this substrate preparation technique to the ultimate stage used by Heavens et al, by the evaporation of a 1000 ~ 2000 Å epitaxial layer of copper, since it was not possible with the evaporation conditions used (U.H.V.), to obtain well orientated (100) films of copper without a considerable proportion of (111) orientation also. This was exactly in accordance with the findings of Ino et al[I2], who observed a similar deterioration of the epitaxy of Cu on rock-salt when moving from ordinary high vacuum to U.H.V., even when the rock-salt was cleaved in vacuum.

Air cleaved rock-salt and lithium fluoride were also used as substrates. The quality of the resulting films, both magnetically and structurally, indicated that there had been no great

disadvantage in not using vacuum-cleaving, which may have been considered more desirable in any low-contamination evaporation procedure. It could even be postulated that the exposure of the cleaved face to the moist atmosphere would tend to smooth out the cleavage steps on a small scale, by means of a micro-solution and recrystallisation process. Such a suggestion could find support in the fact that good decoration of cleavage steps is only usually possible on vacuum-cleaved substrates. All substrates were heated before deposition, for up to $\frac{1}{2}$ hour at a temperature not exceeding 400° C for the NaCl, as explained in section 5.6. The lithium fluoride substrates were preheated at 425° C, the limit of the substrate heater with the power supply available (75 amps.). This preheat was necessary to remove any surface contamination, particularly in the case of the polished films. Such a thermal etch, involving the removal of a microscopic layer of the surface, was also thought to be beneficial to the film growth because of the release of some of the surface stresses resulting from the cleavage or polishing process.

The substrate temperature used was usually 300° C for the NaCl and 365° C for LiF. This latter temperature was chosen as being above the Curie temperature of nickel (355° C). The applied

field, when used, was 150 oe. This was considered quite adequate since the rapid fall of K_1 with rise in temperature ensured that such a field was always several times the anisotropy field even at the low temperatures at which the magneto-stress properties of the film were probably established. (100 ~ 200° C; see below, sections 6.5. - 6.5.1.)

Attempts were made to measure the films on NaCl both before and after release from the substrate. In this way, it was hoped that the stress contribution to K_u could be easily determined. Unfortunately, one or other of these two measurements was not always possible. In some cases, the films were physically damaged during the floating-off procedure. In other cases, the substrate-to-film bond was so weak that even the moisture in the atmosphere caused a relief of the stress system in the film by allowing it partially to detach itself on a microscopic scale. This was recognised macroscopically by a sudden clouding-over of the shiny nature of the film surface. On inspection under an optical microscope, the surface was seen to be wrinkled in a random manner where the compressive stress in the film (to be discussed below) had proved too large for the moisture-exposed NaCl surface to maintain. It was for this reason that a number of evaporations were performed on LiF substrates for the purpose of making the primary investigations of the constraint energy.

LiF is almost insoluble in water (2·7 gm/l at 18°. C) and so maintains a good bond to the film even in moist atmospheric conditions. LiF also has two other incidental advantages over NaCl. The lattice misfit of Ni on LiF is much smaller than for Ni on NaCl. (Lattice constant for Ni = 3·524 Å, LiF = 4·02 Å, NaCl = 5·64 Å.) It is thus likely that the Ni films would grow epitaxially on LiF with a lower density of lattice faults than on NaCl. The second advantage is that the sublimation temperature of LiF is considerably higher than that of NaCl. It was thus possible to carry out better thermal cleaning of the LiF before deposition than in the case of NaCl, and also to evaporate at a higher temperature without danger of damaging the surface. This gave the incident atoms higher mobility on the substrate and so would tend to contribute to better crystal perfection of the films. It was not possible, unfortunately, to use LiF for the whole of the current investigation because of the difficulty of removing the films intact from the substrates. Small electron microscope specimens (1 mm. in diameter) were, however, easily stripped by the action of a hot saturated ammonium chloride solution, lithium chloride being more soluble than lithium fluoride (640 gm/l at 0° C).

$$NH_4Cl + LiF \rightleftharpoons LiCl + NH_4F$$

All magnetic measurements were performed on the as-grown films,

i.e., no attempt was made to anneal the films. (The two exceptions to this rule are noted below in section 6.7.) It was considered that the effect even of so-called "zero field" anneals would only be to complicate the situation as regards mechanisms operating to produce K_u. It should be borne in mind in this context, that at 300° C, the magnetostatic energy arising from a "stray" field of only 1 oersted is probably the dominant term in the total energy determining the film's magnetic properties. This is because anisotropy constants fall exceptionally rapidly with rising temperature, whilst M_s at 300° C is still over half its room temperature value so that the anisotropy field $H_K = {}^{2K}/_{M_s}$ will be very small. Likewise large stresses are unlikely to be maintained at this temperature so that magnetoelastic effects will be small. The only annealing effect the films were subjected to, therefore, was in cooling down to room temperature after the deposition, as mentioned in section 5.6.

The main structural features of the films are apparent from the electron micrographs and electron diffraction patterns shown in figure 6.1. All the films showed broad extinction contours at low magnification, and were very well orientated, with parallel growth: (100)Ni || (100)LiF or NaCl. The rock-salt films usually showed some twinning along (111) type planes though in general, those from the polished substrates showed

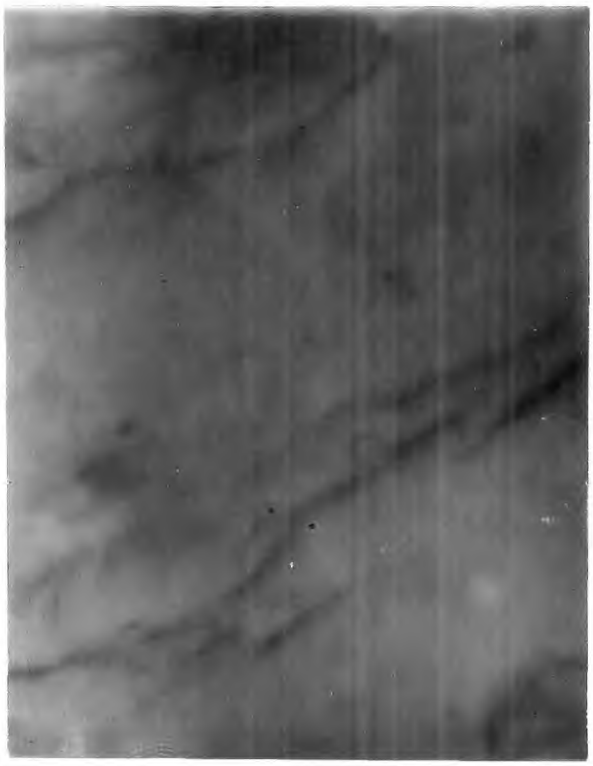

Fig. 6.1(a).

Mag. = 75,000

Micrograph typical of large areas of U.H.V. films on LiF.
No sharp features at all are visible.

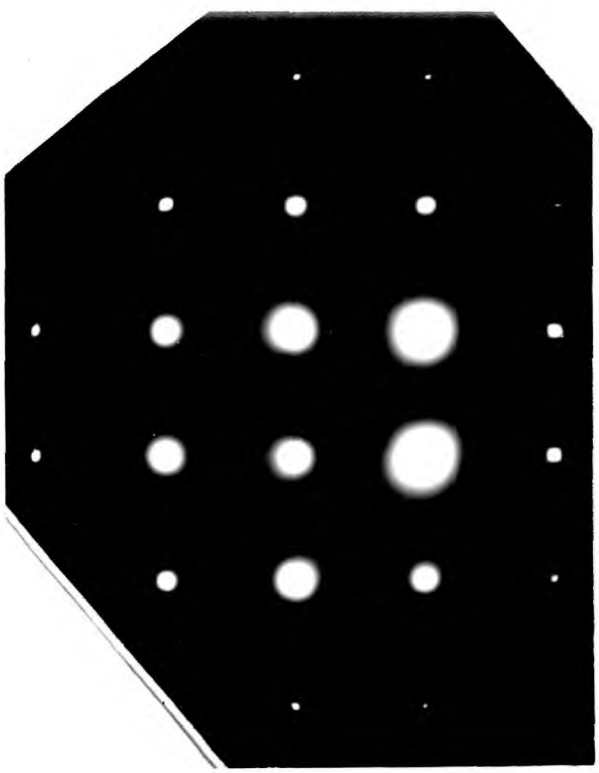

Fig. 6.1(b)

Electron diffraction pattern of selected area of the above.

Fig. 6.1(c).

Electron diffraction pattern of large area of U.H.V. film on LiF, showing well-defined Kikuchi pattern.

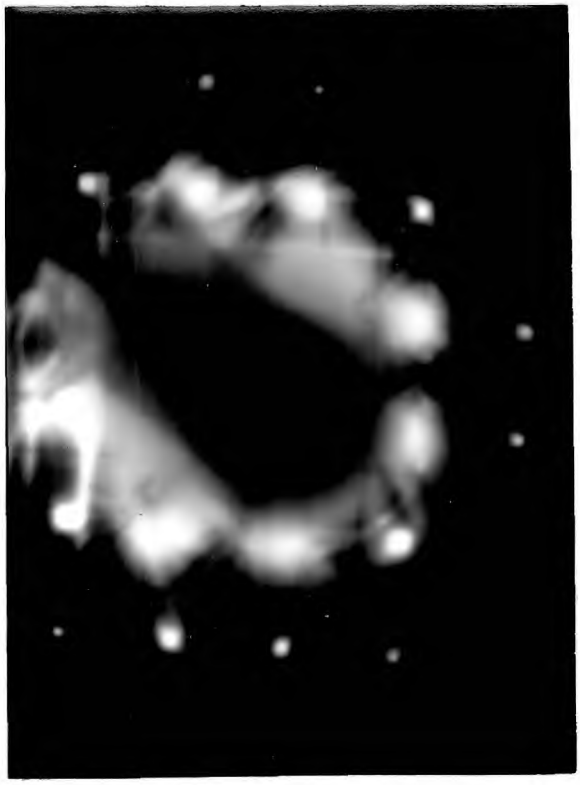

Fig. 6.1(d).

Mag. = 75,000

Micrograph typical of the worst areas of U.H.V. films on LiF. The broad black band is an extinction contour due to the film bending. The fine black features are defects of some sort.

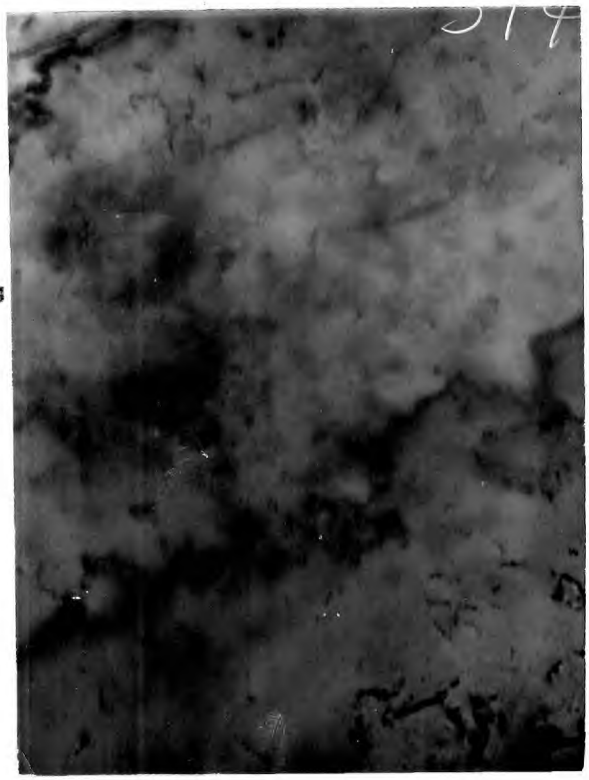

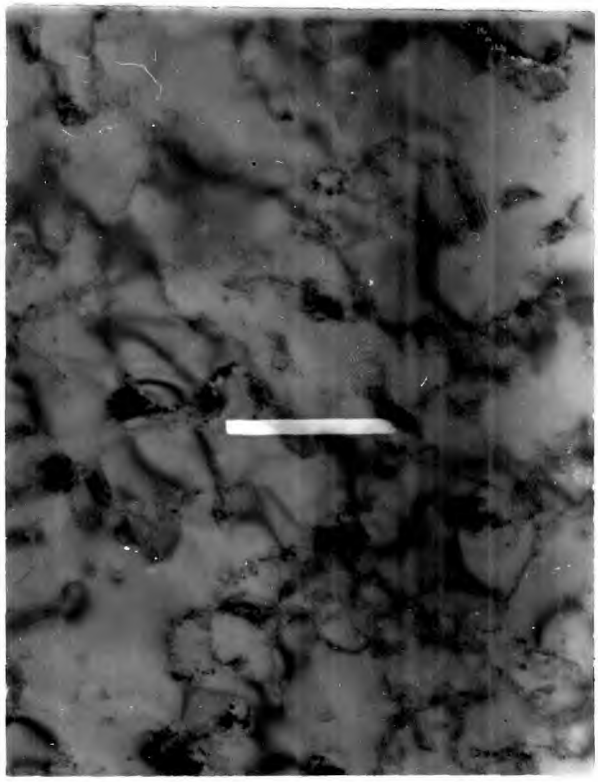

Fig. 6.1(e).

Mag. = 75,000

Micrograph typical of U.H.V. films on polished NaCl. A few stacking faults and also some very fine detail are visible.

Fig. 6.1(f).

Mag. = 75,000

Micrograph typical of film grown in ordinary high vacuum (1 x 10^{-5} torr) on polished NaCl.

Fig. 6.1. (g).

Mag. = 75,000

Typical area of Ni 32, showing grainy appearance and high density of stacking faults.

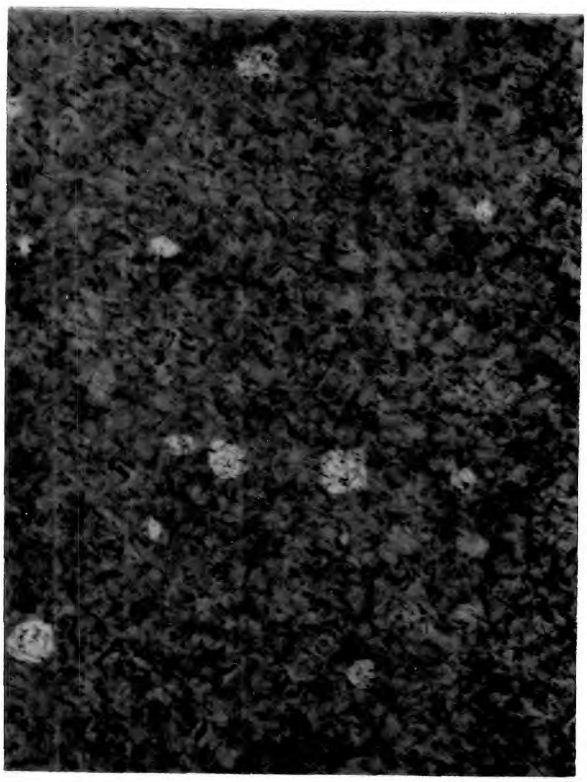

much less than did the cleaved substrates. On the other hand, some areas of the polished substrates' films were very grainy. The micrographs of all the U.H.V. films were very featureless, the occasional twin or stacking fault being the only sharp identifiable features. The U.H.V. films on LiF were exceptionally perfect. Their diffraction patterns showed no twinning at all, and the well defined Kikuchi patterns testified to the crystalline perfection. The imperfection density was of the order of $10^{10} \sim 10^{11}$ visible defects per cm^2 of film, this being a very low figure. More specific correlation of structure with magnetic properties will be attempted in the relevant sections below.

6.1.2. Colour Centres in LiF.

It was observed that the films grown on LiF in the absence of a magnetic field displayed a distinct yellow colour when viewed from the back, i.e., through the LiF substrate. Such a colouration, though of a deeper reddish brown colour, had been previously observed by Chambers and Prutton[C11] in similar circumstances. They showed that this colouration was probably due to the presence of F-centres produced in the substrate near its surface, as a result of the heavy incident electron flux from the electron bombardment evaporation source. They also

attributed the excellent crystalline orientation and the low defect density of the resulting films to the effect of this electron bombardment. Since, in the present programme, it was noted that the application of a field during deposition completely supressed the appearance of the colour centres, and yet the resultant films were indistinguishable as far as crystalline perfection was concerned, a simple experiment was performed to attempt to clarify the nature of the ionic plasma from the furnace incident on the substrate.

The electron gun source was turned on and stabilised at a fixed input power of 100 mA of emission at 7 KV (water-cooled hearth earthed, furnace body at -7 KV). The system pressure was $4 \sim 6 \times 10^{-6}$ torr. The ratemeter vane was collecting 90 μA of electronic current, and since it was effectively earthed through the AVO-meter, it was at the same potential as the substrate and surroundings during evaporation. The magnetic field was then gradually applied, and the ratemeter current noted as a function of field. The result is shown in fig. 6.2. The shape of the curve can be explained by assuming that the incident flux of electrons contained electrons of all energies up to 7 KeV, the operating voltage of the furnace. As the field is increased, more and more of these electrons are deflected away from the vapour beam, until at about 65 oe., a residual current

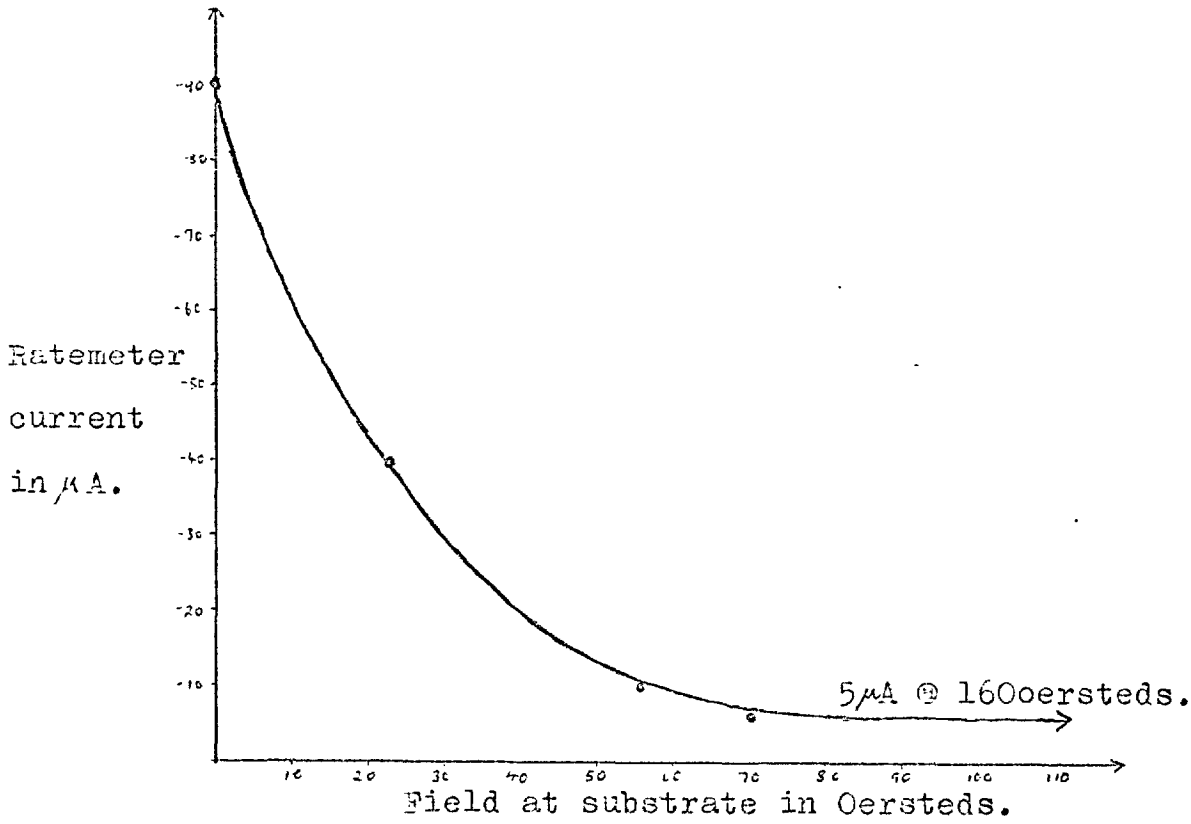

Fig. 6.2.

of -5μA is reached, and is not reduced by further increase in the field up to 160 oe. Now, from electron-optics tables of functions[K8], it is observed that a 7 KeV beam of electrons has momentum $2{\cdot}83 \times 10^{-4}$ Webers/metre, where the electron momentum is given by $(Br)_e$, the product of the radius of curvature, r, of the electron in a magnetic field, B. Substituting in our value of critical field, $6{\cdot}5 \times 10^{-3}$ web./m^2 (65 oe), the radius of curvature of the electron beam is calculated as approximately $4\frac{1}{2}$ cm. When it is borne in mind that the effective field from the Helmholtz coils extends to about 6 cm below the

substrate level (this is the point at which the field has fallen to $\frac{1}{5}$ of its axial value), it seems reasonable to suppose that at that field of 65 oe., the most energetic electrons in the beam are just being diverted sufficiently so as not to hit the ratemeter, and hence the substrate. The residual 5 μA of current could possibly be due to residual gases ionised in the intense electron flux present within the furnace. Since the gaseous ions have a large mass they would be virtually undeflected by fields of only hundreds of oersteds.

In order to test this postulated behaviour, the effect of applying a potential to the ratemeter vane was investigated. With increasing negative potential, the initial -90 μA current fell, reaching zero at about -800 volts and rising approximately linearly to a plateau of + 550 μA at -7 KV. At this voltage, application of a field made no difference to the current. Decreasing the furnace operating voltage to -6 KV also decreased the voltage at which this saturation set in to -6 KV. It is therefore supposed that in this mode of operation, positive Ni ions were being collected, with energies of up to the furnace operating potential. Such ions would, of course, be undeflected by the field applied. In normal operation, such ions would not reach the substrate because of the high electric field opposing their passage away from the furnace body, which was at a high

negative potential.

When a positive potential was applied to the ratemeter, the current collected rose steadily from -90μA to a maximum of -600μA at + 7 KV. Application of an increasing magnetic field at this stage decreased the current collected, until by about 90 oe., the current had become approximately constant at -100μA. It is therefore proposed that this effect can again be explained by means of a combination of electrons and residual gas ions. The accelerating electric field makes the flux collected higher than in the normal operating mode where the collector is at earth potential.

From measurements of the geometry of the ratemeter vane, the normal -90μA current represents an electron flux of about 2×10^{13} elecs./cm^2/sec. This is over an order of magnitude less than that reported in Chambers and Prutton's experiment. This may be due to their smaller source-substrate distance.

In conclusion, it is therefore proposed that the yellow colour in the LiF substrates of films prepared in the absence of a magnetic field are indeed colour centres, as suggested by Chambers and Prutton. The paler colour could be due to the lower electron flux in the present author's experiments. The application of the magnetic field normally used virtually

completely deflects this electron flux, thereby preventing the formation of the F-centres. Since this does not lead to deterioration of the films' structural properties, it seems that the incident electron flux under these experimental conditions is not instrumental in producing the excellent structural properties.

6.2. Features of the Torque Curves.

Before taking any torque curves, films were always brought into a cyclic state magnetically by making them perform several complete revolutions in the field. After the curve had been plotted in one direction, spot checks were made whilst rotating the field back in the opposite direction. In no case was any rotational hysteresis observed at the field used (5·1 K Oe.).

As expected, the torque curves showed a predominantly 4θ dependence. Typical examples are shown in figure 6.3. The computer output from the Fourier analysis consisted of three separate sets of coefficients and phase angles, resulting from three separate analyses performed at 5° intervals on the input curve. An example of the output is shown in fig. 6.4. As is observed, the variation of coefficients between the three analyses

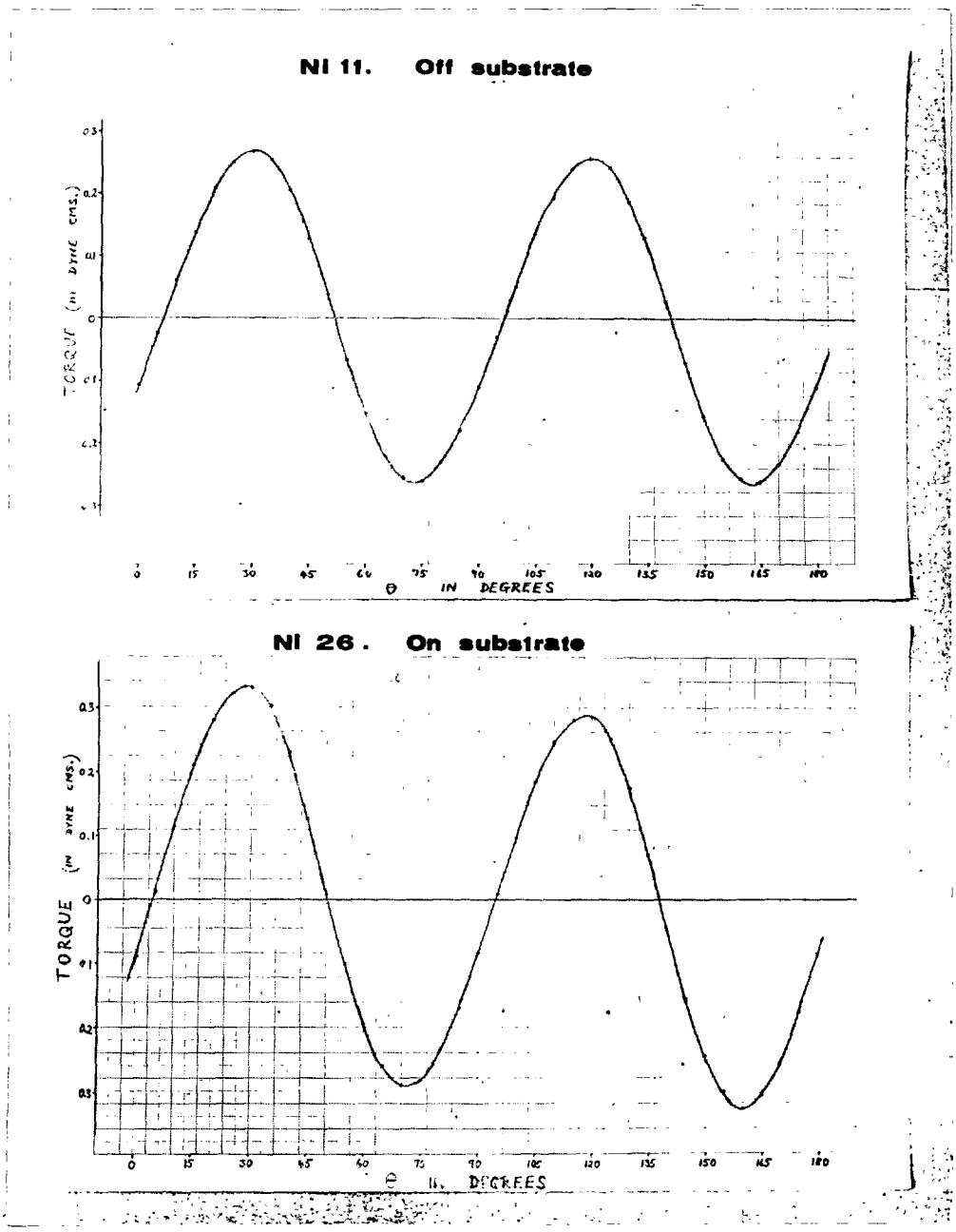

Fig. 6.3 Examples of torque curves.

RESULT OF CALCULATION OF PHASE 1

J = 1	A(J) =	1.4192	B(J) =	0.	COEFF(J) =	1.4192	PHI =	90.0
J = 2	A(J) =	0.0023	B(J) =	0.0634	COEFF(J) =	0.0635	PHI =	2.1
J = 3	A(J) =	-0.2442	B(J) =	0.7607	COEFF(J) =	0.7989	PHI =	-17.8
J = 4	A(J) =	-0.0017	B(J) =	0.0033	COEFF(J) =	0.0037	PHI =	-26.6
J = 5	A(J) =	0.0108	B(J) =	-0.0274	COEFF(J) =	0.0295	PHI =	158.4
J = 6	A(J) =	-0.0006	B(J) =	-0.0001	COEFF(J) =	0.0006	PHI =	-98.2
J = 7	A(J) =	-0.0008	B(J) =	0.	COEFF(J) =	0.0008	PHI =	-90.0

RESULT OF CALCULATION OF PHASE 2

J = 1	A(J) =	1.4196	B(J) =	0.	COEFF(J) =	1.4196	PHI =	90.0
J = 2	A(J) =	0.0094	B(J) =	0.0657	COEFF(J) =	0.0664	PHI =	8.2
J = 3	A(J) =	0.0312	B(J) =	0.7989	COEFF(J) =	0.7995	PHI =	2.2
J = 4	A(J) =	-0.0042	B(J) =	0.0083	COEFF(J) =	0.0093	PHI =	-26.6
J = 5	A(J) =	-0.0146	B(J) =	-0.0325	COEFF(J) =	0.0356	PHI =	-155.8
J = 6	A(J) =	0.0022	B(J) =	0.0051	COEFF(J) =	0.0056	PHI =	23.5
J = 7	A(J) =	0.0063	B(J) =	0.	COEFF(J) =	0.0063	PHI =	90.0

RESULT OF CALCULATION OF PHASE 3

J = 1	A(J) =	1.4158	B(J) =	0.	COEFF(J) =	1.4158	PHI =	90.0
J = 2	A(J) =	0.0203	B(J) =	0.0659	COEFF(J) =	0.0690	PHI =	17.1
J = 3	A(J) =	0.2975	B(J) =	0.7390	COEFF(J) =	0.7966	PHI =	21.9
J = 4	A(J) =	0.0042	B(J) =	0.0058	COEFF(J) =	0.0072	PHI =	35.5
J = 5	A(J) =	-0.0250	B(J) =	-0.0202	COEFF(J) =	0.0328	PHI =	-128.0
J = 6	A(J) =	0.0030	B(J) =	0.0024	COEFF(J) =	0.0039	PHI =	51.3
J = 7	A(J) =	0.0050	B(J) =	0.	COEFF(J) =	0.0050	PHI =	90.0

Fig. 6.4. Computer output for film Ni 26.

was very small. This signifies that no part of the curve is seriously inaccurate. It is also expected that the angles "PHI" of the 2θ and 4θ components should move 10° and 20° respectively between each of the three analyses (in which the angle θ moved 5°). Each PHI represents the angular displacement of each particular coefficient from the origin of the analysis. The degree to which this is so is a second check on the consistency of the input curve.

The misalignment angle of the 2θ component (representing K_u) from the 4θ component (representing $\frac{1}{2}K_1$), is given by $\phi = \beta - \alpha$ in the terminology of equation (15) of section 3.4.2. It could be found by subtracting half the value of PHI for 2θ from a quarter of the value of PHI for 4θ. A simpler method for finding this phase angle is to observe by interpolation or extrapolation where the origin of the 4θ component lies, i.e., where PHI (4θ)= 0°. ϕ is then simply obtained by observing the value of PHI (2θ) at this point, which is then 2ϕ away from the value 0°. This is illustrated in fig. 6.5.

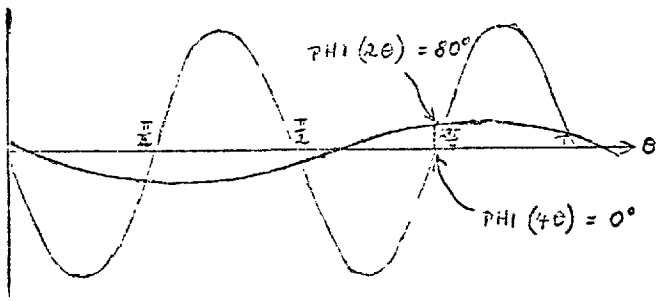

Where PHI(4θ)= 0°,
PHI(2θ)=80°.

$\therefore \phi = \frac{80 - 0}{2} = 40°.$

Fig. 6.5.

6.2.1. M-Deviation Results, and K_3.

It is now proposed to investigate how far the results of the M-deviation calculations carried out in section 3.4.5. are upheld by the experimental results. From equation (22) of that section, it is expected that the predominant pseudo-torque term will be $\frac{K_1^2}{2MH}\sin 8\theta$, since $K_1 \gg K_u$ in all of the curves obtained. Since K_1 for Ni is negative, $\frac{K_1^2}{2MH}$ should be of opposite sign to the 4θ coefficient, $\frac{K_1}{2}$. Scrutiny of the results showed that the 8θ coefficient was indeed always in antiphase to the 4θ coefficient at the latter's origin. In order to check the magnitude of the 8θ term, a number of the torque curves were graphically replotted, adjusting each point according to the deviation expected in the 5·1 K oe. field by the relationship $\alpha = -\frac{L}{MH}$. The resulting curves were analysed, and in all cases, the net effect was to reduce the 8θ component considerably, whilst leaving the other components virtually unchanged. For example, in the results for Ni26 given in fig. 6.4., the following table compares the mean coefficients before and after graphical M-deviation correction.

Component	Uncorrected Coeffs.	Corrected Coeffs.
2θ	0·0663	0·0635
4θ	0·7987	0·7974
6θ	0·0067	0·0099
8θ	0·0326	0·0124
10θ	0·0034	0·0043
12θ	0·0040	0·0028

Now, since the 8θ-coefficient after M-deviation correction was still larger than the expected random noise level for an 8θ component, a closer investigation was made of the magnitudes of the 8θ components in all of the curves. In Ni26, for instance:

$$K_1 = -7{\cdot}98 \times 10^4 \text{ erg/cc.}$$

$$\therefore \frac{K_1^2}{2MH} = 1{\cdot}28 \times 10^3 \text{ erg/cc.}$$

(assuming M = 490 gauss.)

Experimentally, the coefficient of 8θ was, however, $1{\cdot}56 \times 10^3$ erg/cc. In all cases, the experimental values of the 8θ components were in excess of the expected theoretical values, on average by $0{\cdot}3 \times 10^3$ erg/cc. By means of a comparison with the random noise levels of the other components of the analysis, a maximum value of about $0{\cdot}2 \times 10^3$ erg/cc was expected. This suggests the possibility that the excess 8θ is due to the presence of the $\frac{K_3}{16}$ sin 8θ term in the torque expression derived in section 3.4.2. to 8th order in the α_i. Support for this is derived from the fact that the excess 8θ component is always of the same sign as the M-deviation part of 8θ. This will be so if it comes from $\frac{K_3}{16}$ sin 8θ, since this acts in concert with $\frac{K_1^2}{2MH}$ sin 8θ, both having the same angular origin. Random fluctuations, on the other hand, would sometimes tend to make the 8θ component bigger than its expected value of $\frac{K_1^2}{2MH}$, and sometimes smaller. That this interpretation is

reasonable is supported by the fact that the values of the excess 8θ component fluctuated from 0·07 to 0·54 x 10^3 erg/cc, i.e., over approximately the range either side of 0·3 x 10^3 erg/cc expected from a random noise fluctuation of 0·2 x 10^3 erg/cc. The only alternative source for this 8θ component could be found in the lack of justification in the assumption that M_s for the films has the same value as for bulk Ni. A reduction in M_s of about 30% would, however, be necessary to bring the average $\frac{K_1^2}{2M}$ value up to the average experimental 8θ component, and this is thought to be very unlikely.

It is therefore concluded that the effect observed is in fact the $-\frac{K_3}{16}\sin\theta$ term, and it becomes possible to state that the sign of K_3, as observed here, is negative (since the sign of $\frac{K_1^2}{2M}$ is positive). This disagrees with the results of Krause and Patz[K1] and of Hofmann[H10], but probably could agree with Aubert[A4]. It is very difficult to ascribe a value to K_3 because of the uncertainties mentioned above. In particular, it seems that even randomly positive and negative noise contributions to the individual sine and cosine parts of 8θ will always make second order positive contributions to the total 8θ coefficient. The value 0·3 x 10^3 erg/cc could thus be taken as the maximum possible value of $\frac{K_3}{16}$, giving $|K_3| \leqslant 5 \times 10^3$ erg/cc at room

temperature. This is of the same order as both Krause and Patz and Hofmann obtained (3×10^3 erg/cc), but is probably too large compared with Aubert's results. The good agreement in magnitude with Krause and Patz is encouraging, in that they too were deducing their K_3 values from an otherwise unexplained difference in two anisotropy terms. It would not be out of place to quote here their concluding remarks, since they are almost equally applicable to the current result: "Der Fehler muss in unserem Fall jedoch zu etwa $\frac{\Delta K_3}{K_3} = 1{\cdot}00$ angegeben werden, so dass kaum mehr als eine Aussage über das Vorzeichen übrig bleibt." (The probable error assigned to K_3 must be approaching 100%, so that one can say little more than a comment as to the sign of K_3.)

6.3. Results of the Analyses.

The values of K_u, K_1, $\frac{K_u}{K_1}$ and the misalignment angle ϕ (measured from the K_1 easy axis) are given below in table 6.1. for all the films produced, together with details of the production conditions for each. The order of film number is chronological. In the table, POL refers to a polished substrate, and CL to a cleaved one. The residual gas pressure, substrate temperature, deposition rate and deposition field particulars are noted. The

Table 6.1.

Film No.	On or Off Substrate	$K_u \times 10^{-3}$ in erg/cc.	$-K_1 \times 10^{-4}$ in erg/cc.	$\frac{K_u}{K_1}$	ø
		Films on NaCl.			
Ni 8	POL	2×10^{-8} torr	350° C	4½Å/sec	No H
	On	Released on exposure to atmosphere			
	Off	1·07	5·41	0·020	40°
Ni 11	CL	$5\text{-}6 \times 10^{-9}$	300° C	4⅝Å/sec	H along ⟨110⟩
	On	3·69	7·19	0·051	22°
	Off	0·51	5·74	0·009	20°
Ni 20	CL	7×10^{-9}	300° C	6½Å/sec	No H
	On	5·61	8·10	0·069	½°
	Off	1·54	6·64	0·023	20½°
Ni 32	HCL etched	$2\text{-}3 \times 10^{-8}$	365° C	7¼Å/sec	No H
	On	Released on exposure to atmosphere			
	Off	4·28	5·36	0·080	24°
	Annealed	2·21	5·23	0·042	10°
Ni 18	POL	4×10^{-8} O_2	300° C	5½Å/sec	H along ⟨110⟩
	On	6·72	9·00	0·075	1°
	Off	8·13	5·78	0·141	19°
Ni 17	POL	2×10^{-7} O_2	300° C	5½Å/sec	H along ⟨110⟩
	On	3·84	6·84	0·056	4½°
	Off	3·49	5·70	0·061	3°

Table 6.1. (Cont.)

Ni 15	POL	1×10^{-6} O_2	300° C	4Å/sec	H along ⟨110⟩
	On	2·56	7·82	0·033	12°
	Off	5·16	5·97	0·087	12°
	Annealed	2·65	5·65	0·047	22°
Ni 21	POL	7×10^{-6} O_2	300° C	7½Å/sec	H along ⟨110⟩
	On	2·79	4·17	0·067	25°
	Off	2·90	3·32	0·087	33½°
Ni 22	POL	6×10^{-6} O_2	300° C	4Å/sec	H along ⟨110⟩
	On	8·95	7·77	0·12	31½°
	Off	1·57	4·53	0·035	10°
Ni 34	CL	2×10^{-5} O_2	300° C	4Å/sec	No H
	On	Released on exposure to atmosphere			
	Off	1·96	6·02	0·033	5°
Ni 35	CL	2×10^{-5} O_2	300° C	5⅜Å/sec	H along ⟨110⟩
	On	1·61	8·93	0·018	42°
	Off		Damaged		
Ni 36	CL	2×10^{-5} O_2	305° C	6⅜Å/sec	H along ⟨110⟩
	On	4·65	7·60	0·061	2°
	Off	1·19	6·08	0·020	23°

Table 6.1. (Cont.)

Ni 16	POL	$1 \cdot 2 \times 10^{-6}$ N_2	300° C	$5\frac{3}{4}$Å/sec	H along ⟨110⟩
	On	Accidentally released			
	Off	2·64	5·26	0·050	27°
Ni 37	CL	2×10^{-5} N_2	300-340° C	6Å/sec	H along ⟨110⟩
	On	4·35	7·60	0·057	10°
	Off	1·88	6·45	0·029	20°

Table 6.1. (Cont.)

Films on LiF.

Ni 23	CL	1×10^{-8}	350° C	5Å/sec	No H
	On	1·64	5·35	0·030	22°
Ni 25	CL	$5\text{-}10 \times 10^{-7}$	365° C	9Å/sec	No H
	On	4·22	7·34	0·058	17°
Ni 26	CL	8×10^{-9}	365° C	7½Å/sec	No H
	On	3·18	7·98	0·040	3½°
Ni 27	CL	$1\text{-}1\frac{1}{2} \times 10^{-8}$	365° C	7Å/sec	H midway between ⟨100⟩ and ⟨110⟩
	On	4·04	7·31	0·055	29°
Ni 28	CL	2×10^{-8}	365° C	7Å/sec	H along ⟨110⟩
	On	2·61	7·73	0·034	21°
Ni 31	CL	$1\text{-}2 \times 10^{-8}$	365°	7Å/sec	H along ⟨110⟩
	On	3·05	7·21	0·042	2°
Ni 29	CL	2×10^{-8}	365°	6Å/sec	H along ⟨100⟩
	On	5·29	7·17	0·074	35°
Ni 30	CL	9×10^{-9}	365°	6Å/sec	H along ⟨100⟩
	On	4·81	7·58	0·063	34°

films fall into two groups, Ni 8-22, Ni 32-37, which were made on NaCl substrates at different pressure, and Ni 23-31, which were on cleaved LiF and with one exception, at U.H.V.

Different aspects of the results are then dealt with in subsequent sections.

6.4. Magnitude of K_1 for Ni.

The values obtained for K_1 from films floated off their substrates and picked up on cleaned glass cover slips are as follows:

Ni	8	$- 5{\cdot}41 \times 10^4$ erg/cc.	
	11	$- 5{\cdot}74$	
	15	$- 5{\cdot}65$	
	16	$- 5{\cdot}26$	
	17	$- 5{\cdot}70$	
	18	$- 5{\cdot}78$	
	20	$- 6{\cdot}64$	rejected.
	21	$- 3{\cdot}32$	rejected.
	22	$- 4{\cdot}53$	
	32	$- 5{\cdot}23$	
	34	$- 6{\cdot}02$	
	36	$- 6{\cdot}08$	
	37	$- 6{\cdot}45$	rejected.

The three rejected values fall too far from the mean value to be acceptable as reliable. The result then becomes:

$$\text{Mean } K_1 = -5{\cdot}54 \times 10^4 \text{ erg/cc.}$$

at 304° K. (If all the films are included, the mean comes to $-5{\cdot}52 \times 10^4$ erg/cc., so it would appear that the rejection mechanism is not biased in one direction or another.)

This value can be compared with all the other recent values for K_1 quoted in the literature:

Author	$K_1 \times 10^{-4}$ erg/cc. @ 300° K.
Aubert (A4) (1968)	-5·0
Tatsumoto et al. (T6) (1965)	-5·6
Krause and Patz (K1) (1965)	-5·0
Rodbell (R1) (1965)	-4·7
Puzei (P7) (1957)	-5·0

The data of Tatsumoto et al. were not regarded as being quite so reliable as that of the others quoted, as they had obtained positive values for K_2, contrary to the currently accepted most probable data. Rodbell's data, though of unquestionable quality, were obtained from microwave resonance experiments, which may not give the same results as static measurements (see discussion in section 3.3. above). Thus, it may be concluded from a consensus of all of the most recent work, that the most likely value of K_1 is $-5{\cdot}0 \times 10^4$ erg/cc. Since the difference from the result obtained here, $-5{\cdot}5 \times 10^4$ erg/cc., was rather larger than

could be explained by the errors in the present experiment, a source for this discrepancy was sought.

6.4.1 Intrinsic and Effective Magnetic Anisotropy.

The magnetic anisotropy of an undeformed single crystal is known as the intrinsic magnetic anisotropy. An undeformed crystal is one which has not been allowed to deform either due to magnetostriction or to externally applied stresses. The effective anisotropy of a single crystal which has been permitted to deform freely is the sum of the intrinsic anisotropy and contributions from the magnetostriction and/or applied stress. It is fortunate that the effective anisotropy energy and the intrinsic anisotropy energy can be simply expressed in the same form with respect to the direction cosines α_i, as was shown by Kittel[K9]:

$$\text{i.e., } (E_K)_{\text{intrinsic}} = (K_1)_{\text{int.}}(\alpha_1^2\alpha_2^2 + \alpha_2^2\alpha_3^2 + \alpha_3^2\alpha_1^2) + (K_2)_{\text{int.}}\alpha_1^2\alpha_2^2\alpha_3^2 + \ldots$$

$$\text{or } (E_K)_{\text{effective}} = (K_1)_{\text{eff.}}(\alpha_1^2\alpha_2^2 + \alpha_2^2\alpha_3^2 + \alpha_3^2\alpha_1^2) + (K_2)_{\text{eff.}}\alpha_1^2\alpha_2^2\alpha_3^2 + \ldots$$

as appropriate. This means that the term $(K_1)_{\text{eff.}} - (K_1)_{\text{int.}}$ is a constant independent of α_i. The evaluation of this difference

was first performed to first order only by Becker and Döring[B7], (p. 145) and by Kittel[K9]. More recently, Baltzer[B9] has produced an expression for this difference to 2nd order in K (i.e., 6th order in α):

$$(K_1)_{eff.} - (K_1)_{int.} = (C_{11} - C_{12})(h_1^2 + \tfrac{7}{3}h_1h_4 - h_1h_6 - h_4h_6) - 2C_{44}h_2^2 + 3(C_{11} + 2C_{12})(\frac{h_3^2}{5} + \frac{h_3h_8}{105})$$

where the C are the standard elastic moduli of the crystal and the h_i the usual magnetostriction constants.

When magnetic measurements are normally made, no external constraints are usually applied, and the sample is allowed to deform freely due to magnetostriction, thereby involving the effective anisotropy constants. This is the situation in all the experiments mentioned above, from which K_1 data has been derived. Now, in the present experiments, the Ni films were floated off the substrate and mounted on cover slips which had been previously well cleaned, using both ultrasonic and vapour degreasing techniques. Under these conditions, the films were found on drying to adhere extremely tightly to their new substrates, (c.f. Boyd[B12]), so much so that even prolonged soaking in water subsequently failed to detach any part of the film from the glass. It is therefore proposed that such films

are so constrained to the substrate as to approximate the case of the undeformed single crystal. The measured anisotropy constant in this case is therefore the intrinsic K_1. Some values are now inserted into Baltzer's expression to determine the magnitude of $(K_1)_{eff.} - (K_1)_{int.}$. The terms involving h_6 and h_8 are neglected since no data is available on these. The elastic constants of Alers et al.[A7] and the magnetostriction data of Benninger and Pavlovic[B13] are used, these being the most reliable currently available. Substituting:

$$C_{11} - C_{12} = 1{\cdot}008 \times 10^{12} \text{ dyne/cm}^2$$

$$C_{44} = 1{\cdot}235 \times 10^{12} \text{ dyne/cm}^2$$

$$C_{11} + 2C_{12} = 5{\cdot}508 \times 10^{12} \text{ dyne/cm}^2$$

$$h_1 = -85 \times 10^{-6}$$

$$h_2 = -41 \times 10^{-6}$$

$$h_3 = -4 \times 10^{-6}$$

$$h_4 = -9 \times 10^{-6}$$

whence $(K_1)_{eff.} - (K_1)_{int.} = +4{\cdot}9_8 \times 10^3$ erg/cc.

(If the 2-constant expression is used, this difference comes to only $+3{\cdot}1_3 \times 10^3$ erg/cc.)

When this adjustment is made to the K_1 value from this experiment, in order to obtain $(K_1)_{eff.}$, the result becomes:

$$K_1 = -5{\cdot}0_4 \times 10^4 \text{ erg/cc.}$$

in good agreement with the most reliable results at present available.

6.5. The Effects of Stress on K_1.

Because of the qualifications made in section 6.1.1. about the lack of reliability of NaCl substrates for maintaining the film-substrate bond against the effects of film stress, only the LiF films are used for the primary quantitative measurements of stress effects.

As derived in section 2.4.1., an isotropic planar stress, σ, in the film will produce an extra contribution to K_1, of magnitude $\sigma(\frac{2}{3}h_4 - 2h_3)$. The values of K_1 obtained from the films on their LiF substrates are:

	$K_1 \times 10^{-4}$ in erg/cc.	
Ni 23	- 5·35	..... rejected
25	$-7{\cdot}33_5$	
26	- 7·98	
27	- 7·31	
28	- 7·73	
29	- 7·20	
30	- 7·17	
31	- 7·58	

Ni 23 was rejected by electron microscopic inspection, where it was seen to have some areas of (111) orientation. The

torque curve also showed an abnormally large 8θ component (10% of the 4θ component). From the remaining films, the mean value of K_1 is $-7{\cdot}52 \times 10^4$ erg/cc. Subtracting from this the intrinsic K_1 value obtained above, the stress contribution to K_1 becomes $-2{\cdot}0 \times 10^4$ erg/cc.

$$\therefore \sigma(\tfrac{2}{3}h_4 - 2h_3) = -2 \times 10^4 \text{ erg/cc.}$$

The two most recent sets of data for the magnetostriction constants are by Tatsumoto et al.[T7] (1965) and by Benninger and Pavlovic[B13] (1967). The discrepancy between them is so great that one of them must be regarded as far less reliable. Birss and Wallis[B14] have preferred to use Benninger and Pavlovic's results because they were performed at higher field and were a least squares fit from data obtained on disc shaped specimens, rather than differencing measurements on rods. They are also substantially in agreement with the previously best available data, by Bozorth and Hamming[B15].

$$\therefore \text{ Substituting in } h_3 = -4{\cdot}0 \times 10^{-6}$$

$$\text{and } h_4 = -9{\cdot}0 \times 10^{-6}$$

from Benninger and Pavlovic, the result is:

$$\sigma = -1{\cdot}0 \times 10^{10} \text{ dyne/cm}^2$$

This result agrees exactly with the stress obtained by Freedman[F5] by direct X-ray observation of the strain in his Ni films on NaCl.

It is also interesting to note that by the current calculation, he obtained a value for σ of -7×10^{10} dyne/cm^2, having only Bozorth and Hamming's h values at his disposal (and admittedly, a ΔK_1 twice as large as the one obtained here). Tolutaka et al.(T8) have obtained for permalloy films evaporated at 400° C on to (110) LiF faces, a value $\sigma = -1{\cdot}8 \times 10^{10}$ dyne/cm^2, again in fair agreement with the present result.

The result here is within the elastic limit of nickel films, of $\sigma \approx 1{\cdot}3 \times 10^{10}$ dyne/cm^2 as obtained by Grunes(G2). Existing data for the so-called intrinsic stress in Ni films is of little use in the present case. All available data are for films on glass, and with the exception of Prutton's(P8) results (for permalloy), and Klokholm and Freedman's(K10), do not extend to sufficiently high temperature to be of any use. Even in these two cases, no guidance is given at all as to the origins of the component parts of the stress observed, but in any case it appears to be comparatively small (1×10^9 dyne/cm^2) in the region of 300° C substrate temperature. It would therefore appear that no great error would be incurred by assuming, after Freedman(F5), that the origin of the stress in this experiment lies in the differential thermal expansions of the LiF and Ni.

To calculate the strains, ε, classical elasticity theory is used:

$$\varepsilon_x = S_{11}\sigma_x + S_{12}\sigma_y$$

$$\varepsilon_y = S_{12}\sigma_x + S_{11}\sigma_y$$

$$\varepsilon_z = S_{12}\sigma_x + S_{12}\sigma_y$$

where the S_{ij} are elastic compliances. ($\sigma_z = 0$ since the film is unconstrained normal to its surface. ε_z is then simply the Poisson contraction due to ε_x and ε_y.)

$$\varepsilon_x = \varepsilon_y \text{ by symmetry.}$$

$$\therefore \sigma_x = \sigma_y = \frac{\varepsilon_x}{S_{11} + S_{12}}$$

(Note that $\frac{1}{S_{11} + S_{12}}$ is simply E, Young's modulus.)

Using the data of Alers et al.[A7] and the relationships:

$$S_{11} = \frac{C_{11} + C_{12}}{(C_{11} - C_{12})(C_{11} + 2C_{12})} \text{ and } S_{12} = \frac{- C_{12}}{(C_{11} - C_{12})(C_{11} + 2C_{12})},$$

the result for Ni at 300° K is:

$$S_{11} = 0.722 \times 10^{-12} \text{ cm}^2/\text{dyne}$$

$$\text{and } S_{12} = - 0.270 \times 10^{-12} \text{ cm}^2/\text{dyne}.$$

$$\therefore \varepsilon_x = 0.452 \times 10^{-12}\sigma$$

$$= - 4.52 \times 10^{-3}$$

$$= \left[\left(\frac{\Delta l}{l}\right)_{Ni} - \left(\frac{\Delta l}{l}\right)_{LiF}\right] \Delta T$$

where the $\frac{\Delta l}{l}$ are expansion coefficients and ΔT is the temperature range over which the substrate with bonded film

must cool in order to set up the strain ε_x. This ΔT is the object of the calculation. Since the $\frac{\Delta l}{l}$ are temperature dependent, it is necessary to use a trial and error method of selecting the correct temperature range to give values of the $\frac{\Delta l}{l}$ which then produce a value for ΔT from the above equation, consistent with the original choice of the temperature range for the $\frac{\Delta l}{l}$.

The $\frac{\Delta l}{l}$ are taken from Combes et al.(C12) for the LiF, and from a consensus of a number of different tables for Ni.

Between 20° and 180° C, $\left(\frac{\Delta l}{l}\right)_{LiF} = 41 \times 10^{-6}$

and $\left(\frac{\Delta l}{l}\right)_{Ni} = 13\frac{3}{4} \times 10^{-6}$

$\therefore \left(\frac{\Delta l}{l}\right)_{Ni} - \left(\frac{\Delta l}{l}\right)_{LiF} = -27\frac{1}{4} \times 10^{-6}$

$$\therefore \Delta T = \frac{-4{\cdot}52 \times 10^{-3}}{-27\frac{1}{4} \times 10^{-6}}$$

$$\approx 165 \text{ deg. C}$$

i.e., $T_{constraint} \approx 190°$ C.

This temperature is well below the substrate temperature of 365° C. Its significance is, therefore, that the film-substrate combination cools quite considerably before the film-substrate bond is established, and that, as suggested by West(W5) in his theory, the constraint temperature is not

necessarily equal to the substrate temperature.

It therefore is of interest to see how this "constraint temperature" compares with the constraint temperature derived from the magnitude of the uniaxial anisotropy set up in the films.

6.5.1. The Effects of Stress on K_u.

Chikazumi[C13] was the first to show that the magnitude of an induced uniaxial anisotropy depends upon the direction of application of the annealing field for a process such as pair-ordering, which involves direction cosines of magnetisation within the single crystal sample. He later showed a similar effect with pure monocrystal Ni films[C14], without specifying the origin of the anisotropy.

The general expression for the constraint energy of a cubic single crystal is given by West[W5] as:

$$W(\alpha_i\,\beta_i) = -\frac{9}{4}(C_{11} - C_{12})\lambda_{100}\lambda_{100}^{1}(\alpha_1^2\beta_1^2 + \alpha_2^2\beta_2^2 + \alpha_3^2\beta_3^2) - 9C_{44}\lambda_{111}\lambda_{111}^{1}(\alpha_1\alpha_2\beta_1\beta_2 + \alpha_2\alpha_3\beta_2\beta_3 + \alpha_3\alpha_1\beta_3\beta_1)$$

where the α and β are direction cosines of M_s at T and T^1, the measuring and constraint temperatures respectively. Now, because of the dependence of W on β_i, the constraint anisotropy of a single crystal will vary with the crystallographic direction of the applied field used to establish the mechanism. The full

derivation of this effect for a (100) type of film is carried out in appendix 5, and the result shows two particularly simple cases, as might be expected. When H lies along a cube edge, the anisotropy energy is:

$$(E_K)_{100} = -\frac{9}{4}(c_{11} - c_{12})\lambda_{100}\lambda_{100}^{1}\cos^2\theta$$

where θ is the angle M_s makes with the uniaxial easy axis (the cube edge). When H lies along a $\langle 110 \rangle$ direction, the anisotropy energy is:

$$(E_K)_{110} = -\frac{9}{2}c_{44}\lambda_{111}\lambda_{111}^{1}\cos^2\psi$$

where ψ is the angle M_s makes with the uniaxial easy axis (the $\langle 110 \rangle$ direction). Thus, the anisotropy constants depend on the direction of applied field during deposition:

$$\text{e.g., } (K_u)_{100} = -\frac{9}{4}(c_{11} - c_{12})\lambda_{100}\lambda_{100}^{1}$$

$$\text{and } (K_u)_{110} = -\frac{9}{2}c_{44}\lambda_{111}\lambda_{111}^{1}$$

(These results could have been deduced on sight from Baltzer's[B9] expression for the effective anisotropy energy within a domain wall. Indeed, Baltzer's 180° domain wall is exactly analogous to the magnetostrictive constraint mechanism, in that within the wall, M_s has to rotate against the magnetostrictive effects of a constant elastic deformation resulting from the magnetostriction in the two antiparallel domains on either side of the wall.)

From the K_u results on films Ni 28 - 31, the following averages are obtained:

$$(K_u)_{100} = 5{\cdot}0 \times 10^3 \text{ erg/cc.}$$

$$(K_u)_{110} = 2{\cdot}8 \times 10^3 \text{ erg/cc.}$$

$$\therefore\ 5{\cdot}0 \times 10^3 = -\frac{9}{4}(C_{11} - C_{12})\lambda_{100}\lambda_{100}^{1}$$

$$\text{and } 2{\cdot}8 \times 10^3 = -\frac{9}{2}C_{44}\lambda_{111}\lambda_{111}^{1}$$

From the data of Birss and Lee[B16], the values of λ_{100} and λ_{111} at 300° K are $-50{\cdot}6 \times 10^{-6}$ and $-23{\cdot}3 \times 10^{-6}$ respectively. Using the data of Alers et al.[A7],

$$C_{11} - C_{12} = 1{\cdot}008 \times 10^{12} \text{ dyne/cm}^2$$

$$\text{and } C_{44} = 1{\cdot}235 \times 10^{12} \text{ dyne/cm}^2,$$

the following is obtained for the unknowns λ_{100}^{1} and λ_{111}^{1}:

$$\lambda_{100}^{1} = -\frac{5{\cdot}0 \times 10^3}{\frac{9}{4} \times 1{\cdot}008 \times 5{\cdot}06 \times 10^7} = -43{\cdot}6 \times 10^{-6}$$

whence T = 110° C.

$$\lambda_{111}^{1} = -\frac{2{\cdot}8 \times 10^3}{\frac{9}{2} \times 1{\cdot}235 \times 2{\cdot}33 \times 10^7} = -21{\cdot}7 \times 10^{-6}$$

whence T = 85° C

More reliance for a mean value of T constraint was placed on the ⟨100⟩ result (110° C) than on the ⟨110⟩ (85° C), since

the angular position of the uniaxial easy axis was more consistent with theory for the ⟨100⟩ cases, the misalignment from the cube edges being only 10° and 11° in the two films produced.

Comparing this result with the constraint temperature of 190° C derived from the stress effect of ΔK_1, the agreement is considered to be very reasonable for a number of reasons.

In the first place, looking at the problem the other way round, if the value $T_{constraint} = 190°$ C is used, what values for $(K_u)_{100}$ and $(K_u)_{110}$ are expected? From the data of Birss and Lee(B16), at 190° C,

$$\lambda_{100} = -32{\cdot}0 \times 10^{-6}$$
$$\lambda_{111} = -17{\cdot}3 \times 10^{-6}$$

from which on substitution are obtained the values:

$$(K_u)_{100} = 3{\cdot}7 \times 10^{3} \text{ erg/cc.}$$
$$(K_u)_{110} = 2{\cdot}2_5 \times 10^{3} \text{ erg/cc.}$$

i.e., approximately $\frac{2}{3}$ the experimentally obtained values. The first suggestion, therefore, is that in assuming that the whole of K_u in the LiF films is due to the constraint term, too low a value of $T_{const.}$ has resulted. A small contribution to $(K_u)_{stress}$ of only 500 erg/cc from another source aligned with K_{stress} would bring the values of $T_{const.}$ up to 140° C and 190° C for the ⟨100⟩ and ⟨110⟩ cases respectively, in much better

agreement with the ΔK_1 constraint temperature. Such a small contribution could readily be ascribed to an imperfection ordering mechanism. No attempt could be made to anneal out this contribution since an anneal may also affect the constraint term itself and so render the result useless.

Another suggestion on these lines comes from a consideration of the magnitude of the anisotropic stresses involved in producing the K_u. These are calculated to be about 7×10^7 dyne/cm^2 for both of the K_u orientations, i.e., over 2 orders of magnitude less than the isotropic stress. It is thus feasible that even only a tiny directional inhomogeneity in the substrate structure could cause an anisotropic stress large enough to affect K_u. Such a source of inhomogeneity could, for instance, be found in the cleavage steps on the LiF substrates. (Misorientation of parts of the film would produce a biaxial anisotropy, and so would affect K_1 but not K_u.)

The third possibility is that not all of the isotropic stress is indeed due to thermal expansion effects between film and substrate, as assumed in section 6.5., and that intrinsic stress also contributes to σ. If this is so, then it is difficult to understand why such a similar value for σ ($-1{\cdot}1 \times 10^{10}$ dyne/cm^2) is obtained from the NaCl results (to be discussed in the next section), when:

a) the lattice misfit of Ni on LiF is only 14% compared with 60% for Ni on NaCl;

b) the defect density, perhaps as a result of a), and perhaps as a result of the higher substrate temperature used, was much lower for the LiF films than for the NaCl films under equivalent vacuum conditions.

This suggestion is therefore rejected.

The fourth, and probably major part of the discrepancy, lies in the accuracy of the h_3 and h_4 values used to calculate σ. Measurements of the magnetostriction constants beyond h_2 are notoriously difficult. h_4 and h_5 are particularly susceptible to experimental error (Baltzer[B9]). Indeed, Bozorth and Hamming had put probable errors of 130% and 70% respectively on h_3 and h_4, so that, as pointed out by Freedman[F5], the error in the combination $(\frac{2}{3}h_4 - 2h_3)$ could well be several hundred percent. It is in this respect that Benninger and Pavlovic's[B13] data have produced such an improvement of the present author's estimation of σ over that of Freedman, since their data was taken from smooth continuous curves of the h with temperature, whilst Bozorth and Hamming's were a single determination at room temperature. Benninger and Pavlovic were even able to detect the presence of h_6 and h_7, thereby indicating the high accuracy of their experiments. For this

reason, the probable error in σ obtained by using their magnetostriction data was only in the region of a few tens of percent.

Certainly, the reasonable consistency of the change of K_u with field angle suggests that this is not badly in error, and that the greater part of the $T_{const.}$ discrepancy arises from errors in the estimation of σ. This is also indicated by the fact that film Ni 27, produced in a field midway between $\langle 100 \rangle$ and $\langle 110 \rangle$ type directions, showed an intermediate K_u value and orientation angle.

The only doubtful feature of the experiment is that it is the measured value of misorientation angle which should determine the magnitude of K_u, and not the actual applied field direction. Only one of the films, Ni 28, showed any great error however ($\phi = 21^\circ$ instead of 0°). This problem will be discussed further in the section below on the NaCl results.

In conclusion, a constraint temperature for Ni films grown on LiF under U.H.V. conditions of probably no more than 150° C has been established. One consequence of this is a reinterpretation of the effect, observed by Freedman, that the effect of stress on K_1 was independent of substrate temperature above about 250 - 300° C. This he interpreted as the effect of plastic flow in the film once the limit of elasticity had been

exceeded. It is apparent from the present work that this is not necessarily so, and that the independence of the σ of substrate temperature is simply because the true constraint temperature is well below that of the substrate.

6.6. Stress effects on K_1 of films grown on NaCl

The values of K_1 for films before removal from their NaCl substrates were as follows:

	$K_1 \times 10^{-4}$ erg/cc		Preparation conditions
Ni11	7.19		U.H.V.
15	7.82		1×10^{-6} O_2
17	6.84		2×10^{-7} O_2
18	9.00		4×10^{-8} O_2
20	8.10		U.H.V.
21	4.17	. . . . rejected	7×10^{-6} O_2
22	7.77		7×10^{-6} O_2
35	8.93		2×10^{-5} O_2
36	7.60		2×10^{-5} O_2
37	7.60		2×10^{-5} N_2

Film Ni21 was rejected outright, as in section 6.4 as its K_1 values were much too low for it to be regarded as a "well behaved" sample ferromagnetically. After consideration Ni18 and Ni35 were also rejected for the purpose of calculating the mean K_1. The value for Ni35 could have been accounted for by the presence of an abnormally high constraint temperature (c 275°C), since the associated value of K_u on the substrate

was exceptionally low. This would indicate a very energetic substrate-film bond which could perhaps be attributed to substrate contamination conditions peculiar to that particular evaporation. No such correlation between K_1 and K_u could, however, be found for Ni18. One possible cause for any of the rejections could be an inaccurate estimation of the film thickness, this being the only experimental measurement not carried out by the author. Certainly, in the case of Ni21 the errors could be attributed to an incorrect thickness being given, since the K_1 values both on and off the substrate were below the expected values by equal proportions. There was very little trace of polycrystalline Ni which could also have caused such an error in the K's.

The mean K_1 of the remaining films was 7.56×10^4 erg/cc, corresponding to an isotropic stress, σ, of about $-1.0_2 \times 10^{10}$ dyne /cm^2. Taking the temperature range 20 - 180°C, $(\frac{\Delta l}{l})_{Ni} - (\frac{\Delta l}{l})_{NaCl}$ is calculated as $27\frac{3}{4} \times 10^{-6}$.

$$\therefore \quad 1.02 \times 10^{10} = \frac{27\frac{3}{4} \times 10^{-6}}{0.452 \times 10^{-12}} \cdot \Delta T.$$

whence ΔT = 167 deg. C.

i.e. $T_{constraint} \approx 195°C$

- almost exactly as obtained for the LiF substrates. Indeed, it would have been considered strange if the result had been otherwise. Whether the nature of the film-substrate bond is a chemi-sorption process or a Van der Waals type of force, the differences between the properties of the various alkali halides would not be expected to be significant enough to materially alter this bond.

After measurement on the substrate, the films were floated off in distilled water and picked up on cleaned glass cover slips. When first picked up on the cover slips, the films are separated from the slip by a layer of water. It was noticed that the films exhibited a convex shape, and this was attributed to strain resulting from the compressive stress built into the film during its production whilst flat on its substrate. A simple attempt to obtain a direct measurement of this strain was therefore made on one film (Ni16). After picking up the film, the glass cover slip was supported horizontally and upside down with the film "floating" on its layer ~~surface~~ of water on the bottom surface of the cover slip. A vernier microscope was used to obtain the degree of convexity of the film surface by measuring the excess "height" of the centre of the film below

its edge. This was found to be approximately 0.5 mm. Using the results of appendix 6, this represents the effect of an initial stress in the film of -2×10^{10} dyne/cm^2., which is in order-up-magnitude agreement with σ obtained magnetically.

6.6.1. Stress effects on K_u of films grown on NaCl

As will be observed from the table of film results in section 6.3, there does not appear to be the same sort of correlation as there was for the films on LiF between the values of K_u on the substrates and the angle of applied field during deposition.

In view of the rather large values of K_u in some of the films even after stripping, this in itself cannot be considered significant. If, however, the change in K_u on stripping is observed, then the true contribution to K_u from the constraint theory should be obtained. The addition or subtraction of anisotropies (of the same order only) can be carried out by simple vector addition and subtraction, provided that the angles used in the process are twice the angles actually present between the various easy axes in the film. Even when this construction is performed for each of the films, however, there still appears to be no correlation between the various ΔK_u

and the film preparation conditions. All the ΔK_u, so obtained, with only two exception, fell within the range 2.6 to 4.8×10^3 erg/cc. These results are in agreement, as to magnitude, with the expected values of $K_{constraint}$.

6.7. Residual Anisotropy Mechanisms

The values of K_u obtained after stripping all the films from their NaCl substrates are shown below. They are grouped according to deposition conditions.

a) Grown in U.H.V:

Ni8 POL. 1.07×10^3 erg/cc

11 CL. 0.51 "

20 CL. 1.54

32 HCl etch. 4.28 falling to 2.21×10^3 erg/cc. on anneal.

b) Grown in residual gas pressures quoted:

Ni18	POL	4×10^{-8}	O_2	8.13×10^3 erg/cc
17	"	2×10^{-7}	"	3.49 "
15	"	1×10^{-6}	"	5.16 falling to 2.65 on anneal
21	"	6×10^{-6}	"	2.90 (rising to 4.80 on correction)
22	"	7×10^{-6}	"	1.57
34	CL	2×10^{-5}	"	1.96
36	"	2×10^{-5}	"	1.19

Ni16	POL.	1~2 x 10^{-6}	N_2	2.64
37	CL.	2 x 10^{-5}	"	1.88

The U.H.V. results are considered first. Two of them, Ni8 and Ni11, showed, for Ni films, remarkably low levels of uniaxial anisotropy. In the case of Ni11, K_u was only 500 erg/cc., i.e. less than 1% of K_1. This was approaching the limit of confidence of K_u measurement in the presence of K_1. The micrographs of Ni8 and 11 were very featureless, as observed in fig. 6.1. There were, however, some lattice defects or vacancy agglomerations visible. In this respect, they were a little inferior to the best U.H.V. grown LiF films. Ni32 was a trial film grown on an NaCl substrate which had been treated for 10 secs. with a solution of 2 parts hydrochloric acid to 1 part of water. Such an etchant acts very slowly and controllably on NaCl because of the very high Cl^- ion content of the solution. The aim was to achieve the same surface advantages as obtained with a water etch, but without the accompanying rapid pitting. As seen from the tables, the result was disappointing. The Ni film auto-released from the substrate immediately on exposure to the laboratory air, and the value of K_u was unexpectedly high. A micrograph of the film, shown in fig. 6.1., showed a very grainy structure,

which was nevertheless very well orientated. It was therefore thought that the high K_u could perhaps be associated with some anisotropic structural defect orientation, which was not present (or present to a much lesser extent) in the other U.H.V. grown films. To apply a qualitative test to this suggestion, the film was annealed at 250°C for 10 mins. Care was taken to carefully align the K_u easy axis with the direction of the residual field present, which was due to incomplete cancellation of the substrate heater field, and in any case was less than 1 oe. In this way, it was hoped that no anisotropy changes could occur because of the annealing in of processes in a direction perpendicular to the initial easy axis. The result of the anneal was a reduction of K_u to 2.21×10^3 erg/cc., approaching the low level expected from the other U.H.V. films. It was thus supposed that the reduction in K_u was due to the annealing out of mobile lattice defects which had become anisotropically orientated. Since only one anneal was performed, it was not possible to obtain values of the activation energy and τ for the annealing process.

It is thus reasonable to state that the assumption made in section 2.5.6. is upheld by the results of the U.H.V. grown films - namely, that if a pure Ni film is grown under

U.H.V. conditions, and is then released from its substrate without straining, it shows an exceptionally small uniaxial anisotropy, subject to its possessing a sufficiently high level of structural perfection.

This result in itself is of some importance. It represents the first reported occasion in which such a low level of K_u has been observed in films grown under conditions specifically controlled to prevent any of the proposed mechanisms for K_u from acting.

6.8. The Effects of Deposition Atmosphere on K_u

The majority of the evaporations were performed with a view to determining the effect of the residual gas atmosphere during deposition on the resulting K_u. In view of the importance of oxygen in theories involving residual gas sources of K_u, as discussed in section 2.5.5.4., most of the films were grown in varying partial pressures of oxygen. Two films were also grown in nitrogen atmospheres for comparison purposes.

The first films, Ni13 - 22, grown on polished substrates, showed unexpectedly high residual K_u values, with wide variations from film to film unrelated to evaporation pressure. The high K_u values are explicable if it is assumed that the polishing

process has the same effect on nucleating density for film growth as a water etch-viz, to increase the number of nucleating centres. If this is so, far more defect centres will be formed in the film when the increased number of individual grains grow together. It was for this reason that films Ni34 - 37 were subsequently grown on cleaved substrates. The results are shown in fig. 6.6.

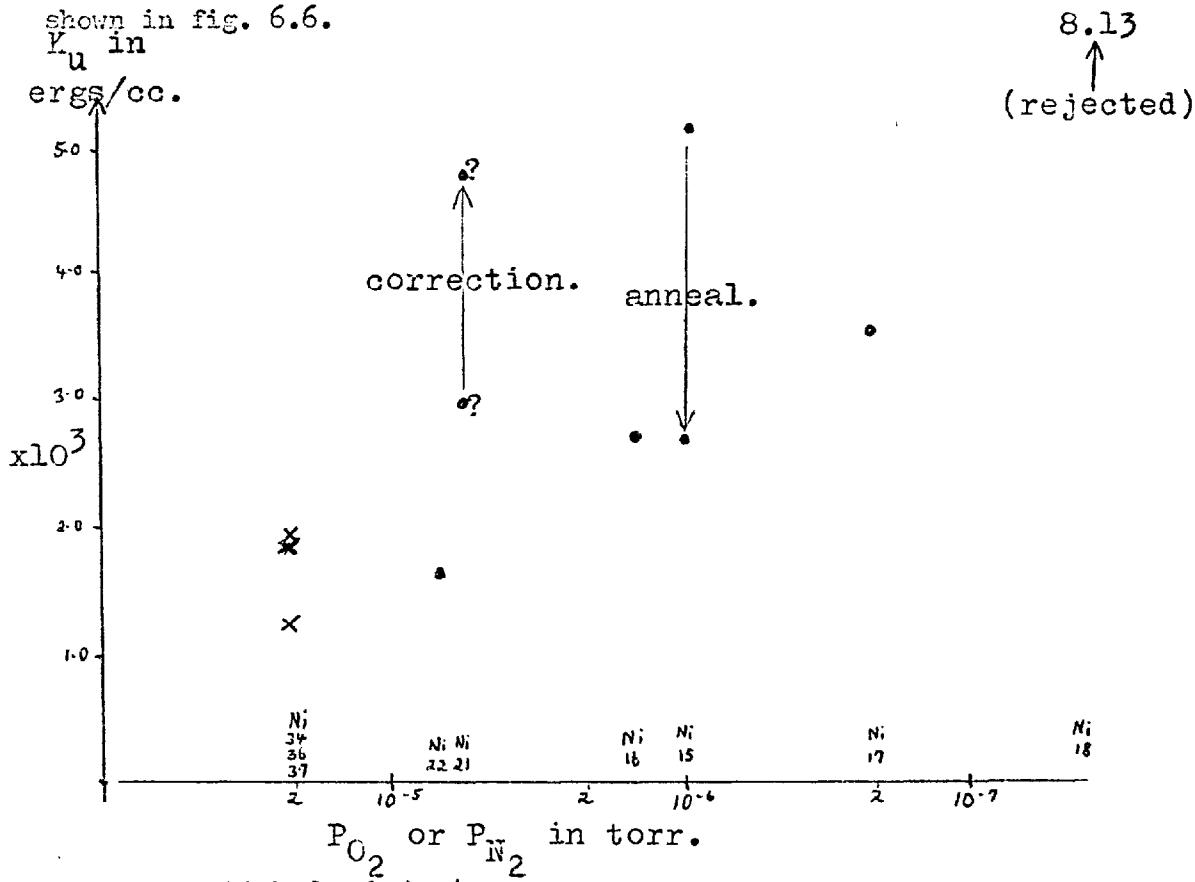

Polished substrates = •

Cleaved substrates = X

Oxygen residual atmosphere in black, • X

Nitrogen " " " red • X

FIG. 6.6.

Ni15 was annealed by exactly the same procedure as that outlined in section 6.7, since it had shown a large increase in K_u on floating off its substrate. The annealed value was a more reasonable result. Ni18 was rejected outright, as in section 6.6, as being much too high a value to be considered realistic. Ni21 is the film whose K_1 values were consistently too low, due perhaps to a faulty thickness estimation. If all the K values of that film are corrected to bring K_1 to its expected value, the value of K_u rises to the position shown on the graph.

There are several significant features of this graph. In the first place, the spread in K_u results on the polished films did not really permit any meaningful conclusion to be drawn from them. The most probable reason for this spread could lie in the varying microstructure from film to film. This must be a result of the random nature of the quality of the NaCl surface after polishing. This contrasts with cleaved surfaces, which, cleavage step density aside, are always of the same nature atomically. More conclusive, however, are the results of the cleaved substrates films. Besides the different substrate surface, another, perhaps significant, detail is that the films were always demagnetised before

removal from the torque magnetometer for floating off after the first measurements. This, it was hoped, would not provide any internal aligning field by means of which a Kneer and Zinn type of constraint mechanism could act on the dislocations formed in the film on floating off. The previous films had always been floated off immediately after removal from the torque magnetometer in a saturated state. Though this suggestion - that the dislocations could be rendered magnetically active in contributing to K_u because of the remanent state of the films -does seem rather remote, all precautions were nevertheless taken for the final films. The significant feature about the three cleaved films is their closely similar values of K_u, despite the fact that two were grown in 2×10^{-5} torr of oxygen, and one in 2×10^{-5} torr of nitrogen. Indeed, Ni36 and 37 are practically identical magnetically, both on and off their substrates (the former because of the great care taken to shield the films from moisture before insertion in the magnetometer for measurement). In the case of the nitrogen grown film, the partial pressure of oxygen was certainly below 1×10^{-9} torr, since U.H.V. procedures had been followed in all cases before admission of any gas. The oxygen content of the nitrogen itself was quoted by the suppliers as less than 5 parts per million. Thus, these results would appear to suggest strongly that there is

no gross effect of oxygen on K_u, at least up to pressures of 2×10^{-5} torr. Further support for this conclusion is obtained from the fact that the magnitudes of the K_u on these three films were lower than those of the films grown at lower oxygen pressures. Notwithstanding the discussion on defect density above, if some significant oxygen mechanism for K_u were active at 2×10^{-5} torr, it would be expected that the values of K_u would have risen with increasing P_{O_2}.

The fact that the K_u observed for these three "good" films is higher than for the U.H.V. films is quite easily accountable for by the existance of many more opportunities for vacancy and defect ordering than in the case of the U.H.V. films.

The micrographs and diffraction patterns of these films are shown in fig. 6.7. They show that at 2×10^{-5} torr O_2, the oxygen is incorporated in the film mainly as polycrystalline NiO, whilst at 2×10^{-7} torr O_2, the quantity of oxygen involved is so small that it can all easily grow as NiO in an oriented state. The diffraction pattern for Ni37 showed no trace of oxide at all, as expected. The bright and dark field micrographs of Ni36 indicate that at 2×10^{-5}, most of the oxygen

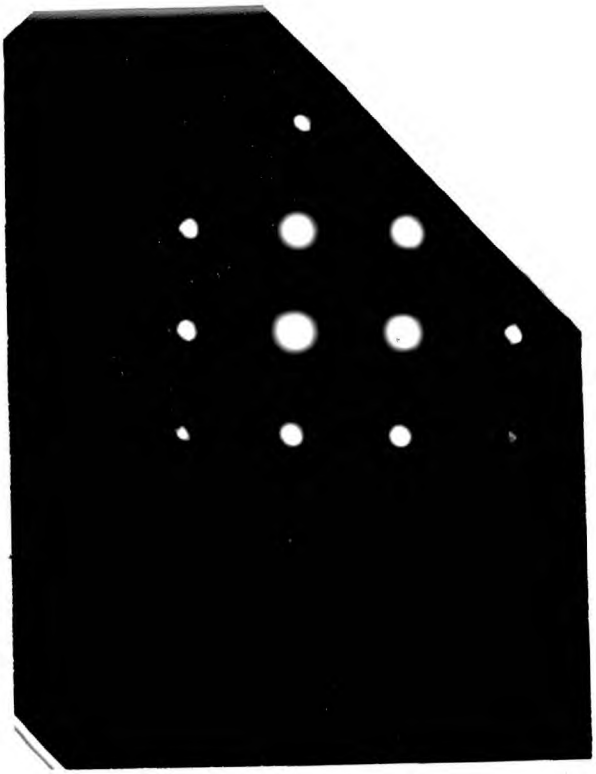

Fig. 6.7 (a).

Ni 37. 2×10^{-5} N_2.

Pattern indistinguishable from U.H.V. films.

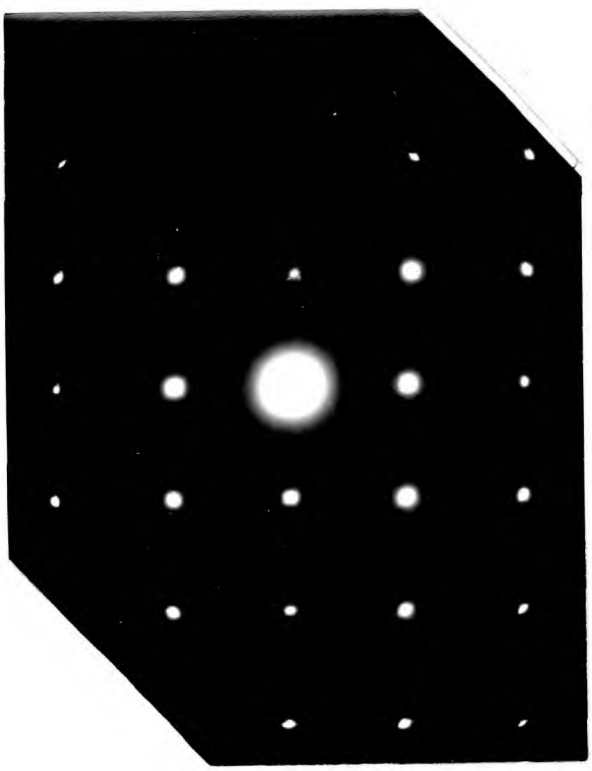

Fig. 6.7 (b).

Ni 17. 2×10^{-7} O_2
Oriented NiO just visible.

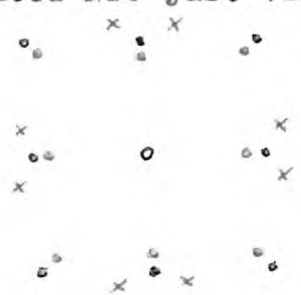

• = Ni (020) & (220) spots
◦ = NiO (020) & (220) spots
× = NiO twin spots on (111) planes

Fig. 6.7(c).

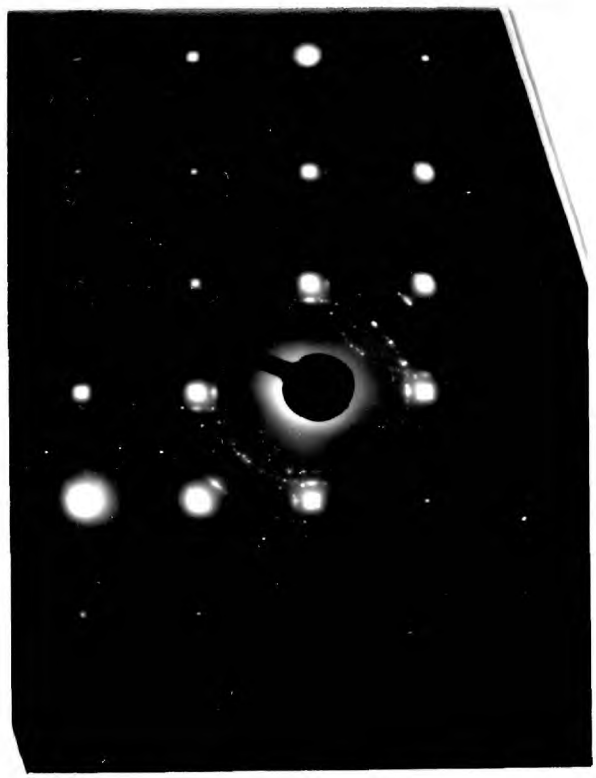

Ni 22.7 x 10^{-6} O_2

Highly orientated poly-crystalline NiO showing.

The (020) type and (220) type NiO spots are clearly visible within their poly-crystalline rings.

Streaking in all four [111] directions is also visible.

Fig. 6.7(d).

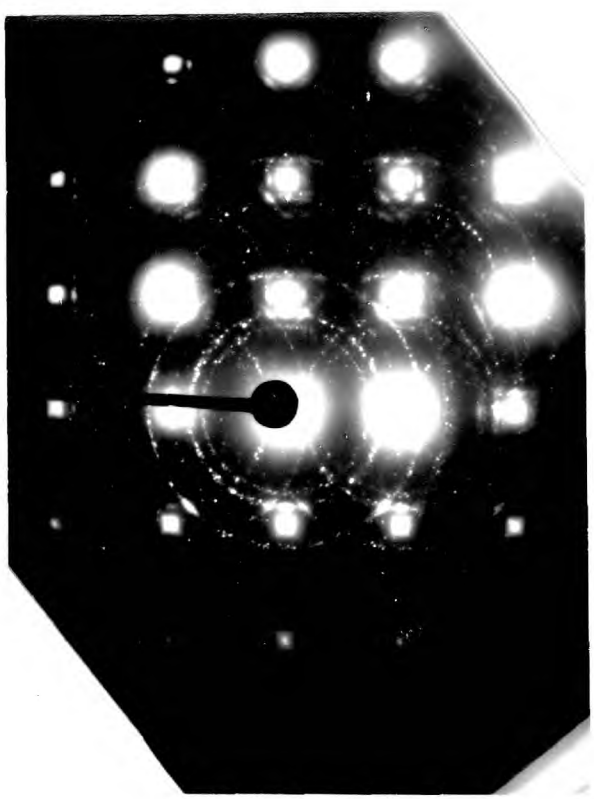

Ni 36 2 x 10^{-5} O_2

High density of Poly-crystalline NiO.

Secondary diffraction patterns from many of the Ni planes.

Some orientated NiO visible in the rings. Innermost ring is probably from NiO twin spots.

Fig. 6.7(e).

Ni 36. $2 \times 10^{-5} O_2$

Mag. = 75,000.

Sharp black areas are probably agglomerates of NiO.

Fig. 6.7(f)

Ni 36.

Mag. = 75,000

Dark field micrograph of the above, using two innermost NiO rings for image formation.

Some of the white areas line up with dark patches in the bright field micrograph.

exists as distinct agglomerations of NiO within the film, but there is also a small percentage distributed throughout the Ni lattice, as is evident from the dark field picture. Electron probe microanalysis was performed on one of the 2×10^{-5} O_2 films, and gave a value of about 5 atomic percent oxygen content, though at this level, the background count is of the same order as the oxygen count, so that this figure may be considerably in error.

It therefore seems that a not insignificant atomic percentage of oxygen, as NiO, is contained within the film lattice, both as orientated and as polycrystalline material, and in both an agglomerated form and diffusely spread throughout the lattice. Additionally, streaking was detected in all four [111] directions. Alessandrini,(A8) in her experiments on the annealing of Ni films in high O_2 partial pressures, has associated this with the lattice distortion caused by the presence of (111) planes of interstitial oxygen. This is thus the extension of Heidenreich and Nesbitt's observations to films. The complex Ni + O phase observed by her was not detected here.

Consequently, it would appear that oxygen is incorporated in the film in almost all the ways possible for it to become so, and yet the films still show, to within the accuracy justified

by the magnetic results, no uniaxial anisotropy specifically attributable to the special effects of this oxygen. It is therefore considered profitable to investigate all the literature references to oxygen mechanisms for K_u, to see how far the present result agrees with previous work.

As already mentioned in section 2.5.5.4., the work of Paul and Hanson (P 6) indicated no distinct oxygen effects on H_k from below 10^{-9} torr to a few x 10^{-5} torr, above which pressure H_k rose. Since the Heidenreich and Nesbitt mechanism needs a minimum oxygen level of only 10 p.p.m. to enable it to operate, Paul and Hanson thought that such a low saturation level may already have been passed in all of their experiments. That this interpretation is unlikely can be deduced from the results of Graham and Lommel,[43] whose Ni films showed no meaningful change in K_u from evaporation pressures of 2 x 10^{-10} to c.10^{-5} torr.

The partial pressures of oxygen at which the various structural effects of oxygen on the Ni lattice were observed by Alessandrini were also in the range from 3 x 10^{-5} torr upwards at 400°C. Such a comparison of pressures is not strictly valid, since the structural effects which she observed were all the result of annealing initially perfect Ni films in varying oxygen

atmospheres and at varying temperatures, rather than processes occuring during film growth itself. It certainly seems reasonable to assume, however, that these effects should be similar to within an order of magnitude measurement of pressure. Thus, the fact that Alessandrini found no structural change in her Ni films if annealed for 1 hour at 500°C in the upper 10^{-6} torr range of oxygen, or for 1 hour at 450° even at 1×10^{-5} torr of oxygen, seems to indicate that oxygen effects are not active in films below this level.

The results of Freedman (F7) on Ni films evaporated at pressures of from $1\frac{1}{2} \times 10^{-9}$ to $3\frac{1}{2} \times 10^{-7}$ torr of oxygen are not directly comparable with the K_u results presented here. Freedman had shown that such a change in oxygen pressure caused a marked shift in the resonance field and in the perpendicular anisotropy. This result is however not unexpected, since both of these measurements are known to be notoricusly sensitive to the presence of the antiferromagnetic NiO, either at the film surface, or at the film substrate interface. Indeed, Lykken et al (L6) had shown that the pinning of spins, probably on antiferromagnetic surfaces, exists in 81/19 permalloy films in a total pressure of only 1×10^{-7} torr, even before the films have been exposed to the atmosphere. The same reservations

apply to the U.H.V. results of Usami et al[U2] who only made $K_{\perp}$ measurements, and by means of resonance techniques.

With regard to the possible effects of the antiferromagnetic NiO on K_u of the Ni films, it should be pointed out that the usual results of a ferromagnetic-antiferromagnetic exchange interaction are twofold.

i) A unidirectional component in the torque curves

ii) Rotational hysteresis even at fairly high fields.

There has been only one reported experimental result in which the exchange interaction gave rise to a uniaxial anisotropy. This was the work of Glazer et al[G4] using NiFe - NiFeMn system. Their results were interpreted in terms of a mechanism proposed earlier by Vlasov et al[V3], which relies on the existence of a low-anisotropy antiferromagnetic region. When the ferromagnetic spins are reversed by means of an external field, the spins of the weakly anisotropic antiferromagnet also rotate 180° because of the exchange coupling. The easy direction controlled by these regions is, therefore, also reversed. Such a small unidirectional anisotropy thus has the same effect in the system as a uniaxial anisotropy. Since, however, in the case of the current author's films, the NiO was certainly very evident, and

if ordered has a very strong anisotropy energy, such a mechanism could be excluded. The very fact that neither rotational hysteresis nor unidirectional torque components were observed seems to imply that the NiO was not formed in a single-domain state, but was ordered in random directions in different parts of the film. This may have been a result of the low value of aligning field used, at least as regards antiferromagnetic ordering experiments.

6.9. Conclusions

Summarising the main features of the experimental results, the following can be stated:

1) Single crystal nickel films show magnetic behaviour in excellent agreement with bulk material as far as the magnetocrystalline anisotropy and magnetostriction properties are concerned.

2) Films grown under sufficiently rigorous conditions, as specified above, show exceptionally small values of uniaxial anisotropy.

3) The effects of stress mechanisms, both on K_1 and on K_u are well understood. In particular, a constraint temperature well below the substrate temperature during evaporation has been established.

4) There seems to be no contribution to K_u, within the limits of the experimental accuracy, from mechanisms involving impurity oxygen in these films. This may not be the situation in films which have monodomain ordered NiO present.

5) The effects of lattice imperfections and impurities (other than the special effects of oxygen) are quite important in the as-grown films, and can be the predominant K_u source. In this respect, imperfections arising from the growth mechanism itself seem more important than imperfections arising from included gas atoms, or the effects of the gas atoms themselves.

Appendix A1

Computational Method for Fourier Analysis

The method first used was a library subroutine entitled FORIT, from the I.B.M. 360 series scientific package. This programme uses a recursive technique devised by Goertzel, and described in "Mathematical Methods for Digital Computers", edited by A. Ralston and H. Wilf, John Wiley, New York, 1960. The results using this programme, showed, however, large deviations from the expected results, this being particularly noticeable in the large magnitude of the higher order terms, which were nominally zero. In order to test the programme therefore, calculated values of a known function were inserted. The function used was

$$f = \sin\theta + 0.5 \sin 2\theta$$

On inserting values of f to four significant figures for every 10° degrees (i.e. 36 points), the resulting output was:

J = 1 A(J) = 0.0000 B(J) = -0.

J = 2 A(J) = 0.0850 B(J) = 0.9984

J = 3 A(J) = 0.0765 B(J) = 0.4462

J = 4 A(J) = -0.0141 B(J) = -0.0543

J = 5 A(J) = -0.0114 B(J) = -0.0322

J = 6 A(J) = -0.0105 B(J) = -0.0233

The output should have been B (J) = 1.0000 for J = 2, B (J) = 0.5000 for J = (3) and all other coeffs. zero. In fact, errors of up to 10% were occuring in some of the coefficients. In an attempt to find

the source of these errors, the number of input points was doubled to 72, i.e. every 5°. The output was then:

J = 1	A(J) = 0.0000	B(J) = -0.
J = 2	A(J) = 0.0431	B(J) = 1.0007
J = 3	A(J) = 0.0410	B(J) = 0.4754
J = 4	A(J) = -0.0035	B(J) = -0.0273
J = 5	A(J) = -0.0029	B(J) = -0.0166
J = 6	A(J) = -0.0027	B(J) = -0.0122

As is observed, the errors are approximately halved, but were still surprisingly high. The reason for this level of error was not fully understood. The method uses as its starting point the classical solution for a Fourier analysis:

$$a_r = \frac{2}{n} \sum_{k=0}^{n-1} f_k \cos \frac{2\pi kr}{n}$$

$$b_r = \frac{2}{n} \sum_{k=0}^{n-1} f_k \sin \frac{2\pi kr}{n}$$

$$a_o = \frac{1}{n} \sum_{k=0}^{n-1} f_k$$

The only possible suggestion is that in the attempt to make the method universally applicable to any order of analysis, the recursive relationships used have necessitated loss of accuracy

when only a finite number of input points are used, however accurately those points may be specified.

An alternative method was therefore sought. A suitable method was found in "The Calculus of Observations" by E. Whittaker and G. Robinson, Blackie, London, 1944.

Starting with the expressions mentioned above, substitutions were made for n = 12, i.e. for input points every 30°, and from the series of equations so produced, an ingeneous table was drawn up which enabled the coefficients to be rapidly calculated up to 6th. order (see p. 270 of Whittaker and Robinson). The table was, of course, designed for hand computation, but a simple transcribing process soon enables it to be converted into a programming language. Since this method is really a trigonometric interpolation, i.e. finding a trigonometric series with a finite number of terms which fits a given finite number of data points, rather than a true Fourier Analysis, it was expected to be more accurate for the problem in hand. Indeed, insertion of the test function calculated every 30°, i.e. 12 points, accurate to only 2 significant figures, produced the output:

J = 1	A(J) = -0.	B(J) = 0.
J = 2	A(J) = 0.	B(J) = 0.9994
J = 3	A(J) = 0.	B(J) = 0.4994
J = 4	A(J) = -0.	B(J) = -0.0000
J = 5	A(J) = 0.	B(J) = -0.0029
J = 6	A(J) = -0.	B(J) = 0.0006
J = 7	A(J) = 0.	B(J) = 0.

This was thus regarded as a totally satisfactory method. Since the data from the torque magnetometer was obtained effectively every 10° (really every 5°, but over only 180°), three interlocking analyses (called phases of the computation in this programme) of every third point of the data were performed, the origin moving 10° (5° in reality) between each phase.

Appendix A.2. Evaluation of torque expression for mixed uniaxial and biaxial anisotropies in non-infinite field.

For a (100) plane measurement on a cubic crystal whose uniaxial anisotropy is aligned along a cube edge:

$$E_K = K_u\sin^2\theta + K_1\sin^2\theta.\cos^2\theta + \ldots$$

$$\therefore -L = K_u\sin 2\theta + \frac{K_1}{2}\sin 4\theta$$

Substituting $\alpha = -\frac{L}{MH} = \frac{K_u\sin 2\theta + \frac{1}{2}K_1\sin 4\theta}{MH}$:

$$-L = K_u\sin\left(2\theta + \frac{2K_u\sin 2\theta + K_1\sin 4\theta}{MH}\right) + \frac{K_1}{2}\sin\left(4\theta + \frac{4K_u\sin 2\theta + 2K_1\sin 4\theta}{MH}\right)$$

Rearranging the first term, the following is obtained:

$$K_u\sin 2\theta.\cos\tfrac{1}{MH}(2K_u\sin 2\theta + K_1\sin 4\theta) + K_u\cos 2\theta.\sin\tfrac{1}{MH}(2K_u\sin 2\theta + K_1\sin 4\theta)$$

Expanding the small angle sine and cosine terms:

$$K_u\sin 2\theta.\left(1 - \frac{1}{M^2H^2}(4K_u^2\sin^2 2\theta + K_1^2\sin^2 4\theta + 4K_uK_1\sin 2\theta.\sin 4\theta)\right)$$
$$+ K_u\cos 2\theta.\frac{1}{MH}(2K_u\sin 2\theta + K_1\sin 4\theta),$$

$$= K_u\sin 2\theta\Big\{1 - \underbrace{\frac{1}{M^2H^2}(2K_u^2(1 - \cos 4\theta) + \frac{K_1^2}{2}(1 - \cos 8\theta) + 2K_uK_1(\cos 2\theta - \cos 6\theta))}_{\text{2nd. order in } 1/MH}\Big\}$$
$$+ \frac{2K_u^2}{MH}\sin 2\theta.\cos 2\theta + \frac{K_1K_u}{MH}\sin 4\theta.\cos 2\theta$$

$$= K_u\sin 2\theta + \frac{K_u^2}{MH}\sin 4\theta + \frac{K_1K_u}{2MH}(\sin 6\theta + \sin 2\theta) \quad \ldots\ldots\ (1)$$

From the second term, the following is obtained:

$$\frac{K_1}{2}\sin 4\theta.\cos\frac{2}{MH}(2K_u\sin 2\theta + K_1\sin 4\theta) + \frac{K_1}{2}\cos 4\theta.\sin\frac{2}{MH}(2K_u\sin 2\theta + K_1\sin 4\theta)$$

$$= \frac{K_1}{2}\sin 4\theta.\left[1 - \frac{4}{M^2H^2}(4K_u^2\sin^2 2\theta + K_1^2\sin^2 4\theta + 4K_uK_1\sin 2\theta\sin 4\theta)\right]$$

$$+ \frac{K_1}{2}\cos 4\theta.\frac{2}{MH}(2K_u\sin 2\theta + K_1\sin 4\theta)$$

$$= \frac{K_1}{2}\sin 4\theta\left\{1 - \underbrace{\frac{4}{M^2H^2}\left[2K_u^2(1-\cos 4\theta) + \frac{K_1^2}{2}(1-\cos 8\theta) + 2K_uK_1(\cos 2\theta - \cos 6\theta)\right]}_{\text{2nd. order in } K/MH.}\right\}$$

$$+ \frac{2K_uK_1}{MH}\sin 2\theta.\cos 4\theta + \frac{K_1^2}{MH}\sin 4\theta.\cos 4\theta$$

$$= \frac{K_1}{2}\sin 4\theta + \frac{K_1^2}{2MH}\sin 8\theta + \frac{K_uK_1}{MH}(\sin 6\theta - \sin 2\theta) \quad \ldots\ldots\ (2)$$

Adding (1) and (2) to obtain full expression for -L in non-infinite field conditions:

$$-L = K_u\sin 2\theta + \frac{K_1}{2}\sin 4\theta + \frac{K_u^2}{MH}\sin 4\theta + \frac{K_1^2}{2MH}\sin 8\theta$$

$$- \frac{K_uK_1}{2MH}\sin 2\theta + \frac{3K_uK_1}{2MH}\cos 6\theta$$

where the normal expression is given by the first two terms.

Appendix A.3. The heating effect on the substrate due to radiation from the source and incident evaporant.

A.3.1. Radiation Effect.

By the Stefan-Boltzmann Law, the rate of radiation of thermal energy $\frac{dE}{dt}$ from a source at temperature $T^{\circ}K$ to its surroundings at $T_o{}^{\circ}K$ is given by

$$\frac{dE}{dt} = \sigma \, A \, \epsilon_t (T^4 - T_o{}^4)$$

where σ is the Stefan-Boltzmann constant,

A is the radiating area,

ϵ_t is the total emissivity of the radiating surface.

If $T_o \ll T$, it can be neglected.

For the vapour source, the ingot, of diameter $\frac{1}{2}$", was regarded as being at a constant temperature of 1850° K. The small areas at the electron focus were about 200° hotter, but their effect could be neglected as their total radiating area was so small.

$$\epsilon_{1850} \text{ for Ni} \approx 0{\cdot}26$$

(extrapolated from 1000° C, the highest temperature at which published data is available)

$$\therefore \frac{dE}{dt} = 5{\cdot}7 \times 10^{-5} \cdot \pi \times (0{\cdot}65)^2 \cdot 0{\cdot}26 \cdot (1850)^4 \text{ ergs/sec.}$$

$$\approx 2{\cdot}2 \times 10^8 \text{ erg/sec.}$$

$$\approx 5 \text{ calories/sec.}$$

Assuming that this energy is radiated uniformly over a hemisphere of radius 20 cm. (the source-substrate distance) with the ingot at its centre point,

∴ Rate of incident energy per unit area at substrate

$$= \frac{5}{2 \times \pi \times (20)^2} \text{ cals/sec/cm}^2$$

$$\approx 2 \times 10^{-3} \text{ cals/sec/cm}^2$$

(By way of comparison, the incident radiant energy from the substrate heater at 1200^0 K is about $\frac{1}{2}$ cal/sec/cm^2.)

Since about 1 cm.^{2} of substrate is exposed to the radiation, the radiant power received is thus 2×10^{-3} cals/sec. This assumes zero reflectivity of the substrate and so represents the maximum theoretical heating effect from the radiant energy.

$$\text{Now, } \frac{dE}{dt} = M C_p \frac{d\theta}{dt}$$

where M = mass of substrate,

C_p = specific heat of substrate,

$\frac{d\theta}{dt}$ = rate of temperature rise.

Substituting values, the result for a 1 gm. substrate is:

$$\frac{d\theta}{dt} = 10^{-2} \text{ deg./sec.}$$

A.3.2. Incident Evaporant Effect.

If it is assumed that the vapour beam has the equilibrium "temperature" of the source, this will give the maximum possible

contribution from this effect.

The thermal energy content of the evaporant flow is given by

$$\frac{dQ}{dt} = R_m C_p T$$

where R_M = mass rate of evaporation,

C_p = specific heat of evaporant,

T = source temperature.

For a deposition rate on the substrate of 10Å/sec., which is

$$1\mu g/cm^2/sec. \text{ for Ni,}$$

$$\frac{dQ}{dt} = 1{\cdot}4 \times 10^{-4} \text{ cals/cm}^2\text{/sec.}$$

This heat flow causes the substrate temperature to rise at the rate of $\frac{d\theta}{dt}$, where $\frac{dQ}{dt} = M C_p \frac{d\theta}{dt}$ for unit area.

Whence, substituting values,

$$\frac{d\theta}{dt} = 1{\cdot}4 \times 10^{-3} \text{ deg/sec.}$$

Thus, the radiant heating term is dominant.

It is assumed that Wilts used an ingot of roughly the same size and temperature as was used in this experiment. (Since vapour pressure is such a sensitive function of temperature, only a small temperature increase gives a comparatively large rate increase.) The radiant energy at the substrates is then of the same order as in this experiment (since Wilts' source-substrate difference was also 20 cm.), i.e., 2×10^{-3} cals/sec/cm^2.

Mass of Wilts' glass substrates $\approx 0{\cdot}15$ gm.

C_p for glass $\approx 0{\cdot}15$

$$\therefore \quad \frac{d\theta}{dt} = \frac{2 \times 10^{-3}}{0{\cdot}15 \times 0{\cdot}15} \text{ deg/sec.} \quad \approx \quad 0{\cdot}1 \text{ deg/sec.}$$

i.e., about one order of magnitude lower than his observed rise.

Appendix A.4. Field due to substrate heater.

Consider a section across the heater strip looking along the current flow direction:

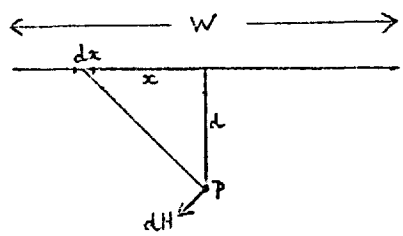

Let i = current per unit of width.

W = width of strip.

At the point P, a distance d from centre of strip, field dH due to current element dx a distant x from centre of strip, is given by:

$$dH = \frac{2i\,dx}{\sqrt{x^2 + d^2}}$$

$\therefore$ Component of dH parallel to strip width

$$= \frac{2i\,dx}{\sqrt{x^2 + d^2}} \cdot \frac{d}{\sqrt{x^2 + d^2}} = \frac{2id \cdot dx}{x^2 + d^2}$$

$$\therefore \text{ Total field } \quad H = \int_{-\frac{W}{2}}^{+\frac{W}{2}} \frac{2id\,dx}{x^2 + d^2}$$

$$= 2i\left[\tan^{-1}\frac{x}{d}\right]_{-\frac{W}{2}}^{+\frac{W}{2}}$$

$$= \frac{4I}{W}\tan^{-1}\frac{W}{2d}$$

where I = total current.

For current series of experiments,

W = 23 mm. $\quad$ d = 4 mm.

$\therefore$ For a current of 50 amps., (= 5 e.m.u.),

$$\underline{\underline{H = 11 \text{ oe.}}}$$

Appendix A.5. The constraint term in single crystal films.

Following West[W.5], the angular-dependent part of the constraint energy of a cubic single crystal film is given by:

$$W(\alpha_i\beta_i) = -\left(\frac{B_1B_1^1}{C_{11}^1 - C_{12}^1}\right)(\alpha_1^2\beta_1^2 + \alpha_2^2\beta_2^2 + \alpha_3^2\beta_3^2)$$

$$-\frac{B_2B_2^1}{C_{44}^1}(\alpha_1\alpha_2\beta_1\beta_2 + \alpha_2\alpha_3\beta_2\beta_3 + \alpha_3\alpha_1\beta_3\beta_1)$$

(from equation (8) of his paper)

where α_i are direction cosines of M_s at measuring temp. T,
and β_i are direction cosines of M_s at measuring temp. T^1.

The B and C are the standard magnetoelastic coupling constants and the pure elastic constants, being primed or unprimed depending on the temperature T^1 or T.

Converting to magnetostriction constants by using the relationships:

$$B_1 = -\frac{3}{2}(C_{11} - C_{12})\lambda_{100} \quad \text{and} \quad B_2 = -3C_{44}\lambda_{111},$$

$$W(\alpha_i\beta_i) = -\frac{9}{4}(C_{11} - C_{12})\lambda_{100}\lambda_{100}^{1}(\alpha_1^2\beta_1^2 + \alpha_2^2\beta_2^2 + \alpha_3^2\beta_3^2)$$

$$- 9\,C_{44}\lambda_{111}\lambda_{111}^{1}(\alpha_1\alpha_2\beta_1\beta_2 + \alpha_2\alpha_3\beta_2\beta_3 + \alpha_3\alpha_1\beta_3\beta_1)$$

Now, for a (100) plane measurement, $\alpha_3 = \beta_3 = 0$.

Putting $-\frac{9}{4}(C_{11} - C_{12})\lambda_{100}\lambda_{100}^{1} = A$

and $-\frac{9}{2}C_{44}\lambda_{111}\lambda_{111}^{1} = B,$

$$W(\alpha_i\beta_i)_{(100)} \longrightarrow A(\alpha_1^2\beta_1^2 + \alpha_2^2\beta_2^2) + 2B\alpha_1\alpha_2\beta_1\beta_2.$$

Now, if ϕ = angle of field during deposition
and θ = angle of field during measurement,
both angles being referred to a cube edge,

then $\alpha_1 = \cos\theta$, $\alpha_2 = \sin\theta$

$\beta_1 = \cos\phi$, $\beta_2 = \sin\phi$.

Also, by definition, $\cos(\theta - \phi) = \alpha_1\beta_1 + \alpha_2\beta_2$

$$\therefore (\alpha_1^2\beta_1^2 + \alpha_2^2\beta_2^2) = \cos^2(\theta - \phi) - 2\alpha_1\alpha_2\beta_1\beta_2.$$

Substituting in expression for W above,

$$W(\alpha_i\beta_i)_{100} \longrightarrow A\cos^2(\theta - \phi) - 2(A - B)\sin\theta\cos\theta.\sin\phi\cos\phi$$

$$= A\cos^2(\theta - \phi) - \frac{(A - B)}{2}\left[\cos^2(\theta - \phi) - \cos^2(\theta + \phi)\right]$$

This is a combination of three uniaxial anisotropy energies, and so is itself a uniaxial anisotropy.

There are two particularly simple cases to be considered:

i) Field applied along cube edge during deposition,

$$\text{i.e.,} \quad \phi = 0$$

$$\therefore W \longrightarrow A\cos^2\theta$$

$$\text{i.e.} \quad W_{H\langle\bar{1}00\rangle} = -\frac{9}{4}(C_{11} - C_{12})\lambda_{100}\lambda_{100}I\cos^2\theta.$$

ii) Field applied along substrate diagonal during deposition,

$$\text{i.e.,} \quad \phi = \frac{\pi}{4}$$

$$\therefore W \longrightarrow A\cos^2\left(\theta - \frac{\pi}{4}\right) - \frac{A - B}{2}\left[\cos^2\left(\theta - \frac{\pi}{4}\right)\cos^2\left(\theta + \frac{\pi}{4}\right)\right]$$

Which, on expanding, becomes:

$$W = \text{const.} + \frac{B}{2}\sin 2\theta$$

$$= \text{konst.} + B\cos^2\left(\frac{\pi}{4} - \theta\right)$$

i.e., a uniaxial anisotropy whose easy axis lies along one of the $\langle\bar{1}10\rangle$ directions,

$$\text{i.e., } W_{H\langle\bar{1}10\rangle} = -\frac{9}{2} C_{44}\lambda_{111}\lambda_{111}^{1}\cos^2\psi + \text{const.}$$

where ψ is the angle between M_s and a $\langle\bar{1}10\rangle$ direction.

Appendix 6. Calculation of film stress from direct strain measurement

Consider a diametric cross section of the film:

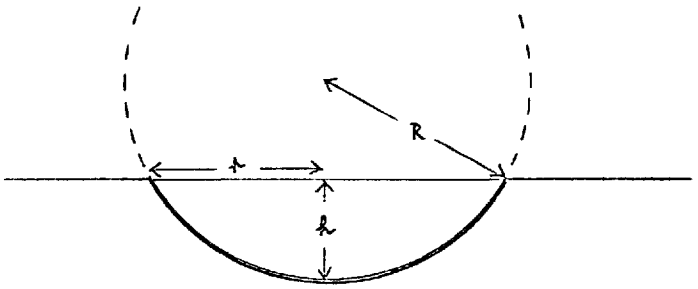

By geometry, length of surface of film

$$= 2r + \frac{2h^2}{r}$$

$$\therefore \text{Strain} = \frac{(2r + \frac{2h^2}{r}) - 2r}{2r}$$

$$= \frac{h^2}{r^2}$$

Now $r = 0.5$ cm.

$h = 0.05$ cm.

$$\therefore \text{Strain} = 10^{-2}$$

$$\therefore \text{Stress} = \text{Strain} \times \text{Young's modulus}$$

$$= \underline{2 \times 10^{10} \text{ dyne/cm}^2}$$

This result is approximate for two reasons:

a) The difficulty of obtaining an accurate measurement of h.

b) The assumption that the weight of the excess liquid beneath the film is exactly counterbalanced by the surface tension effect of the convex surface. An estimate of these two quantities is now made.

Excess pressure inside "bubble" of water beneath film $= \frac{2T}{R}$, where T = surface tension of water, = 75 dyne/cm.

R calculated geometrically = 10 cm.

$\therefore$ P = $\underline{15 \text{ dyne/cm}^2}$.

Mass of water within "bubble" = $\frac{hr^2}{2}$, = 20 mgm.

$\therefore$ Gravitational force = mg $\approx$ 20 dynes.

This acts over an effective area of about $\frac{3}{4}$ cm^2.

$\therefore$ Hydrostatic pressure inside bubble at apex $\approx$ $\underline{27 \text{ dynes/cm}^2}$

These two pressures, therefore, seem to balance in an order of magnitude calculation. Even if this were not so, they are so small in magnitude that they could not appreciably affect the strain already in the film. Thus, supposing that the whole of the gravitational force of 20 dynes were acting <u>tangentially</u> on a strip of the film supposed 1 cm. wide (and 1000 Å thick). The stress involved would still be only 2×10^6 dynes/cm^2. i.e. almost 4 orders of magnitude less than the stresses present during film production.

REFERENCES

A.1. ANDERSON, J.C. (1968), "Magnetism and Magnetic Materials", Chapman and Hall Ltd.

A.2. ANDERSON, J.C. (1962), "Magnetic and Electric Resonance and Relaxation" Proc. XIth Colloque Ampère, Eindhoven, p.471.

A.3. ANDERSON, J.C. and DONAVON, B. (1959), Proc. Phys. Soc., 73, 593.

A.4. AUBERT, G. (1968), J. Appl. Phys. 39, 504.

A.5. ANDRÄ, W., and STEINBECK, K. (1966), Phys. Stat. Sol., 17, 191.

A.6. ASTWOOD, P. and PRUTTON, M. (1963), Brit. J. Appl. Phys., 14, 48.

A.7. ALERS, G.A., NEIGHBOURS, J.R., and SATO, H. (1960), J. Phys. Chem. Solids, 13, 40.

A.8. ALESSANDRINI, E.I. (1964), J. Appl. Phys. 35, 1606.

B.1. BOZORTH, R.M. (1951), "Ferromagnetism", D. van Nostrand Co. Ltd.,

B.2. BLOIS, M.S. (1955), J. Appl. Phys., 26, 975.

B.3. BEAM, W.R., and SIEGLE, W.T. (1965), Rev. Sci.Inst., 36, 641.

B.4. BIRSS, R.R., and WALLIS, P.M. (1963), J. Sci. Inst., 40, 551.

B.5. A suggestion of H.J. Williams in BOZORTH, R.M. (1954) Phys. Rev., 96, 311.

B.6. BOZORTH, R.M., TILDEN, E.F., and WILLIAMS, A.J. (1955), Phys. Rev., 99, 1788.

B.7. BECKER, R. and DÖRING, W. (1939), "Ferromagnetismus", Springer, Berlin.

B.8. BALTZ, A. and DREW, J.B. (1966), I.E.E.E. Trans. Magnetics, MAG-2, 581.

B.9. BALTZER, P.K. (1957), Phys. Rev., 108, 580.

B.10. BIORCI, G., FERRO, A. and MONTALENTI, G. (1961) Nuovo Cim., 20, 617.

B.11. BALTZ, A. (1963), J. Appl. Phys., 34, 1575.

B.12. BOYD, E.L. (1960), I.B.M. J. Res. Develop., 4, 116.

B.13. DEMINGER, G.N. and PAVLOVIC, A.S. (1967), J. Appl. Phys., 38, 1325.

B.14. BIRSS, R.R. and WALLIS, P.M. (1968), J. Appl. Phys., 39, 1347.

B.15. BOZORTH, R.M. AND HAMMING, R.W. (1953), Phys. Rev., 89, 865.

B.16. BIRSS, R.R. and LEE, E.W. (1960), Proc. Phys. Soc., 76, 502.

C.1. CRITTENDEN, E.C., Jr., HUDIMAC, A.A. and STROUGH, R.I. (1951), Rev., Sci. Inst., 22, 873.

C.2. CRITTENDEN, E.C., Jr. and HOFFMANN, R.W. (1953), Rev. Mod. Phys., 25, 310.

C.3. CHAMBERS, A., POMFRET, D, and PRUTTON, M. (1967), J. Sci. Inst., 44, 181.

C.4. CHIKAZUMI, S. (1956), J. Phys. Soc. Japan, 11, 718.

C.5. CALLEN, E.R. and CALLEN, H.B. (1960), J. Phys. Chem. Solids, 16, 310.

C.6. COHEN, M.S. (1968), in "Thin Film Phenomena" edited by K.L. Chopra, McGraw Hill, (to be published 1969).

C.7. COHEN, M.S. (1961), J. Appl. Phys., 32, 87S.

C.8. CARR, W.J. Jr. (1958), J. Appl. Phys., 29, 436.

C.9. CHIKAZUMI, S. (1964), "Physics of Magnetism", John Wiley and Sons Ltd.

C.10 COHEN, M.S. (1962), J. Appl. Phys., 33, 2968.

C.11. CHAMBERS, A. and PRUTTON, M. (1968), Thin Solid Films, 1, 393.

C.12. COMBES, L.S., BALLARD, S.S. and McCARTHY, K.A. (1951), J. Opt. Soc. America., 41, 215.

C.13. CHIKAZUMI, S. (1956), J. Phys. Soc. Japan, 11, 551.

C.14. CHIKAZUMI, S. (1961), J. Appl. Phys., 32, 81S.

D.1. DOYLE, W.D., RUDISILL, J.E. and SHTRIKMAN, S. (1961)., J. Appl. Phys., 32, 1785.

F.1. FRENKEL, J. and DORFMAN, J. (1930), Nature, 126, 274.

F.2. FELDTKELLER, E. (1963), Z. Physik., 176, 510.

FELDTKELLER, E. (1963), Phys. Letters, 7, 9.

F.3. FERGUSON, E.T., (1958), J. Appl. Phys., 29, 252.

F.4. FLANDERS, P.J. (1967), J. Appl. Phys., 38, 1293.

FLANDERS, P.J. (1968), J. Appl. Phys., 39, 1345.

F.5. FREEDMAN, J.F. (1962), I.B.M. J. Res. Develop., 6, 449.

F.6. FERRO, A., GRIFFA, G. and MONTALENTI, G. (1966)., I.E.E.E. Trans Magnetics, MAG-2, 764.

F.7. FREEDMAN, J.F. (1965), J. Appl. Phys., 36, 964.

G.1. GRAHAM, C.D. Jr., (1959) in "Magnetic Properties of Metals and Alloys", American Society for Metals, Cleveland.

G.2. GRUNER, R.L. (1965), M.S. Thesis, Polytechnic Inst. of Brooklyn. Quoted by Schwartzman and D'Antonio (1968), Thin Solid Films, 2, 247.

G.3. GRAHAM, C.D. Jr. and LONMEL, J.M. (1962), J. Phys. Soc. Japan, 17, Supplement B1, 570.

G.4. GLAZER, A.A., POTAPOV, A.P., TAGIROV, R.I., and SHUR, YA.S. (1966), Soviet Phys. - Solid State, 8, 2413.

H.1. HAGEDORN, F.B. (1967) Rev. Sci. Inst., 38, 591.

H.2. HUMPHREY, F.B. (1967), J. Appl. Phys., 38, 1520.

H.3. HARRISON, F... (1956), J. Sci. Inst., 33, 5.

H.4. HUMPHREY, F.B. and JOHNSTON, A.R. (1963), Rev. Sci. Inst., 34, 348.

H.5. HARTE, K.J., SMITH D.C., ANDERSON, R.M. and JOHNSTON, R.C. (1968), J. Appl. Phys., 39, 749.

H.6. HARTE, K.J., SMITH, D.O. and GROSS, M. (1968) to be published.

H.7. HODGES, J.A. (1963), Brit. J. Appl. Phys., 14, 340.

H.8. HEIDENREICH, R.D., NESBITT, E.A. and BURBANK, R.D. Jr. (1959), J. Appl. Phys., 30, 995.

HEIDENREICH, R.D. and REYNOLDS, F.W. (1959) in "Structure and Properties of Thin Films" ed. by C. Neugebauer, Wiley, New York.

H.9. HEAVENS, O.S., MILLER, R.F., MOSS, G.L. and ANDERSON, J.C. (1961), Proc. Phys. Soc. 78, 33.

H.10. HOFMANN, U. (1964) Exper. Techn. Physik, 12, 417.

I.1. IGNATCHENKO, V.A. (1961), Soviet Phys. - J.E.T.P., 13, 863.

I.2. INO, S., WATANABE, DE. and OGAWA, S. (1964), J. Phys. Soc. Japan, 19, 881.

J.1. JÄGER, M. (1964), Z. Metallkunde, 55, 17.

K.1. KRAUSE, D. and PATZ, V., (1966), Z. Angew. Phys., 21, 342.

K.2. KITTEL, C. (1946), Phys. Rev., 70, 965.

K.3. KOBELEV, V.V., (1963), Soviet Phys. Metals and Metallography, 13, 146.

K.4. KOUVEL, J.S. and GRAHAM, C.D. Jr. (1957), J. Appl. Phys., 28, 340.

K.5. KITTEL, C. and GALT, J.K. (1956) "Ferromagnetic Domain Theory" in Solid State Physics, 3, 439, Academic Press (New York).

K.6. KNEER, G. and ZINN, W (1966), Phys. Stat. Sol. 17, 323.

K.7. KNEER, G. and ZINN, W (1966) in "Basic Problems in Thin Film Physics", edited by R. Niedermayer and H. Mayer (Vandenhoeck and Ruprecht), p. 437.

K.8. KLEMPERER, O. (1959) "Electron Physics" Butterworths, London, p.241.

K.9. KITTEL, C. (1949), Revs. Mod Phys., 21, 541.

K.10. KNOCKHOLM, B and FREEDMAN, J.F. (1967), J. Appl. Phys., 38, 1354.

L.1. LAMTON, H. and STEWART, K.H. (1948), Proc. Roy. Soc., A.193, 72.

L.2. LANGFORD, D.A. (1956), Metropolitan-Vickers Research Report, No.5077.

L.3. LEAVER, K.D., (1966), private communication.

L.4. LESNIK, A.G., LEVIN, G.I. and NEDOSTUP, V.M. (1966), Phys. Stat. Sol., 17, 745.

L.5. LUBORSKY, F.E. (1967), J. Apply. Phys., 38, 1445.

LUBORSKY, F.E. and BARBER, W.D. (1968), J. Appl. Phys. 39, 746.

LUBORSKY, F.E. (1968), I.E.E.E. Trans. Magnetics, MAG-4, 19.

L.6. LYKKEN, G.I., HARMAN, W.L. and MITCHELL, E.N., (1966), J. Appl. Phys. 37, 3353.

M.1. MIDDELHOEK, S. (1961), "Ferromagnetic Domains in Thin Nickel Iron Films", PhD Thesis, Amsterdam, 1961.

M.2. METHFESSEL, S. (1966), in "Basic Problems in Thin Film Physics", edited by R. Niedermayer and H. Mayer (Vandenhoeck and Ruprecht, Göttingen), p.422.

M.3. METHFESSEL, S., SEGÜLLER, A. and SCHMERHALDER, R. (1962) J. Phys. Soc. Japan, 17, Suppliment B1, 575.

M.4. METZDORF, W. (1965), Z. Angew. Phys., 18, 534.

M.5. Mullard Reference Manual of Transistor Circuits, p.270.

N.1. NESBITT, E.A., WILLIAMS, H.J. and BOZORTH, R.M. (1954). J. Appl. Phys., 25, 1014.

N.2. NESBITT, E.A. and WILLIAMS, H.J. (1955). J. Appl. Phys., 26, 1217.

N.3. NÉEL, L. (1953), Compt. Rend. Acad. Sci. Paris, 237, 1468 and 1613.

N.4. NÉEL, L. (1963), J. de Physique, 24, 513.

O.1. OSBORNE, J.A. (1945), Phys. Rev., 67, 351.

P.1. PRUTTON, M. (1964) "Thin Ferromagnetic Films", Butterworths.

P.2. PUGH, E.W. (1963) in "Physics of Thin Films", Vol. 1., edited by G. Hass, (Academic Press, New York).

P.3. PRUTTON, M. (1962), Trans. 9th National Vacuum Symposium, American Vacuum Society, pp.59-67.

P.4. PRUTTON, M. (1964), Brit. J. Appl. Phys. 15, 815.

P.5. PAULEVÉ, J., DAUTREPPE, D., LAUGIER, J. and NÉEL, L. (1962), J. Phys. Radium, 23, 841.

PAULEVÉ , J. and DAUTREPPE, D (1963), J. de Physique, 24, 522.

P.6. PAUL, M.C. and HANSON, M.M. (1966), J. Appl. Phys. 37, 3743.

P.7. PUZEI, I.M. (1957), Bull. Acad. Sci., U.S.S.R., Phys. Ser., 21, 1088.

P.8. PRUTTON, M. (1962), Nature, 193, 565.

R.1. RODBELL, D.S. (1965), Physics., 1, 279.

R.2. ROBINSON, G. (1962), J. Phys. Soc. Japan, 17, Supplement B1, 558.

R.3. ROTH, M., ANAGNOSTOPOULOU-KONSTA, A. and PAULEVÉ, J. (1968), J. Appl. Phys. 39, 738.

S.1. STONER, E.C. and WOHLFARTH, E.P., (1948), Phil. Trans Roy. Soc., A240, 599.

S.2. SMITH, D.O. (1956), Conf. on Mag. and Mag. Materials, Boston, p.625.
SMITH, D.O. (1958), J. Appl. Phys., 29, 264.

S.3. SATO, H. and CHANDRASEKHAR, B.S. (1957), J. Phys. Chem. Solids, 1, 228.

S.4. SCHLECHTWEG, H. (1936), Ann. Physik (5), 27, 573.

S.5. SOOHOO, R.F. (1965), "Magnetic Thin Films", Harper and Row, New York.

S.6. SLONCZEWSKI, J.C. (1968), I.E.E.E. Trans Magnetics, MAG-4, 15.

S.7. SMITH, D.O., COHEN, M.S. and WEISS, G.P. (1960), J. Appl. Phys. 31, 1755.

S.8. SPAIN, R. (1963), Compt. Rend. 256, 3262.

S.9. SIEGLE, W.T. and BEAN, W.R. (1965), J. Appl. Phys., 36, 1721.

S.10. SUZUKI, T. and WILTS, C.H. (1967), J. Appl. Phys., 38, 1356.

S.11. SOROHAN, M. (1966), Phys. Stat. Sol. 14, K21.

SOROHAN, M. (1968), Phys. Stat. Sol. 26, K9.

S.12. SMITH, D.O. and WEISS, G.P. (1965), J. Appl. Phys., 36, 962.

S.13. SMITH, D.O., WEISS, G.P. and HARTE, K.J. (1966), J. Appl. Phys., 37, 1464.

S.14. SLONCZEWSKI, J.C. (1966), I.B.M. Research Note, NC 675.

S.15. SELLA, C. and TRILLAT, J.J. (1963), in "Single Crystal Films". Proceedings of Int. Conf. at Philco Scientific Laboratory, Blue Bell, Penn. (Pergamon Press, 1964).

S.16. SCHAEFER, H. Discussion comment after paper by Wilts at Clausthal Conference.

T.1. TOROK, E.J., WHITE, B.A., HUNT, A.J. and GREDSON, H.N. (1962), J. Appl. Phys., 33, 3037.

T.2. TARASOV, L.P. (1939), Phys. Rev. 56, 1224.

T.3. TANIGUCHI, S. and YAMAMOTO, H. (1954), Sci. Rep. Res. Inst. Tohoku Univ. A6, 330.

TANIGUCHI, S. (1955), Sci. Rep. Res. Inst. Tohoku Univ., A7, 269.

T.4. TELESNIN, R.V., SARAEVA, I.M., RYSAK, E.N. and SHISHKOV, A.G. (1966), Bull. Acad. Sci. U.S.S.R., Phys. Ser., 30, 102.

T.5. TAKAHASHI, M. (1962), J. Appl. Phys., 33, 1101.

T.6. TATSUMOTO, E., OKAMOTO, T., IWATA, N. and KADENA, Y, (1965), J. Phys. Soc. Japan, 20, 1541.

T.7. TATSUMOTO, E., OKAMOTO, T., and KADENA, Y., (1965), J. Phys. Soc. Japan, 20, 1534.

T.8. TOKUTAKA, H. and MAEJIMA, R. (1965), J. Phys. Soc. Japan, 20, 362.

U.1. UNVALA, B.A. (1963), PhD Thesis, Cambridge.

U.2. USAMI, S., NAGASHIMA, H. and AOI, H. (1967), J. Phys. Soc. Japan, 22, 877.

V.1. VEERMAN, J. FRANSE, J.J.M. and RATHENAU , G.W., (1963), J. Phys. Chem. Solids, 24, 947.

V.2. VAN VLECK, J.H. (1937), Phys. Rev. 52, 1178

V.3. VLASOV, K.B. and MITSEK, A.I. (1962), Soviet Physics, Metals and Metallography, 14, 487. (in the original).

W.1. WEISS, P. (1905), J. de Physique, 4, 469.

WEISS, P. (1907), J. de Physique, 6, 661.

W.2. WILLS, C.H. and HUMPHREY, F.B. (1968), J. Appl. Phys., 39, 1191.

W.3. WEBSTER, W.L. (1925), Proc. Roy. Soc. 107, 496.

W.4. WILLIAMS, H.J., HEIDENREICH, R.D. and NESBITT, E.A. (1956), J. Appl. Phys. 27, 85.

W.5. WEST, F.G. (1964), J. Appl. Phys., 35, 1827.

W.6. WILTS, C.H. (1966), in "Basic Problems in Thin Film Physics", edited by R. Niedermayer and H. Mayer (Vandenhoeck and Ruprecht, Göttingen), p.422.

W.7. WILLIAMS, C.M. and SCHINDLER, A.I. (1964), J. Appl. Phys., 35, 877.

WILLIAMS, C.M. and SCHINDLER, A.I. (1966), J. Appl. Phys., 37, 1468.

W.8. WILTS, C.H. (1965), Brit. J. Appl. Phys., 16, 1775.